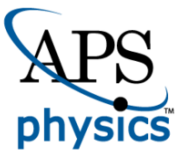

This is the accepted manuscript made available via CHORUS. The article has been published as:

Fluctuation spectroscopy: From Rayleigh-Jeans waves to Abrikosov vortex clusters

A. A. Varlamov, A. Galda, and A. Glatz

Rev. Mod. Phys. **90**, 015009 — Published 27 March 2018

DOI: 10.1103/RevModPhys.90.015009

Fluctuation Spectroscopy: from Rayleigh-Jeans Waves to Abrikosov Vortex Clusters

A.A. Varlamov

CNR-SPIN (Istituto Superconduttori, Materiali Innovativi e Dispositivi), Viale del Politecnico 1, I-00133, Rome, Italy

A. Galda

James Franck Institute, University of Chicago, Chicago, Illinois 60637, USA
Materials Science Division, Argonne National Laboratory, 9700 S. Cass Avenue, Argonne, Illinois 60439, USA

A. Glatz

Materials Science Division, Argonne National Laboratory, 9700 S. Cass Avenue, Argonne, Illinois 60439, USA
Department of Physics, Northern Illinois University, DeKalb, Illinois 60115, USA

(Dated: November 22, 2017)

Superconducting (SC) fluctuations, discovered in the late 1960s, have constituted an important research area in superconductivity as they are manifest in a variety of phenomena. and are therefore of great fundamental and practical importance. Indeed, the underlying physics of SC fluctuations makes it possible to elucidate the fundamental properties of the superconducting state.
The interest in SC fluctuation phenomena was further enhanced with the discovery of cuprate high temperature superconductors (HTS). In these materials, superconducting fluctuations appear over a wide range of temperatures due to the superconductors' extremely short coherence lengths and low effective dimensionality of the electron systems. These strong fluctuations lead to anomalous properties of the normal state in some HTS materials. Within the framework of the phenomenological Ginzburg-Landau theory, and more extensively, in the diagrammatic microscopic approach based on BCS theory, SC fluctuations as well as other quantum contributions (weak localization, etc.), enabled a new way to investigate and characterize disordered electron systems, granular metals, Josephson structures, artificial super-lattices, and others. The characteristic feature of SC fluctuations is its strong dependence on temperature and magnetic field in the vicinity of the superconducting phase transition. This dependence allows the separation of fluctuation effects from other contributions and provides information about the microscopic parameters of a material; in particular, the critical temperature and the zero-temperature critical magnetic field. As such, SC fluctuations are very sensitive to the relaxation processes that break phase coherence and can be used as a versatile characterization instrument for SCs: *Fluctuation spectroscopy* has emerged as a powerful tool for studying the properties of superconducting systems on a quantitative level.
Here, we review the physics of SC fluctuations, commencing from a qualitative description of thermodynamic fluctuations close to the critical temperature and quantum fluctuations at zero temperature in the vicinity of the second critical field. The analysis of the latter allows us to present fluctuation formation as a fragmentation of the Abrikosov lattice. The review highlights a series of experimental findings followed by microscopic description and numerical analysis of the effects of fluctuations on numerous properties of superconductors in the entire phase diagram and beyond the superconducting phase.

CONTENTS

TABLE I: List of symbols. When possible, the equation number, where a symbol is defined is listed in the third column.

c	speed of light (mostly set to one)	
$C^{(\mathrm{fl})}$	fluctuation heat capacity	
$\mathcal{C}_n(\varepsilon_1,\varepsilon_2)$	four-leg Cooperon	(31)
d	effective dimension of the FCP motion	
d_e	effective dimension of the electron motion	
$\mathcal{D}$	electron diffusion coefficient	
$\mathcal{D}_\mathrm{g}$	intragrain diffusion coefficient	
$\mathcal{D}_\mathrm{T}$	intergrain diffusion coefficient	
e	electron unit charge	
E_F	Fermi energy	
E_Th	Thouless energy	
$\mathcal{E}_m(x,t,h)$	Auxiliary function inversely proportional to the fluctuation propagator	(33)
$F^{(\mathrm{fl})}$	fluctuation correction to free energy	(37)
$G(\mathbf{p},\varepsilon)$	one electron Green's function	
g_eff	effective BCS interaction	
$\mathrm{Gi}_{(\mathrm{d})}$	Ginzburg-Levanyuk number	(28)
h	dimensionless magnetic field, $H/\widetilde{H}_{c2}(0)$	
$\hbar$	Planck constant (mostly set to one)	
$\widetilde{h}$	reduced magnetic field, $[H - H_{c2}(0)]/H_{c2}(0)$	
$H_{c2}(0)$	second critical field at zero temperature	
$\widetilde{H}_{c2}(0)$	second critical field extrapolated to zero temperature from the GL region	
$I^{(\mathrm{fl})}$	fluctuation correction to quasiparticle tunneling current	
j_α	electric current density	
$\mathbf{j}^\mathrm{mag}$	density of persistent electric current induced by magnetization gradient	
k_B	Boltzmann constant (mostly set to one)	
l	electron mean free path	
ℓ_H	FCP magnetic length, $\sqrt{\hbar c/(2eH)}$	
ℓ_ϕ	phase relaxation length, $v_\mathrm{F}\tau_\phi$	
l_T	thermal length, $\sqrt{\mathcal{D}/k_BT}$	
$L(\mathbf{q},\Omega_k)$	fluctuation propagator	(24)
$\mathcal{L}(p,p',q)$	two-particle Green's function	(23)
m^*	effective mass of FCPs	
m_e	electron mass	
$m^{(\mathrm{qp})}$	mass of quasiparticles	
$M(h,t)$	magnetization	(50)
$n(\mathbf{q})$	Bose–Einstein distribution	(5)
$N_{(d)}$	FCP concentration in d dimensions	(7)
$\mathfrak{N}$	Nernst signal	(74)
$n_\mathrm{F}(E)$	Fermi distribution	
$\widehat{\mathcal{N}}_{\mathrm{L,R}}$	particle number operator in left/right electrode	
p_F	Fermi momentum	
$Q_{\alpha\gamma}$	"electric current - electric current" response operator	
$\widetilde{Q}_{\alpha\gamma}$	"electric current - heat current" response operator	
R_N	tunnel junction resistance	
$R_\square$	sheet resistance	
r_L	Larmor radius	
s	film thickness	
S	wire cross-section	
T	temperature	
t	dimensionless temperature, T/T_{c0}	
$T_\mathrm{c}(H)$	superconducting critical temperature	
$T_\mathrm{c}^\mathrm{BCS}$	mean field value of superconducting critical temperature followed from BCS theory	
T_{c0}	superconducting critical temperature in zero field renormalized by fluctuations	(1)
$T_{\mathbf{pk}}$	tunnel matrix element between states $\mathbf{p}$ and $\mathbf{k}$	
v_F	electron Fermi velocity	
v	dimensionless voltage, $2\frac{eV}{\Delta_\mathrm{BCS}}$	
V	voltage	
V_max	voltage determining the pseudogap eV_max	(95)
W	NMR relaxation rate	
α	GL parameter	
$\beta^{\alpha\beta}$	thermoelectric tensor relating electric current with temperature gradient	
$\beta_\mathrm{M}^{\alpha\beta}$	part of the thermoelectric tensor related to magnetization currents	
$\gamma^{\alpha\beta}$	thermoelectric tensor relating heat current with electric field	
γ_E	exponential Euler-Mascheroni constant	(40)
γ_ϕ	phase-breaking parameter	(55)
Γ	tunneling rate	
$\Delta(\mathbf{r})$	superconducting order parameter	
Δ_BCS	order parameter at zero temperature	
$\Delta^{(\mathrm{fl})}(\mathbf{r},t)$	fluctuation order parameter	
Δ_q, Δ_q^*	Fourier components of the fluctuating order parameter	
ΔE_s	binding energy of FCP close to T_{c0}	
ΔE_QF	binding energy of FCP close to $H_{c2}(0)$	
δ	phase-breaking parameter	(60)
ϵ	reduced temperature, $[T - T_{c0}]/T_{c0}$	(2)
$\epsilon^{\alpha\beta\zeta}$	Levi-Civita symbol	
$\varepsilon(\mathbf{q})$	kinetic energy of FCP	(6)
ε_n	fermionic Matsubara frequency, $(2n+1)\pi k_\mathrm{B}T$	
$\theta(x)$	Heaviside step function	
$\kappa^{\alpha\beta}$	heat conductivity tensor	
λ_F	electron Fermi length	
$\lambda_n(\varepsilon_1,\varepsilon_1)$	Cooperon	(30)
μ	chemical potential	
$\mu^{(\mathrm{fl})}$	chemical potential of FCP close to T_{c0}	
$\mu^{(\mathrm{QF})}$	chemical potential of FCP close to $H_{c2}(0)$	
$\mu^{(\mathrm{qp})}$	chemical potential of quasiparticle	
$\nu_{(d)}$	Nernst coefficient	(11)
$\nu^{(\mathrm{fl})}$	fluctuation contribution to Nernst coefficient close to T_{c0}	
$\nu^{(\mathrm{QF})}$	fluctuation contribution to Nernst coefficient close to $H_{c2}(0)$	
ν_e	electron contribution to Nernst coefficient	
ρ_e	one-electron density of states	
$\rho_{\mathrm{L,R}}$	density of states of the left (right) electrode	
ξ	superconducting coherence length	(4)
$\xi_{\mathrm{cl},\mathcal{D}}$	coherence length for clean/dirty systems	
ξ_GL	GL coherence length	(3)
ξ_BCS	BCS coherence length at zero temperature	

$\xi_{\rm QF}$	characteristic size of QF	(18)
$\Pi(\mathbf{q},\Omega_k)$	polarization operator	(25)
$\sigma_{\rm xx}^{(AL),(MT)...}$	different fluctuation corrections to longitudinal conductivity	
$\sigma_{\rm xy}^{(AL),(MT)...}$	different fluctuation corrections to Hall conductivity	
$\sigma_{\rm xx}^{(\rm fl)}$	total fluctuation correction to conductivity	(55)
$\sigma_{\rm xx}^{(\rm e)}$	Drude conductivity	
$\delta\sigma_{\rm tun}^{(\rm fl)}$	fluctuation correction to tunneling conductivity	
ς	particle-hole asymmetry parameter	
τ	elastic scattering time	
$\tau_{\rm cp}$	Cooper pair rotation period	(17)
$\tau_{\rm GL}$	GL lifetime of FCP	(1)
$\tau_{\rm tr}$	transport scattering time	
τ_ϕ	phase-breaking time	
$\tau_{\rm QF}$	lifetime of FCP in QF regime	(17)
$\tau_{\rm so}$	spin-orbit scattering time	
$\chi_\pm$	dynamic spin susceptibility	
$\chi^{(\rm fl)}$	fluctuation correction to magnetic susceptibility	(38)
$\chi_{\rm L}$	Landau diamagnetic susceptibility	
$\psi(x)$,$\psi^{(n)}(x)$	digamma, polygamma functions	
ω	frequency	
$\omega_{\rm c}$	electron cyclotron frequency, $\left\lvert\frac{eH}{m_{\rm e}c}\right\rvert$	
$\omega_{\rm c}^{(\rm qp)}$	cyclotron frequency of quasiparticles, $\left\lvert\frac{eH}{m^{(\rm qp)}c}\right\rvert$	
Ω_H	cyclotron frequency of FCP, $\frac{4\mathcal{D}eH}{c}$	
$\omega_{\rm D}$	Debye frequency	
Ω_k	bosonic Matsubara frequency of fluctuation Cooper pair, $2\pi k_{\rm B}Tk$, $(k=0,\pm1,\pm2...)$	
ω_n	bosonic Matsubara frequency corresponding to the external field, $2\pi k_{\rm B}Tn$, $(n=0,1,2...)$	

TABLE II: List of acronyms

AL	Aslamasov-Larkin
BCS	Bardeen-Cooper-Schriefer
BEC	Bose-Einstein condensation
DCR	diffusion coefficient renormalization
BKT	Berezinskii-Kosterlitz-Thouless
DOS	density of states
FCP	fluctuation Cooper pairs
fl	fluctuations
GL	Ginzburg-Landau
GM	Giaever and Megerle
HTS	high-T_c superconductors
ID	(corrections due to) interaction in diffusion channel
LBA	low-bias anomaly
LD	Lawrence-Doniach
LLL	lowest Landau level
MT	Maki-Thompson
(N+SF)	normal state with SF
NE	Nernst-Ettingshausen
NMR	nuclear magnetic resonance
NQR	nuclear quadrupole resonance
pg	pseudogap
QF	quantum fluctuations
qp	quasi-particles
QPT	quantum phase transition
SC	superconductor/superconducting
SF	superconducting fluctuations
STM/STS	scanning tunneling microscopy/spectroscopy
WL	weak localization (corrections)

"Natura non facit saltus",
Gottfried Leibniz, **New Essays** (1704).

I. INTRODUCTION

"Happy families are all alike; every unhappy family is unhappy in its own way." is the famous beginning line of Leo Tolstoy's novel, "Anna Karenina". About a hundred years later, Vladimir Nabokov turned this line on its head and opened his novel "Ada or Ardor: A Family Chronicle" with "All happy families are more or less dissimilar; all unhappy ones are more or less alike." in reference to Tolstoy.

We do not want to say whose assertion is more astute, but can confidently assume that scientists, studying the ramifications of superconducting fluctuations for nearly half a century, are content with their discoveries. Neither can we say whether electrons or Cooper pairs ['coupled' electrons in superconductors (SC)] are happy or not, but we know that while *stable* Cooper pairs in the superconducting state form a sort of condensate below the critical temperature T_{c0} – all conducting in the same way – the behavior of *fluctuating* Cooper pairs (FCPs)[1] beyond the superconducting region is more complex and results in a multitude of interesting physical phenomena.

These FCPs affect thermodynamic and transport properties of a metal, both directly and through changes which they cause in the quasiparticle subsystem. The investigation of superconductivity through superconducting fluctuations (SF) provides valuable information about the microscopic properties of the normal and superconducting state and details about the formation of the latter (Larkin and Varlamov, 2009). For example, direct measurements of the second critical field $H_{c2}(0)$ of some high temperature superconductors is a challenging problem due to its extremely large predicted values, restricting their measurements to only a few available pulsed high-field facilities. Yet, this important material property can be extracted from the study of the fluctuation induced Nernst signal above the critical temperature (Tafti *et al.*, 2014) at considerably lower field ranges.

The phenomenon of superconducting fluctuations came into the focus of the superconductivity community nearly half a century after the discovery of superconductivity. There were several reasons for this suspended interest. For example, the early samples were inhomogeneous, resulting in substantial extrinsic broadening of the superconducting transition, which obfuscated the manifestation of thermal fluctuations. Later, when homogeneous bulk materials became available, the very sharp superconducting transition of these clean materials also concealed the fluctuation phenomena. The temperature region over which the superconducting transition is smeared due to fluctuations is determined by the so-called *Ginzburg-Levanyuk number*, $\mathrm{Gi}_{(3)}$, (Ginzburg, 1960; Levanyuk, 1959). For a three-dimensional superconductor, it has a typical value range of $(10^{-14} - 10^{-6})T_{c0}$ (depending on the concentration of impurities).

The search for superconductors with high critical parameters led scientists to the investigation of disordered superconducting films and quasi-one-dimensional systems, where the transition from the resistive to the superconducting state is smeared over a much wider temperature interval: $\sim (10^{-2} - 10^{-3})T_{c0}$ (Glover, 1967). A careful analysis of the transition region in low dimensional systems resulted in the concurrent formulation of the phenomenological theory of fluctuations based on the Ginzburg-Landau theory (Schmidt, 1968, 1966) and the development of a diagrammatic microscopic approach (Aslamasov and Larkin, 1968; Maki, 1968; Thompson, 1970). These advances explained the experimental observations and opened a new field of interdisciplinary research involving superconductivity and the theory of phase transitions. Furthermore, close to the critical temperature and in relatively weak magnetic field regions of the phase diagram, both approaches essentially led to the same conclusions regarding the effect of FCPs on various superconducting properties.[2]

The fluctuation "boom" started with the investigation of corrections to the heat capacity (Suzuki and Tsuboi, 1977; Tsuboi and Suzuki, 1977), the conductivity (Glover, 1967), the density of states (Abeles *et al.*, 1971; Cohen *et al.*, 1969), and the emergence of collective modes in the superconducting phase (Carlson and Goldman, 1973) close to T_{c0}. All of them were found to be small everywhere beyond the immediate vicinity of the transition. This relatively negligible effect of fluctuations on the SC transition was found to be in striking contrast to the properties of liquid ^{4}He at the transition to the superfluid state, where fluctuations smear the heat capacity jump so strongly that the corresponding temperature was called the λ-point. This discrepancy was explained by the large value of the Cooper pairs coherence length with respect to inter-atomic distances: namely,

[1] One has to distinguish the notion of FCP from that one of a "preformed Cooper pair" appearing in some BEC-BCS scenarios of high temperature superconductivity. While preformed Cooper pairs are supposed to be equilibrium bosons composed of two electrons due to their effective attraction in real space, a FCP is a useful "image" of superconducting-type correlations occurring in a Fermi-liquid of electrons in the normal phase of a superconductor.

[2] The microscopic approach yields additional contributions related to the quantum interference and indirect effects of fluctuation pairing on the properties of the quasiparticle subsystem. The latter are generally less singular in the vicinity of the critical temperature.

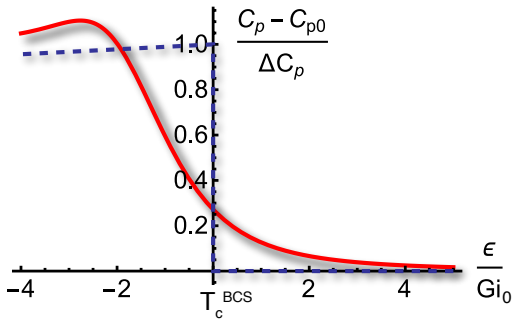

FIG. 1 (Color online) Smearing of the superconducting transition by fluctuations ($\epsilon \approx T/T_{c0} - 1$). The temperature dependencies of the heat capacity of a superconducting grain in the vicinity of the transition temperature in accordance to the BCS theory (dashed line) and the one accounting for fluctuations obtained in Ref. (Schmidt, 1966) (solid line). The typical temperature scale for the change of the heat capacity is given by $\mathrm{Gi}_{(0)}\, T_{c0}$.

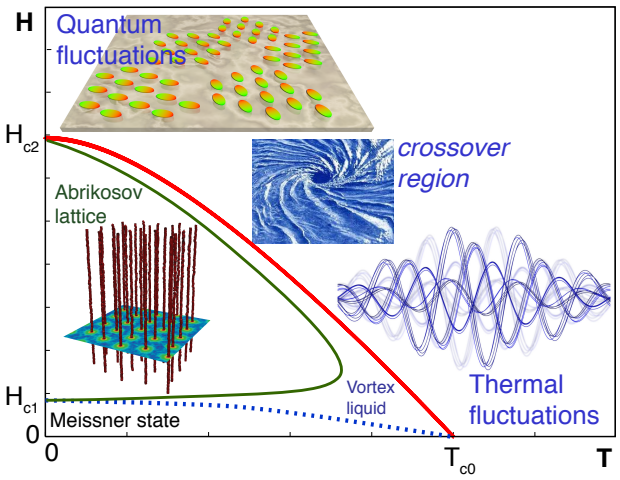

FIG. 2 (Color online) Schematic phase diagram of type-II superconductors, showing the domains of qualitatively different physical behavior.

the inverse ratio of these quantities constitutes a small parameter to the theory of SF –the Ginzburg-Levanyuk number– and determines the weakness of SF in conventional superconductors.

In the vicinity of the superconducting transition temperature, the thermodynamics of SF can be described within the framework of the GL functional. Such description for small, effectively zero-dimensional, SC granules was successfully considered by V. V. Schmidt (Schmidt, 1966). Here, the shape of the superconducting transition, smeared by fluctuations, is essentially determined by the fourth order term in the GL functional (see Fig. 1). Unfortunately, a functional integration over all modes of the fluctuating order parameter in the partition function using the complete GL functional is an infeasible task for higher dimensional ($d = 1, 2, 3$) superconductors. Yet, beyond the immediate vicinity of the critical temperature, the leading fluctuation contribution to the heat capacity arises from low energy (long-wavelength) modes of the fluctuating order parameter. Their scale is characterized by the so-called Ginzburg-Landau coherence length $\xi_{\mathrm{GL}}(T)$, which is much larger then the size of the "true" Cooper pairs emerging in BCS theory. This fact enables the GL functional to describe fluctuation effects with the quadratic approximation, which allows for solving a wide range of problems. However, the description of fluctuations in the immediate vicinity of the transition ($\epsilon \lesssim \mathrm{Gi}_{(\mathrm{d})}$) remains beyond the validity of this approximation and requires renormalization group approaches.

The situation is similar to the effect of fluctuations on transport coefficients: they are mainly determined by low energy/slow modes of the order parameter (Abrahams *et al.*, 1970; Aslamasov and Larkin, 1968; Maki, 1968; Scalapino, 1970).

In the early 1970s, the only experimentally observed characteristic exhibiting a long tail in its temperature dependence was the magnetization, which extended Meissners diamagnetism far into the normal phase of superconductors. It considerably exceeded the values for the electron diamagnetism predicted by Langevin's and Landau's theories over a wide range of temperatures. Moreover, even at temperatures close to the transition difficulties appeared in explaining the field dependence of the fluctuation magnetization in high magnetic fields. For example, it was quite clear that strong magnetic fields should suppress fluctuations (and this was indeed observed experimentally), the GL approach – even in its nonlinear version – failed to explain this behavior (Patton *et al.*, 1969; Prange, 1970; Skocpol and Tinkham, 1975). Furthermore, in the zero- and one-dimensional cases, the precursor of the Meissner signal as function of the magnetic field first increases (in absolute terms) linearly with the field until it reaches a maximum, and finally decreases slowly to zero. In the two-dimensional case, it saturates and in the 3D case it increases indefinitely, in contrast to the experimental results and common sense. The discrepancy between the then available theory and experimental findings demonstrated the important role of short-wavelength and dynamical fluctuation modes, which involve energies much larger than those accessible with the Ginzburg-Landau approach (Kurkijärvi *et al.*, 1972). The sharp contradiction between theory and experiment in this case may be compared to the paradox of the Rayleigh-Jeans catastrophe that led to Planck's theory.

Early results obtained first in the vicinity of the transition temperature T_{c0} were generalized in the 1970s to 1980s to temperature ranges far from the transition (Altshuler *et al.*, 1983; Aslamasov and Varlamov, 1980; Aslamazov and Larkin, 1974; Bulaevskii, 1974; Larkin, 1980; Maki, 1973) and to relatively high fields (Lopes dos San-

tos and Abrahams, 1985). More recently, quantum fluctuations (QF), appearing in SC at low temperatures and fields close to the second critical field $H_{c2}(0)$, have been also considered (Beloborodov and Efetov, 1999; Beloborodov *et al.*, 2000; Galitski and Larkin, 2001a). Focusing on the vicinity of the quantum phase transition one obtains a qualitative picture of superconducting fluctuations quite different from that in the GL region close to T_{c0}. FCPs close to $H_{c2}(0)$ should rather be seen as rotating fluctuating vortices with cyclotron frequency $\Omega_H \sim \Delta_{\rm BCS}/\hbar$ and Larmor radius $r_{\rm L} \sim \xi_{\rm BCS}$ than being considered as long wavelength modes. Since the characteristic coherence length of QFs and their lifetime considerably exceed the corresponding size and period of rotation of a single vortex ($\xi_{\rm QF} \gg r_{\rm L}$, $\tau_{\rm QF} \gg \hbar\Delta_{\rm BCS}^{-1}$) in this region, one can assume that they form a peculiar dynamic state (Glatz *et al.*, 2011b), which consists of clusters of coherently rotating FCPs. These form some kind of quantum liquid (see Fig. 2, top-left).

Finally, renewed interest in superconducting fluctuations was triggered by the observation of a giant Nernst-Ettingshausen signal over a wide range of temperatures and magnetic fields in underdoped phases of high temperature superconductors (Xu *et al.*, 2000) and later also in conventional superconductors above the critical temperature (Pourret *et al.*, 2006a) — now in their most general manifestation, including the quantum regime. The origin of the giant signal generated a lively discussion and was finally explained in Refs. (Levchenko *et al.*, 2011; Michaeli and Finkel'stein, 2009a; Serbyn *et al.*, 2009; Ussishkin *et al.*, 2002). These papers outlined the profound relationship between the fluctuation Nernst-Ettingshausen signal, magnetization currents, and the dominant role of these effects with respect to the other fluctuation entities.

In this review, we emphasize the general approach to describe the fluctuation phenomena in the entire phase diagram of a superconductor above the upper critical field line $H_{c2}(T)$ and its importance for *fluctuation spectroscopy*. We concentrate mainly on the most interesting case of a two-dimensional $s-$wave superconductor, restricting the consideration to the representative limit of a dirty superconductor ($k_B T_{c0}\tau \ll \hbar$). Moving along the $H_{c2}(T)$ line one can see how long-wavelength fluctuations of the order parameter, due to the effect of increasing magnetic field, gradually transform into fluctuation vortices. The crossover between these two, very different, pictures takes place where the FCP's Larmor radius becomes of the order of its coherence length. At higher fields and at lower temperatures the quantum nature of fluctuations becomes more pronounced and the picture starts to resemble an Abrikosov vortex lattice rather than a set of Ginzburg-Landau long waves. Variations in the character of the SFs, determine their contributions to the thermodynamic and transport behavior of the superconductor.

In recent years, a microscopic approach emerged, which accounts for short wavelength and dynamical SFs, elucidating the challenging experimental findings of the last decade over the entire phase diagram. Those include the giant Nernst signal, the non-monotonous temperature behavior of conductivity above the phase transition in disordered SC films, the pseudo-gap opening above the transition line, the peculiarities of the nuclear magnetic resonance relaxation above the Abrikosov vortex state, and many more.

At this point a word of prudence is in order. The theoretical starting point for the microscopic considerations presented in this review is the BCS theory (Bardeen *et al.*, 1957a,b). In its original version it describes the Cooper pair formation as a result of electron-phonon interaction, which was broadly successful in explaining properties of conventional superconductors. Yet, prescinding from its physical nature, one can perceive the BCS theory as a mean-field theory, and the underlying origin of the interaction responsible for the Cooper pair formation is not that important for its applicability. One can replace the phonons mediating the electron-electron interaction in the BCS Hamiltonian by other collective bosonic excitations of the solid. For example, this approach successfully describes the physics of superfluid ^{3}He, where the role of intermediate bosons is played by ferromagnetic paramagnons. Superconductivity mediated by magnetic excitations has been proposed for various organic and heavy fermion superconductors. The collective bosonic degrees of freedom can mediate electron-electron interaction either in spin or in charge channels. The resulting interaction does not even need to be attractive. Also the type of pairing symmetry is not important, as the BCS theory can be extended to *p*-, *d*- and higher angular momenta pairing mechanisms (Chubukov *et al.*, 2008; Scalapino, 2012; Tsuei and Kirtley, 2000; V.M. Loktev, 2015). In this language we can say that fluctuations in the framework of the generic BCS scheme describe thermodynamic and transport properties of superconductors beyond the mean-field approximation.

With the discovery of high-temperature superconductors (HTS) a new field of research was generated - yet a generally accepted mechanism of this phenomenon is still not available. Underdoped cuprates show clear features of electron state localization (Mott physics), such that the BCS theory does not apply to them. HTS oxide superconductors with low superconducting carrier density are characterized by a relatively small phase stiffness and poor screening, both of which imply a significantly larger role for phase fluctuations (Emery and Kivelson, 1995). However, SC properties of optimally doped and overdoped cuprates can be described – at least to first approximation – using models with moderately strong electron-electron interaction. The fundamental properties of such systems are not qualitatively different from BCS superconductors. For this reason, we will also apply the fluctuation spectroscopy approach to analyze the

measurements on optimally and overdoped HTSs in addition to experimental results obtained for conventional superconductors.

The review is organized as follows: In section II we present the qualitative picture of fluctuation phenomena in superconductors by demonstrating how the main results can be obtained from the point of view of the uncertainty principle and basic formulas of condensed matter physics. In section III we report on the main ideas and necessary mathematical elements of the microscopic description of SFs at arbitrary temperatures and magnetic fields. The following sections are organized in a common systematic way: we focus on one physical property of the superconductor at a time, briefly review how it is calculated in the Matsubara diagrammatic technique, present the general analytical expression for the corresponding fluctuation contribution including its asymptotic analysis, when possible present 3D visualization obtained as a result of numerical calculation in the entire phase diagram, and, finally, its comparison with the available experimental data. We start this sequence of properties with the discussion of the fluctuation diamagnetism (Sec. IV), followed by the fluctuation conductivity (Sec. V), Hall conductivity (Sec. VI), Nernst-Ettingshausen effect (Sec. VII), pseudogap and low bias anomaly (Sec. VIII), and NMR relaxation rate (Sec. IX). In section X we discuss some aspects of fluctuation corrections in quasi-2D, two-band, clean, and nanocrystalline superconductors. Finally, we summarize the more technical aspects required for the numerical evaluation of the complete expressions for fluctuation corrections and *numerical fluctuation spectroscopy* in section XI. The numerical codes needed to fit experimental data and, as a result, to extract the fundamental microscopic parameters of the superconducting systems (fluctuation spectroscopy) are supplied as supplementary materials. These codes were also used to produce the 3D surface plots of fluctuation corrections presented in this review.

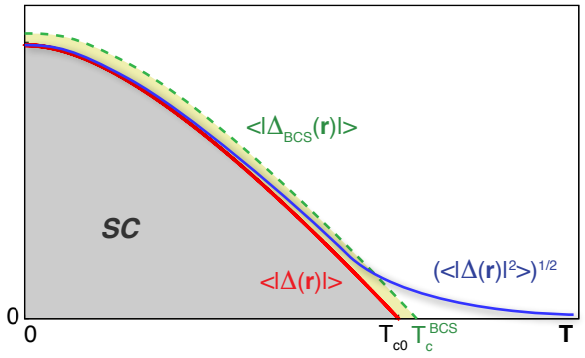

FIG. 3 (Color online) The temperature dependence of the averaged mean square value of the superconducting order parameter (solid, blue line). The dashed, green line corresponds to the mean field BCS picture ($\langle|\Delta_{\rm BCS}(\mathbf{r})|\rangle$ and becomes zero at the point $T_c^{\rm BCS}$). The thick red line describes the same $\langle|\Delta(\mathbf{r})|\rangle$ dependence, but with the fluctuation renormalized transition temperature T_{c0}, which is lower that the mean field value $T_c^{\rm BCS}$ (see Ref (Larkin and Varlamov, 2009)). A finite concentration of fluctuating Cooper pairs, without long-range spatial coherence, exists in the normal phase of superconductor for any temperature above T_{c0}. Their lifetime increases approaching the transition line from the normal state.

II. QUALITATIVE PICTURE

A. Thermodynamic fluctuations in superconductors close to T_{c0}

1. Rayleigh–Jeans waves rather than Boltzmann particles

The BCS theory (Bardeen *et al.*, 1957a,b), being a mean field approximation, only deals with thermally equilibrated Cooper pairs, which form a Bose-Einstein condensate. Any deviations from this mean-field model can be considered fluctuations. For example, four-particle interactions with the formation of one or two non-equilibrium Cooper pairs, or vice versa, interactions resulting in the decay of a Cooper pair belonging to the condensate into two quasiparticles are taken into account in the fluctuation theory (Dinter, 1977; Kulik *et al.*, 1981; Varlamov and Dorin, 1986). Using the language of the Ginzburg-Landau approach, one can say that the BCS approximation corresponds to the saddle point solution of the GL functional. The latter describes the equilibrium distribution of the order parameter in a superconductor and allows for the study of its properties in the mean-field approximation. Yet, any other imaginable $\Delta(\mathbf{r})$ also contributes to the partition function of a superconductor, being weighted by means of the corresponding canonical distribution.

Above the critical temperature of the superconducting transition, T_{c0}, the conditions for the formation of persistent Cooper pairs are not yet fulfilled. Nevertheless, in accordance with the epigraph to this review, these kind of objects appear even in the normal phase of superconductors as fluctuations before the system undergoes the phase transition into the superconducting state. These FCPs appear and decay, without forming a condensate. The corresponding lifetime $\tau_{\rm GL}$, the so-called Ginzburg-Landau time, can be estimated by utilizing the uncertainty principle. Clearly, at the transition temperature, an equilibrium superconducting condensate with infinite lifetime emerges. Hence, for continuity reasons, $\tau_{\rm GL}$ must diverge to infinity when $T \to T_{c0}$. Let us estimate the binding energy of FCPs, ΔE_s, using dimensionality arguments: While the Fermi energy, the Debye temperature, and the critical temperature can be expressed in units of energy, the only quantity that vanishes at the critical temperature is $k_{\rm B}(T - T_{c0})$. Assuming that the binding

energy of a FCP is proportional to this quantity, we immediately see that $\tau_{\rm GL} \sim \hbar/\Delta E_s$ becomes infinite at the phase transition point. The microscopic theory confirms this hypothesis and gives the exact coefficient:

$$\tau_{\rm GL} = \frac{\pi\hbar}{8k_{\rm B}(T-T_{\rm c0})}\,. \tag{1}$$

One can also estimate the characteristic "size" of a FCP, $\xi_{\rm GL}$, which is determined by the distance that two electrons fly away from each other in a time $\tau_{\rm GL}$. In the case of a dirty superconductor, the electron motion is diffusive, with the diffusion coefficient $\mathcal{D} \sim v_{\rm F}^2\tau$ (τ is the electron scattering time) and $\xi_{\mathcal{D}}(T) = \sqrt{\mathcal{D}\tau_{\rm GL}} \sim v_{\rm F}\sqrt{\tau\tau_{\rm GL}}$ [3]. In the case of a clean superconductor, where $k_{\rm B}T\tau \gg \hbar$, impurity scattering no longer affects the electron-electron correlations. In this case, the characteristic time of the ballistic electron motion turns out to be less than the electron-impurity scattering time τ, and is determined by the uncertainty principle, being $\sim \hbar/k_{\rm B}T$. It is this latter time that has to be used to estimate the effective FCP size: $\xi_{\rm cl}(T) \sim v_{\rm F}\sqrt{\hbar\tau_{\rm GL}/k_{\rm B}T}$. In both cases, the coherence length grows as $\epsilon^{-1/2}$ when approaching the critical temperature, where

$$\epsilon \equiv \ln\frac{T}{T_{\rm c0}} \approx \frac{T-T_{\rm c0}}{T_{\rm c0}} \ll 1 \tag{2}$$

is the reduced temperature. In the GL region (close to, but beyond the immediate vicinity of $T_{\rm c0}$, i.e., ${\rm Gi} \lesssim \epsilon \ll 1$) we define the coherence length as

$$\xi_{\rm GL}(\epsilon) = \xi/\sqrt{\epsilon}\,. \tag{3}$$

Here $\xi = \xi_{{\rm cl},\mathcal{D}}$,

$$\xi^2 = -\frac{\tau^2 v_{\rm F}^2}{d_e}\left[\psi\left(\frac{1}{2}+\frac{1}{4\pi T\tau}\right) - \psi\left(\frac{1}{2}\right) - \frac{1}{4\pi T\tau}\psi'\left(\frac{1}{2}\right)\right], \tag{4}$$

where $d_e = 1, 2, 3$ is the effective dimension of the electron motion. [4] This expression was obtained for the first time by Gor'kov (Gor'kov, 1960) as a result of a microscopic calculation. It is important to note that it only differs by a numerical coefficient from the BCS expression for the coherence length at zero temperature $\xi_{\rm BCS}$. We see that the fluctuating order parameter $\Delta^{(\rm fl)}(\mathbf{r},t)$ varies close to $T_{\rm c0}$ on the relatively large scale $\xi_{\rm GL}(\epsilon) \gg \xi_{\rm BCS}$, see (3).

It is important to note that FCPs, strictly speaking, cannot be considered as Landau quasiparticles. Indeed, while the energy of a well-defined quasiparticle has to be much larger than its inverse lifetime, the binding energy ΔE_s for a FCP turns out to be of the same order, $\hbar/\tau_{\rm GL}$. Yet, close to $T_{\rm c0}$, they still can be treated as classical objects, but in the sense of Rayleigh–Jeans waves rather than Boltzmann particles. This means that in the general Bose–Einstein distribution function only small energies $\varepsilon(\mathbf{q}) \ll T$ ($\mathbf{q}$ is the momentum of the center of mass of FCP) are involved, and the exponential function in the Bose-Einstein distribution can be expanded:

$$n(\mathbf{q}) = \frac{1}{\exp(\varepsilon(\mathbf{q})/k_{\rm B}T)-1} \to \frac{k_{\rm B}T}{\varepsilon(\mathbf{q})}\,. \tag{5}$$

For this reason, the more appropriate tool to study fluctuation phenomena is the GL equation written for classical fields rather than the Boltzmann transport equation.

Nevertheless, the treatment of FCPs as particles often turns out to be useful. In this approach, their energy consists of the "binding energy" and the kinetic energy of the center of mass motion:

$$\varepsilon(\mathbf{q}) = k_{\rm B}(T-T_{\rm c0}) + \frac{\mathbf{q}^2}{2m^*}\,, \tag{6}$$

where m^* is the effective mass of FCP.

The concentration of FCPs can be estimated by integration of the distribution function (5) over the momenta in the range $|\mathbf{q}| \le \hbar\xi^{-1}$ (corresponding to the conditions $\varepsilon(\mathbf{q}) \ll T$):

$$N_{(d)} = \int_{|\mathbf{q}|\lesssim\hbar/\xi} n(\mathbf{q})\,\frac{d^d\mathbf{q}}{(2\pi\hbar)^d} = \frac{m^*k_BT_{\rm c0}}{2\pi\hbar^2}\begin{cases} 2\pi\xi_{\rm GL}(\epsilon) & d=1 \\ \ln(1/\epsilon) & d=2 \\ {\rm const} - \xi_{\rm GL}^{-1}(\epsilon) & d=3 \end{cases}. \tag{7}$$

The physical three dimensional concentration for wires and films can be related to (7) by $\tilde{N}_{(3)} = N_{(d)}s^{d-3}$. [5] It turns out to be divergent when approaching the transition in the 1D and 2D cases. Let us recall that these

[3] Strictly speaking, in the majority of expressions below τ has the meaning of the electron transport scattering time $\tau_{\rm tr}$. Nevertheless, as is well known, in the case of isotropic scattering these values coincide; so for the sake of simplicity we will use hereafter the symbol τ.

[4] By introduction of d_e we stress the difference between the effective dimensionality for FCPs, d, and electron motion. When we talk about a 2D superconductor, we mean a superconducting film of thickness $s \ll \xi$, or a strongly layered material with the interlayer distance larger than the perpendicular coherence length. This condition is less restrictive in the GL region, where the requirement $s \ll \xi_{\rm GL}(\epsilon)$ is sufficient for two-dimensional FCP motion. Regarding the effective dimensionality of the electron motion d_e, it is determined by the specifics of its spectrum or confined electron diffusion due to sample geometry.

[5] We define the FCP concentration in d-dimensional space. This means that it determines the number of pairs per volume in the 3D case, the number of pairs per unit square in the 2D case, and the number of pairs per unit length in 1D. Since both wires and films are actual objects in three dimensional space, we can approximate the 3D concentration of FCPs, $\tilde{N}_{(3)}$, by $\tilde{N}_{(3)} = N_{(1)}/s^2$ for wires, where s^2 is the wire cross-section and $\tilde{N}_{(3)} = N_{(2)}/s$ for films, where s is the thickness of the film, respectively.

results were obtained in the long wave-length approximation (i.e., not too far from transition) and does not account for the interaction of fluctuations (i.e. not too close to T_c), which means $\mathrm{Gi} \lesssim \epsilon \ll 1$.

2. Manifestations of SF close to T_c

Using the above estimates for the lifetime, (1), coherence length, (3)) & (4), and concentration of FCPs, (7), we can evaluate their contribution to different physical characteristics of a metal close to (but above) the transition to the superconducting state. For example, we can quantify the smearing of jump of the heat capacity at the transition. We start with the evaluation of the energy density of FCPs in the Rayleigh–Jeans approximation, (5):

$$\frac{E^{(\mathrm{FCP})}}{V} = \int \varepsilon(\mathbf{q}) n(\mathbf{q}) \frac{d^d\mathbf{q}}{(2\pi\hbar)^d} \approx k_B T_{c0} \int_{|\mathbf{q}|\lesssim\hbar/\xi} \frac{d^d\mathbf{q}}{(2\pi\hbar)^d} \sim \frac{k_B T_{c0}}{\xi^d}.$$

One can see that in this approximation this contribution does not depend on ϵ and, hence, does not contribute to the heat capacity. At this point we note that the formation of FCPs is accompanied by a depletion of the quasiparticles subsystem, i.e., the concentration of the latter is reduced by $2N_{(d)}$, see (7). Therefore, the total energy density of the system changes by $E^{(\mathrm{fl})} \sim -2k_BTN_{(d)}$ with related correction to heat capacity

$$C_V^{(\mathrm{fl})} = \left(\frac{dE^{(\mathrm{fl})}}{dT}\right)_V \sim -2k_B \frac{dN_{(d)}(\epsilon)}{d\epsilon} \sim \frac{k_B}{\xi^d} \epsilon^{\frac{d}{2}-2}.$$

Similarly, a qualitative understanding of the increase in the diamagnetic susceptibility above the critical temperature can be obtained from the well-known Langevin expression for the atomic susceptibility (Kittel, 2012). Identifying the concentration of FCPs with (7), their mass with m^*, their charge with $2e$, and the average square rotation radius by $\xi^2_{\mathrm{GL}}(\epsilon)$, one finds

$$\Delta\chi^{(\mathrm{fl})} = -\frac{2e^2}{3c^2}\frac{\tilde{N}_{(3)}}{m^*}\xi^2_{\mathrm{GL}}(\epsilon) \to -\frac{e^2}{c^2}\frac{k_B T_{c0}}{\pi\hbar^2 s^{3-d}}\xi^{4-d}_{\mathrm{GL}}(\epsilon). \quad (8)$$

This expression is valid for $d = 2, 3$ (with logarithmic accuracy in $d = 2$).

Analogously, one can evaluate the direct contribution of FCPs to the conductivity (Aslamazov-Larkin paraconductivity). It may be done by using the Drude formula. It is important to remember that impurities do not present obstacles for the FCP motion in an applied electric field. Indeed, the diffusive character of electron motion was already taken into account when we estimated the size of FCPs. Its square ξ^2 determines the inverse effective mass m^*, i.e., its inertia. The motion of FCPs in an electric field has ballistic character and applying the Drude formula, one should use for the lifetime τ_{GL} rather than the elastic scattering time τ, $2e$ for the carrier charge, m^* for its mass, and $N_{(d)}(\epsilon)$ for the concentration of FCPs. Using (1) and (7) one finds:

$$\sigma_{xx}^{(\mathrm{AL})} = \frac{4\tilde{N}_{(3)}(\epsilon)e^2\tau_{\mathrm{GL}}(\epsilon)}{m^*} \sim \frac{e^2}{\hbar s^{3-d}}\xi^{2-d}\epsilon^{\frac{d}{2}-2}. \quad (9)$$

This contribution to conductivity of the normal phase of a superconductor corresponds to the opening of a new channel of charge transfer above T_{c0} due to the formation of FCPs.

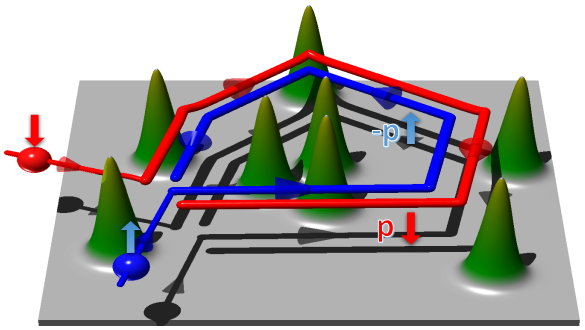

FIG. 4 (Color online) Anomalous MT Cooper pairing. One electron moves clockwise with momentum $\mathbf{p}$, scattering at impurity potentials (green Gaussian peaks), while interacting with another electron with momentum $-\mathbf{p}$ on almost the same path (counter-clockwise).

Besides the direct FCP effect on the properties of a superconductor in its normal phase, indirect manifestation of SFs can be found due to their influence on the quasiparticle subsystem. These have purely quantum nature and, in contrast to paraconductivity, require microscopic consideration.

The first of them is the Maki-Thompson (MT) contribution (Maki, 1968; Thompson, 1970), which is relevant for transport coefficients of dirty SCs near T_c, where its singular temperature dependence is similar to that of paraconductivity. The physical origin of the MT contribution is a result of the fact that in a system with impurities, an electron can move along a self-intersecting trajectory during the process of diffusion and return to its origin after some time. The interference of the wave-functions of two electrons, moving along such trajectories in the opposite directions, leads to the decrease of the Drude conductivity (this is the phenomenon of weak localization (Abrikosov, 1988)). This quantum effect is nothing else than the precursor of the metal–insulator transition.

One can imagine that along such trajectory, two electrons with opposite spins move simultaneously with opposite momenta, interacting with each other (see Fig. 4). They can form some specific FCPs. Here one should note, that the amplitude of the BCS interaction of electrons

drastically increases when $T \to T_{c0}$ (see Ref. (Bardeen *et al.*, 1957a,b)):

$$g_{\rm eff} = \frac{g}{1 - \rho_e g \ln \frac{\omega_D}{2\pi T}} = \frac{1}{\ln \frac{T}{T_c}} = \frac{1}{\epsilon}\,,$$

where ω_D is the Debye frequency and ρ_e is the one-electron density of states. What is the reason for this increase? One possible mechanism is electron-electron scattering accompanied by the formation of virtual Cooper pairs. The probability of such induced pair irradiation (let us remember that Cooper pairs are Bose particles) is proportional to their number in the final state, i.e. $n(\mathbf{p})$ (see Eq. (5)). For small momenta $n(\mathbf{p}) \sim 1/\epsilon$.

During the diffusive motion of an electron, the volume it explores grows as $(\mathcal{D}t)^{d/2}$. During a time dt the electron covers the elementary volume $\lambda_F^{d-1} v_F dt$. Hence the probability to return to the initial point is (Abrikosov, 1988)

$$w \sim \int_{t_{\rm min}}^{t_{\rm max}} \frac{\lambda_F^{d-1}}{(\mathcal{D}t)^{d/2}} v_F dt\,.$$

Since we are interested in fluctuation Cooper pairing of electrons, the corresponding minimal time on such trajectories is τ_{GL}. The upper limit of the integral is governed by the phase-breaking time τ_φ since for larger time intervals the phase coherence, which is necessary for the pair formation, is broken. As a result, the relative correction to conductivity due to such processes is equal to the product of the self-intersecting trajectory probability and the effective interaction constant: $\sigma_{xx}^{(MT)}/\sigma = w g_{\rm eff}$. In the $2D$ case,

$$\sigma_{(2)}^{(MT,an)} \sim \frac{e^2}{8\epsilon\hbar} \ln \frac{\tau_\varphi}{\tau_{GL}}\,.$$

One can see that the MT contribution is extremely sensitive to the electron phase-breaking processes and to the type of symmetry of orbital pairing; this is why it can often be suppressed.

However, the AL and MT contributions, which are positive and singular in ϵ close to T_{c0}, do not capture the full picture of fluctuation effects on conductivity. The involvement of quasiparticles in the fluctuation pairing results in the depletion of their density of states at the Fermi level, i.e., in the opening of a pseudo-gap in the one-electron spectrum and the consequent decrease of the one-particle Drude-like conductivity. This indirect effect of FCP formation is usually referred to as the density of states (DOS) contribution and can be estimated using the Drude formula with doubled concentration of FCPs compared to the concentration of electrons missing at the Fermi level:

$$\sigma_{xx(2)}^{(DOS)} \sim -\frac{2N_{(2)}e^2\tau}{m_e} \sim -\frac{e^2}{\hbar} \ln \frac{1}{\epsilon}\,. \qquad (10)$$

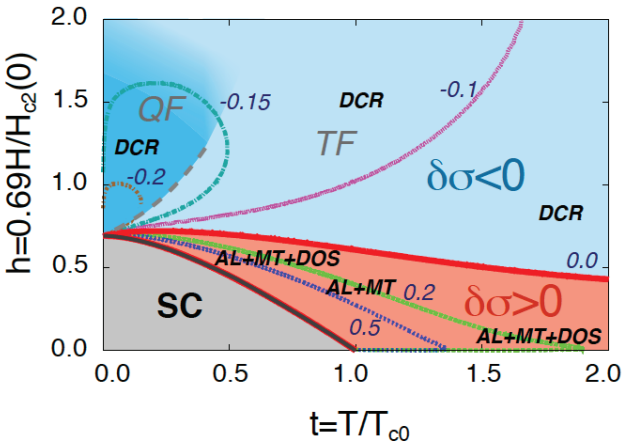

FIG. 5 (Color online) Contours of constant fluctuation conductivity $[\sigma_{xx}^{(fl)}(t,h)$ is shown in units of $e^2/\hbar]$. The dominant fluctuation contributions are indicated in bold-italic labels (**AL** for Aslamazov-Larkin, **MT** for Maki-Thompson, **DOS** for density of states, and **DCR** for diffusion coefficient renormalization). The dashed line separates the domain of quantum fluctuations (QF) [dark area of $\sigma_{xx}^{(fl)} > 0$] and one of thermal fluctuations (TF). After Ref. (Glatz *et al.*, 2011a).

It is seen that the DOS contribution has an opposite sign compared to the AL and MT contributions. In the close vicinity of T_{c0} it does not compete with them, since it has a weaker dependence on temperature (Larkin and Varlamov, 2009). Let us point out the different roles FCPs play in the cases of heat capacity and conductivity: In the former their formation is very "cheap" in terms of energy, and the main change in heat capacity of the system is related to the removal of quasiparticles. In the case of conductivity, the opening of a new channel for the charge transfer due to the formation of FCPs dominates over the changes in the one-particle conductivity.

Finally, a renormalization of the one-electron diffusion coefficient (DCR) in the presence of fluctuation pairing happens. Close to T_{c0}, this contribution is not singular in ϵ:

$$\sigma_{xx}^{(DCR)} \sim \frac{e^2}{\hbar} \ln\ln \frac{1}{T_{c0}\tau} + O(\epsilon)\,.$$

For this reason it was ignored until recently. A few years ago it was shown in Refs. (Glatz *et al.*, 2011a; Serbyn *et al.*, 2009) that the renormalization of the one-electron diffusion coefficient becomes of primary importance relatively far from T_{c0}, and at very low temperatures. Due to the term $\sigma_{xx}^{(DCR)}$, the sign of the overall contribution of fluctuations to the conductivity, $\sigma_{xx(2)}^{(fl)}$, is changed in a wide region of the phase diagram, especially close to $T = 0$, in the region of quantum fluctuations (Glatz *et al.*, 2011a) (see Fig. 5, where regions with dominating fluctuation contributions to magneto-conductivity are shown).

Special attention has been paid to the giant Nernst-Ettingshausen effect observed in the pseudogap state of

underdoped phases of high-temperature superconductors (HTS) (Xu *et al.*, 2000). After the observation in HTS, a giant Nernst-Ettingshausen signal (three orders of magnitude larger than the value of the corresponding coefficient in typical metals) was detected in a wide range of temperatures in the conventional, disordered superconductor Nb_xSi_{1-x} (Pourret *et al.*, 2006b). These groundbreaking experiments have led to vivid experimental and theoretical activities in the last decade (Behnia and Aubin, 2016; Chang *et al.*, 2012; Kavokin and Varlamov, 2015; Levchenko *et al.*, 2011; Michaeli and Finkel'stein, 2009a; Serbyn *et al.*, 2009; Ussishkin *et al.*, 2002).

The origin of the giant contribution of fluctuations to the thermomagnetic signal is closely related to giant fluctuations in the diamagnetic susceptibility occurring in the normal phase of superconductors. It was noticed half a century ago (Obraztsov, 1964) that non-compensated magnetization currents, which appear in non-homogeneously heated samples, can play a crucial role for the correct calculation of the Nernst coefficient, in particular, validating the third law of thermodynamics.

In the case of measurements of the Nernst-Ettingshausen coefficient with a high resistive voltmeter, its thermodynamic part (without the contribution of magnetization currents) can be related to the temperature derivative of the chemical potential (Serbyn *et al.*, 2009; Varlamov and Kavokin, 2009)

$$\nu_{(d)}^{(\mathrm{th})} = \frac{\sigma_{(d)}}{N_{(d)} c e^2} \left(\frac{d\mu_{(d)}}{dT} \right) . \tag{11}$$

For the electron gas in a normal metal $\mu(T) \approx \mu(0) - \pi k_{\mathrm{B}}^2 T^2 / [12\mu(0)]$ and Eq. (11) leads to the known Sondheimer result (Sondheimer, 1948) for the case of electron scattering on elastic impurities:

$$\nu_e = -\frac{\pi\tau}{6 m_{\mathrm{e}} c} \left(\frac{k_{\mathrm{B}} T}{\mu(0)} \right) ,$$

proportional to the small electron-hole asymmetry factor.

Alternatively, one could also try to use Eq. (11) with the values $\sigma_{\mathrm{xx}(d)}^{(\mathrm{AL})}(\epsilon)$ and $N_{(d)}(\epsilon)$ found above. However, one needs to clarify what the chemical potential of fluctuating Cooper pairs, $\mu^{(\mathrm{fl})}$, is, since it is known that in thermal equilibrium, the chemical potential of a system with variable number of particles is zero, like the textbook examples of photon or phonon gases. A naïve application of this "theorem" to the FCP "gas" leads to the wrong conclusion that $\mu^{(\mathrm{fl})} = 0$. However, one needs to be careful when dealing with Cooper pairs, since they do not form an isolated system, but are rather only one subsystem with the other being formed by fermionic quasiparticles, which always have to be taken into account as well. In a multicomponent system, the chemical potential of the ith component, μ_i, is defined as the derivative of the free energy with respect to the number of particles of the i-th kind:

$$\mu_i = \left(\partial F^{(\mathrm{fl})} / \partial N_i \right)_{V,T,N_j} , \tag{12}$$

provided the numbers of particles of all other species are fixed, $N_{j\neq i} = \mathrm{const}$. In deriving the condition for thermodynamic equilibrium, one should now take into account that the creation of a Cooper pair must be accompanied by removing two quasiparticles from the fermionic subsystem. This leads to $\mu^{(\mathrm{fl})} - 2\mu^{(\mathrm{qp})} = 0$, where $\mu^{(\mathrm{qp})}$ is the chemical potential of quasiparticles. Therefore, the equilibrium condition does not fix $\mu^{(\mathrm{fl})}$, $\mu^{(\mathrm{qp})}$ to zero, even though the numbers of Cooper pairs and quasiparticles are not conserved. The simplest way to estimate $\mu^{(\mathrm{fl})}$ is to identify it with the "binding energy" of FCPs, ΔE_s, taken with the opposite sign: $\mu^{(\mathrm{fl})} = T_{\mathrm{c}0} - T$.

A more consistent consideration performed in the framework of the Ginzburg-Landau fluctuation theory confirms this estimate. The fluctuation part of free energy close to $T_{\mathrm{c}0}$ takes form (Larkin and Varlamov, 2009)

$$F_{(2)}^{(\mathrm{fl})}(\epsilon) = -\frac{T_{\mathrm{c}0}}{4\pi\xi^2} \epsilon \ln \frac{1}{\epsilon} . \tag{13}$$

Similarly, the coefficient in Eq. (7) can be expressed in terms of the correlation length, Eq. (4), due to the relation between the coefficients of the Ginzburg-Landau functional (see (Larkin and Varlamov, 2009)):

$$N_{(2)}^{(\mathrm{fl})}(\epsilon) = \frac{1}{4\pi\xi^2} \ln \frac{1}{\epsilon} . \tag{14}$$

Substituting these expressions to Eq. (12) one finds

$$\mu_{(2)}^{(\mathrm{fl})} = \left(\frac{\partial F_{(2)}^{(\mathrm{fl})}}{\partial N_{(2)}^{(\mathrm{fl})}} \right)_{V,T} = \frac{\partial F_{(2)}^{(\mathrm{fl})} / \partial \xi}{\partial N_{(2)}^{(\mathrm{fl})} / \partial \xi} = -T_{\mathrm{c}0} \epsilon . \tag{15}$$

Applying this formula to the subsystem of FCPs close to $T_{\mathrm{c}0}$ and identifying its conductivity with Eq. (9), one finds the Nernst-Ettingshausen coefficient generated by FCPs in weak fields close to $T_{\mathrm{c}0}$:

$$\nu_{(2)}^{(\mathrm{th}),(\mathrm{fl})} = -\frac{\sigma_{\mathrm{xx}(2)}^{(\mathrm{AL})}}{(2e)^2 N_{(2)}^{(\mathrm{fl})} c} = -\frac{\tau_{\mathrm{GL}}(\epsilon)}{m^* c} \sim -\frac{k_{\mathrm{B}} \xi^2}{c\hbar} \frac{1}{\epsilon} , \tag{16}$$

which dramatically exceeds Sondheimer's value. These strong fluctuation effects are a consequence of the extremely strong dependence of the chemical potential of FCPs on temperature and the relatively small concentration of FCPs.

B. Quantum fluctuations in superconductor above $H_{\mathrm{c}2}(0)$

1. Dynamic clustering of fluctuation Cooper pairs

The qualitative picture for SF in the quantum region, at very low temperatures and close to $H_{\mathrm{c}2}(0)$, drastically differs from the Ginzburg-Landau one, valid close

to T_{c0}. As we saw above, the latter can be described in terms of a set of long-wavelength fluctuation modes (with $\lambda \sim \xi_{GL}(T) \gg \xi_{BCS}$) of the order parameter, with characteristic lifetime $\tau_{GL} = \pi\hbar/8k_B(T - T_{c0})$. In the former, the order parameter oscillates on much smaller scales, such that fluctuation modes with wave-lengths up to ξ_{BCS} and frequencies up to $\Delta_{BCS}/\hbar$ are excited.

Indeed, one can visualize the situation in this region as rotating FCPs, analogously to Cooper pairs within Abrikosov vortices, just a little bit below $H_{c2}(0)$. The period of Cooper pairs rotating in an Abrikosov vortex in that region is $\tau_{cp} \sim \Omega^{-1}_{H_{c2}(0)} \sim \Delta_{BCS}$ ($\Omega_H = 4\mathcal{D}eH/c$ is the cyclotron frequency of Cooper pairs) and the corresponding Larmor radius is $r_L \sim \xi_{BCS}$.

The microscopic theory (Galitski and Larkin, 2001a; Glatz *et al.*, 2011a) shows that close to $H_{c2}(0)$ at zero temperature SF are characterized by the lifetime

$$\tau_{QF} \sim \frac{\Delta^{-1}_{BCS}}{\widetilde{h}} \gg \tau_{cp},\ \widetilde{h} = (H - H_{c2}(0))/H_{c2}(0), \quad (17)$$

and by the spatial scale

$$\xi_{QF}\left(\widetilde{h}\right) \sim \frac{\xi_{BCS}}{\sqrt{\widetilde{h}}} \gg \xi_{BCS}. \quad (18)$$

One sees that the dependence of both these values on the parameter governing the transition is completely symmetric to that of $\tau_{GL}(\epsilon)$ and $\xi_{GL}(\epsilon)$: it is sufficient to notice that $\Delta_{BCS} \sim k_B T_{c0}$ and to replace the reduced temperature ϵ by the reduced field $\widetilde{h}$.

The strong inequalities obtained allow us to assume that at zero temperature, slightly above $H_{c2}(0)$, in the normal phase of type II superconductor, the regions of superconducting coherence are extended to distances much larger than the size of an Abrikosov vortex and such "superconducting puddles" remain coherent for times much longer than τ_{cp}.

Eq. (17) can be also obtained from the uncertainty principle. Indeed, the energy characterizing the proximity to the quantum phase transition is $\Delta E = \hbar\Omega_H - \hbar\Omega_{H_{c2}(0)} \sim \Delta_{BCS}\widetilde{h}$ and it is this value that should be used in the Heisenberg relation instead of $k_B(T - T_{c0})$, as was done in the vicinity of T_{c0}. The spatial coherence scale $\xi_{QF}\left(\widetilde{h}\right)$ can be estimated from the value of τ_{QF} analogously to the case close to T_{c0}. Indeed, two electrons with given phase shift starting from the same point get separated by the distance

$$\xi_{QF}\left(\widetilde{h}\right) \sim (\mathcal{D}\tau_{QF})^{1/2} \sim \xi_{BCS}/\sqrt{\widetilde{h}},,$$

after time τ_{QF}

In order to clarify the physical meaning of τ_{QF} and ξ_{QF}, we note that near the quantum phase transition (QPT) at zero temperature, where $H \to H_{c2}(0)$, the fluctuations of the order parameter $\Delta^{(fl)}(\mathbf{r}, t)$ become highly inhomogeneous, contrary to the situation near T_{c0}. Indeed, slightly below $H_{c2}(0)$ (but in the region where the notion of vortices is still adequate), the spatial distribution of the order parameter reflects the existence of an Abrikosov vortex lattice with average spacing

$$a(H) = \xi_{BCS}/\sqrt{H/H_{c2}(0)} \to \xi_{BCS}\,.$$

Therefore, one expects that close to and above $H_{c2}(0)$ the fluctuation order parameter $\Delta^{(fl)}(\mathbf{r}, t)$ also has a "vortex-like" spatial structure varying on the scale of ξ_{BCS}. This structure is preserved for the lifetime of the "superconducting puddle", which is of the order τ_{QF}.

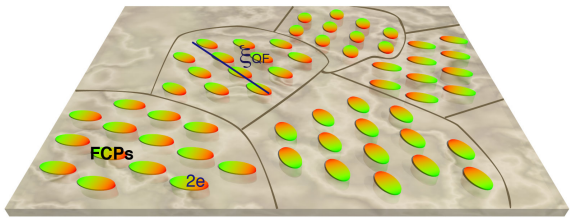

FIG. 6 (Color online) Sketch of the cluster structure of fluctuation Cooper pairs above the upper critical field. After Ref. (Glatz *et al.*, 2011b).

In the language of FCPs one can describe this situation in the following way: A FCP at zero temperature and in a magnetic field close to $H_{c2}(0)$ rotates with the Larmor radius $r_L \sim \xi_{BCS}$, which represents its effective size. During time τ_{QF} two initially selected electrons participate in multiple fluctuating Cooper pairings, maintaining their coherence. The coherence length $\xi_{QF}\left(\widetilde{h}\right) \gg \xi_{BCS}$ is thus a characteristic size of a cluster of such coherently rotating FCPs (which we called above "superconducting puddle"), and τ_{QF} estimates the lifetime of such flickering cluster. One can view the whole system as an ensemble of flickering domains of coherently rotating FCPs, precursors of vortices (see Fig. 6).

Let us return to the scenario of "defragmentation" of the Abrikosov lattice by fluctuations in view of the described qualitative picture of SF in the regime of the QPT. Approaching $H_{c2}(0)$ from below, puddles of fluctuating vortices, which are nothing other than FCPs rotating in the magnetic field, are formed. Their characteristic size is $\xi_{QF}\left(|\widetilde{h}|\right)$, and they flicker with characteristic time $\tau_{QF}\left(|\widetilde{h}|\right)$. At this stage supercurrents still can flow through the sample until these puddles do not break the last percolating superconducting channel. The magnetic field for this to happen determines the value of the second critical field renormalized by QFs: $H^*_{c2}(0) = H_{c2}(0)\left[1 - 2\mathrm{Gi}_{(2)}\ln\left(1/\mathrm{Gi}_{(2)}\right)\right]$ (see Ref. (Larkin and Varlamov, 2009)). Above this field, no supercurrent can flow through the sample anymore – i.e., one reaches the normal state of a type-II superconductor.

Nevertheless, as demonstrated by our estimates above,

the properties of the normal phase are also affected by quantum fluctuations. The fragments of the Abrikosov lattice can be still be observed in the normal phase as can be demonstrated by the following *Gedanken experiment*: Clusters of rotating FCPs (*ex-vortices*) of size $\xi_{\rm QF}$ with some kind of the superconducting order should be found in the background of the normal metal when one takes a picture with exposure time shorter than $\tau_{\rm QF}$. When the exposure time is chosen longer than $\tau_{\rm QF}$ the picture is smeared out and no traces of the Abrikosov vortex state can be found. However, what kind of the order can be detected there is still unclear. It would be very interesting to identify these clusters as remains of the Abrikosov lattice, but more probably is that this is some kind of FCP quantum liquid. Indeed, the presence of structural disorder can result in the formation of a hexatic phase close to $H^*_{c2}(0)$, where the translational invariance no longer exists although it still conserves the orientational order in the vortex positioning. (Halperin and Nelson, 1978; Nelson and Halperin, 1979; Nelson and Kosterlitz, 1977)

2. Manifestation of QF above $H_{c2}(0)$

At zero temperature and fields above $H_{c2}(0)$, the systematics of fluctuation contributions to conductivity change considerably compared to that close to T_{c0}. The collision-free rotation of FCPs (let us recall, that they do not "feel" the presence of elastic impurities, all information related to electron scattering is already included in the effective mass of the Cooper pairs) results in the absence of a direct contribution to the transverse electric transport along the applied electric field (analogously to the suppression of the one-electron conductivity in strong magnetic fields ($\omega_c\tau \gg 1$): $\sigma_{xx}^{(e)} \sim (\omega_c\tau)^{-2}$, see Ref. (Abrikosov, 1988)) and the AL contribution to $\delta\sigma_{(2)}^{(fl)}$ vanishes. The anomalous MT and DOS contributions become zero as well but due to different reasons. Namely, the former vanishes since magnetic fields as large as $H_{c2}(0)$ completely destroy the phase coherence, whereas the latter disappears since the magnetic field suppresses the fluctuation gap in the one-electron spectrum. Therefore the effect of fluctuations on the conductivity at zero temperature is reduced to the renormalization of the one-electron diffusion coefficient. In this region FCPs occupy the lowest Landau level, but all dynamic fluctuations in the frequency interval from 0 to $\Delta_{\rm BCS}$ should be taken into account:

$$\sigma_{xx}^{(\rm DCR)} \sim -\frac{e^2}{\Delta_{\rm BCS}}\int_0^{\Delta_{\rm BCS}} \frac{d\omega}{\widetilde{h}+\frac{\hbar\omega}{\Delta_{\rm BCS}}} \sim -\frac{e^2}{\hbar}\ln\frac{1}{\widetilde{h}}\,. \quad (19)$$

In terms of the above introduced characteristics $\tau_{\rm QF}$ and $\xi_{\rm QF}$ for QF, one can understand the meaning of the QF contributions to different physical values in the vicinity of $H_{c2}(0)$ and derive others, which are essential in this region. For example, one could estimate the direct contribution of the FCPs to conductivity by merely replacing $\tau_{\rm GL} \to \tau_{\rm QF}$ in the classic AL formula, which would give $\sigma_*^{(\rm AL)} \sim \left(e^2/\hbar\right)\tau_{\rm QF}$. Nevertheless, as we already noticed, FCPs at zero temperature cannot drift along the electric field but only rotate around fixed centers. As temperature deviates from zero, the FCP can change their state due to the interaction with the thermal bath, i.e., hopping to an adjacent rotation trajectory along the applied electric field becomes possible. This means that FCPs can participate in longitudinal charge transport as well. This process can be mapped to the paraconductivity of a granular superconductors (Lerner *et al.*, 2008) at temperatures above T_{c0}, where the tunneling of FCPs between grains occurs in two steps: first one electron jumps, then the second follows. The probability of each hopping event is proportional to the inter-grain electron tunneling rate Γ. To conserve the superconducting coherence between both events, the latter should occur in the FCP lifetime $\tau_{\rm GL}$. The probability of FCP tunneling between two grains is determined by the conditional probability of two one-electron hopping events and is proportional to $W_\Gamma = \Gamma^2\tau_{\rm GL}$. Returning to the situation of FCPs above $H_{c2}(0)$, one can identify the tunneling rate by the temperature T, while $\tau_{\rm GL}$ corresponds to $\tau_{\rm QF}$. In order to get a final expression, $\sigma_*^{(\rm AL)}$ should be therefore multiplied by the probability factor $W_{\rm QF} = T^2\tau_{\rm QF}$ of the FCP hopping to a neighboring trajectory:

$$\sigma_{xx}^{(\rm AL)} \sim \frac{e^2}{\hbar}\left(\frac{T}{T_{c0}}\right)^2\frac{1}{\widetilde{h}^2}\,.$$

In order to estimate the contribution of QF to the fluctuation magnetic susceptibility of the SC in the vicinity of $H_{c2}(0)$, one can apply Langevin's formula to a coherent cluster of FCPs and, identify its average size with the rotator radius; one finds

$$\chi_{(2)}^{(\rm AL)} = \frac{e^2 N_{(2)}^{\rm QF}}{c^2 m^*}\left\langle \xi_{\rm QF}^2\left(\widetilde{h}\right)\right\rangle \sim \frac{e^2\Delta_{\rm BCS}}{c^2}\frac{\xi_{\rm BCS}^2}{\widetilde{h}}\,, \quad (20)$$

in complete agreement with the result of Ref. (Galitski and Larkin, 2001a). Here it was assumed that the ratio of the FCP concentration over its mass in the region of quantum fluctuations is $N_{(2)}^{\rm QF}/m^* \sim \Delta_{\rm BCS}$ — with logarithmic accuracy and in analogy to Eq. (7).

Finally, one can reproduce the contribution of QF to the Nernst coefficient. Close to $H_{c2}(0)$, the chemical potential of FCP can be written as $\mu^{(\rm QF)} = -\Delta_{\rm BCS}\,\widetilde{h}$ (in analogy to that one close to T_{c0}). Its temperature derivative differs from zero due to the temperature dependence of $H_{c2}(T)$:

$$d\mu^{(\rm QF)}/dT \sim dH_{c2}(T)/dT \sim -T/\Delta_{\rm BCS}\,. \quad (21)$$

Using the relation between the latter and the Nernst coefficient, it is possible to reproduce one of the results of

Ref. (Serbyn *et al.*, 2009) (with accuracy up to the numerical factor):

$$\nu^{(\mathrm{QF})} \sim \frac{\tau_{\mathrm{QF}}}{m^* c}\left(\frac{d\mu^{(\mathrm{QF})}}{dT}\right) \sim -\frac{k_{\mathrm{B}}\xi^2_{\mathrm{BCS}}}{c\hbar}\left(\frac{k_{\mathrm{B}}T}{\Delta_{\mathrm{BCS}}}\right)\frac{1}{\widetilde{h}}\,. \quad (22)$$

III. BASIC ELEMENTS OF MICROSCOPIC DESCRIPTION OF SF IN MAGNETIC FIELD

Let us begin by recalling the basic ideas of the microscopic description of fluctuations in the normal phase of a superconductor. For this purpose one can employ the formalism of the Matsubara diagrammatic technique. In the BCS theory, the electron–electron attraction leads to the reconstruction of the ground state of the electron system of a normal metal upon approaching the critical temperature from above ($T \to T_{\mathrm{c}0}+0$). Formally, this fact is manifest by the appearance of a pole in the two-particle Green's function

$$\mathcal{L}(p,p',q) = \langle T_\tau[\widetilde{\psi}_{p+q,\sigma}\widetilde{\psi}_{-p,-\sigma}\widetilde{\psi}^+_{p'+q,\sigma'}\widetilde{\psi}^+_{-p',-\sigma'}]\rangle\,, \quad (23)$$

where $\widetilde{\psi}_{p+q,\sigma}$ are electron field operators, T_τ is the time ordering operator, and $4D$ vector notations for electron momentum (or other quantum numbers) are used. The two-particle Green's function can be expressed in terms of the vertex part (Abrikosov *et al.*, 1965). It is this vertex part of the electron–electron interaction in the Cooper channel, $L(\mathbf{q},\Omega_k)$, that is called the *fluctuation propagator* below.

The Dyson equation for $L(\mathbf{q},\Omega_k)$, accounting for the electron–electron attraction in the ladder approximation, is represented graphically in Fig. 7. The solid lines denote the single-particle Green's functions, wavy line corresponds to the fluctuation propagator. The equation can be written analytically as

$$L^{-1}(\mathbf{q},\Omega_k) = -g^{-1} + \langle\langle \Pi(\mathbf{q},\Omega_k)\rangle\rangle_{\mathrm{imp}}\,, \quad (24)$$

where the polarization operator $\Pi(\mathbf{q},\Omega_k)$ is defined as a loop of two single-particle Green's functions in the particle–particle channel[6]:

$$\Pi(\mathbf{q},\Omega_k) = T\sum_{\varepsilon_n}\int \frac{d^3\mathbf{p}}{(2\pi)^3} G(\mathbf{p}+\mathbf{q},\varepsilon_{n+k})G(-\mathbf{p},\varepsilon_{-n})\,. \quad (25)$$

Here $\Omega_k = 2\pi T$ and $\varepsilon_n = (2n+1)\pi T$ are bosonic and fermionic Matsubara frequencies, the symbol $\langle\langle ...\rangle\rangle_{\mathrm{imp}}$ denotes averaging over the position of impurities.

Let us emphasize that the two quantities, $\mathcal{L}(p,p',q)$ and $L(\mathbf{q},\Omega_k)$, are closely connected to each other (Larkin and Varlamov, 2009). Upon integration over the momenta p and p', the former becomes an average of the product of two Fourier components of the superconducting order parameter (Abrikosov *et al.*, 1965):

$$\int dpdp'\,\mathcal{L}(p,p',q) = \frac{1}{g^2}\left\langle \Delta_q \Delta^*_q\right\rangle\,. \quad (26)$$

From the Dyson equation in the ladder approximation for the two-particle Green's function (23) – similar to that one shown in Fig. 7 – it follows that the expression in Eq. (26) can be written in terms of the polarization operator Π and the quantity L:

$$\int dpdp'\,\mathcal{L}(p,p',q) = -\frac{\Pi}{1-g\Pi} = \frac{\Pi}{g}L\,. \quad (27)$$

After analytic continuation to real frequencies, the fluctuation propagator $L(\mathbf{q},i\Omega)$ coincides (up to a constant) with the quantity defined by Eq. (26).

Below we consider a disordered 2D superconductor characterized by the diffusion coefficient $\mathcal{D} = v_{\mathrm{F}}^2\tau/d_e$, placed in a perpendicular magnetic field H at temperatures $T > T_{\mathrm{c}}(H)$. In order to be in the regime of Gaussian superconducting fluctuations, i.e., to avoid the region of critical fluctuations, the temperature must be above a certain value, which for transport properties is determined by the condition $T/T_{\mathrm{c}}(H) - 1 \gg \sqrt{\mathrm{Gi}_{(2)}(H)}$. The Ginzburg-Levanyuk number close to $T_{\mathrm{c}0}$ has the form

$$\mathrm{Gi}_{(2)} = \frac{7\zeta(3)}{32\pi^3}\frac{1}{\rho_e T_{\mathrm{c}0}\xi^2_{(2)}}\,, \quad (28)$$

with a slight dependence on the applied magnetic field away from $T_{\mathrm{c}0}$, see Ref. (Larkin and Varlamov, 2009). Here ρ_e is the one-electron density of states. The Ginzburg-Levanyuk parameter is of the order of $(p_{\mathrm{F}}^2 ls)^{-1}$ on both ends of the line $H_{\mathrm{c}2}(T)$, and can reach values of up to 10^{-2}. The constant $\xi_{(2)}$, already introduced in Eq. (4), coincides with the BCS coherence length of Cooper pairs at zero temperature, up to a numerical factor. In the case of a superconductor with impurities, it is related to the electron diffusion coefficient: $\xi^2 = \frac{\pi\mathcal{D}}{8T_{\mathrm{c}0}}$.

We assume for the temperature $T \ll \min\{\tau^{-1},\omega_{\mathrm{D}}\}$ in order to stay both in the diffusive regime of electron scattering and in the framework of the BCS model (τ is the electron elastic scattering time at impurities). The magnitude of the magnetic field is limited by two conditions: (i) remain below the regime of Shubnikov-de Haas oscillations, $\Omega_H\tau \lesssim 1 \Longleftrightarrow H \lesssim (T_{\mathrm{c}0}\tau)^{-1} H_{\mathrm{c}2}(0)$, and (ii)

FIG. 7 (Color online) The Dyson equation for the fluctuation propagator (wavy line) in the ladder approximation. Solid lines represent one-electron Green's functions, circles represent the electron–electron interaction, and the triangle corresponds to the Cooperon (see Fig. 8).

[6] In the following we use units with $\hbar = k_{\mathrm{B}} = c = 1$.

stay below the Clogston limit, $H \lesssim (\varepsilon_{\rm F}\tau)\, H_{c2}(0)$, i.e., $H/H_{c2}(0) \ll \min\left\{(T_{c0}\tau)^{-1}, \varepsilon_{\rm F}\tau\right\}$.

The single-electron state in magnetic field in presence of impurity scattering can be described by the Green's function written in the form of a series over Landau state eigenfunctions $\varphi_k\left(x - l_{\rm H}^2 p_y\right)$:

$$G(x,x',p_y,p_z,\varepsilon_l) = \sum_k \frac{\varphi_k(x-\ell_{\rm H}^2 p_y)\varphi_k^*(x'-\ell_{\rm H}^2 p_y)}{i\widetilde{\varepsilon}_l - \xi\,(k,p_z)}\,, \tag{29}$$

where $\widetilde{\varepsilon}_l = \varepsilon_l + \frac{1}{2\tau}{\rm sign}\varepsilon_l$ is the fermionic Matsubara frequency, $\xi(k,p_z) = \omega_c(k+1/2)+\xi_z(p_z)$ is the quasiparticle energy at the corresponding Landau level ($\omega_{\rm c}$ is its cyclotron frequency), and $\xi_z(p_z)$ is its part related to the motion along the direction of the magnetic field. The latter will be omitted in the discussion of the properties of 2D superconductors. For the energy-independent width of the Landau levels, a closed expression for the Green's function can be obtained by a straightforward summation over quantum numbers, or by using Schwinger's proper time method (see, for example, Ref. (Gusynin *et al.*, 1995)).

In addition to the appearance of the imaginary part of the self-energy in the one-particle Green's function, see Eq. (29), the effect of coherent electron scattering on impurities results in the renormalization of the vertex part in the particle–particle channel. It is determined by the Dyson equation in ladder approximation (see Fig. 8).

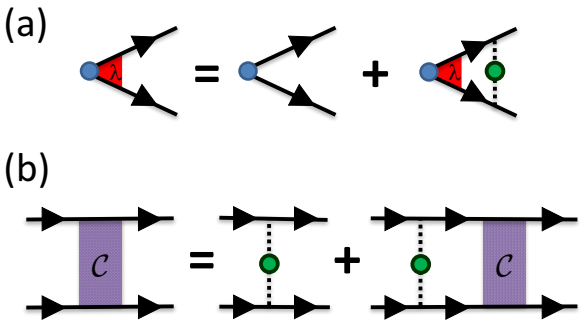

FIG. 8 (Color online) (a) Dyson equation for Cooperon, i.e. the vertex that accounts for the result of averaging over elastic impurity scattering of electrons in the ladder approximation. Solid lines correspond to bare one-electron Green's functions. Dashed line is associated with an impurity correlator, $\langle U^2\rangle = 1/(2\pi\rho_e\tau)$. (b) Analogous Dyson equation for the four-leg Cooperon in the ladder approximation.

The details of the derivations can be found in Ref. (Larkin and Varlamov, 2009); here we only present the results necessary for further discussions. The Cooperon shown in Fig. 8 has the following form in Landau representation:

$$\lambda_n(\varepsilon_1,\varepsilon_2) = \frac{\tau^{-1}\theta(-\varepsilon_1\varepsilon_2)}{|\varepsilon_1-\varepsilon_2| + \Omega_H(n+1/2) + \tau_\varphi^{-1}}\,, \tag{30}$$

where n is the quantum number of the Landau state of Cooper pairs , $\theta(x)$ is the Heavyside step-function, ε_1 and ε_2 are the fermionic frequencies, and τ_φ is the phase-breaking time of electron scattering. In the process of impurity averaging, one also encounters the corresponding four-leg vertex, which differs from Eq. (30) only by the factor $\langle U^2\rangle$:

$$C_n(\varepsilon_1,\varepsilon_2) = \frac{1}{2\pi\rho_e\tau}\frac{\tau^{-1}\theta(-\varepsilon_1\varepsilon_2)}{|\varepsilon_1-\varepsilon_2| + \Omega_H(n+1/2) + \tau_\varphi^{-1}}\,. \tag{31}$$

Finally, the expression for the fluctuation propagator in this representation takes the form:

$$L_n^{-1}(\Omega_k) = \tag{32}$$
$$-\rho_e\left[\ln\frac{T}{T_{c0}} + \psi\left(\frac{1}{2}+\frac{|\Omega_k|+\Omega_H(n+\frac{1}{2})}{4\pi T}\right) - \psi\left(\frac{1}{2}\right)\right].$$

An important characteristic property of Eqs. (30)–(32) is that they are valid in a large region of the phase diagram of a superconductor above the line $H_{c2}(T)$ for magnetic fields $H/H_{c2}(0) \ll \min\left\{(T_{c0}\tau)^{-1}, \varepsilon_{\rm F}\tau\right\}$, temperatures $T \ll \min\{\tau^{-1},\omega_{\rm D}\}$, frequencies $|\Omega_k| \ll \tau^{-1}$, and Landau levels with $n \ll (T_{c0}\tau)^{-1}$.

In the following, it is convenient to use the dimensionless temperature and magnetic field

$$t = \frac{T}{T_{c0}}\,, \quad h = \frac{H}{\widetilde{H}_{c2}(0)}.$$

Since it is more convenient, the latter is normalized by the value of the second critical field obtained by linear extrapolation of its temperature dependence near T_{c0}:

$$\widetilde{H}_{c2}(0) = \frac{\Phi_0}{2\pi\xi^2}\,,$$

where $\Phi_0 = \pi/e$ is the magnetic flux quantum. The magnetic field $\widetilde{H}_{c2}(0)$ is $8\gamma_{\rm E}/\pi^2 = 1.45$ times larger than the true second critical field $H_{c2}(0)$:

$$h = \frac{H}{\widetilde{H}_{c2}(0)} = \frac{\pi^2}{8\gamma_{\rm E}}\frac{H}{H_{c2}(0)} = 0.69\frac{H}{H_{c2}(0)}\,.$$

In these dimensionless units, the fluctuation propagator (32) acquires the form

$$L_n^{-1}(\Omega_k) = -\rho_e\mathcal{E}_n(t,h,|k|)\,.$$

The function

$$\mathcal{E}_n(t,h,x) \equiv \ln t + \psi\left[\frac{x+1}{2} + \frac{4h}{\pi^2 t}\left(n+\frac{1}{2}\right)\right] - \psi\left(\frac{1}{2}\right) \tag{33}$$

and its derivatives with respect to the argument x,

$$\mathcal{E}_n^{(n)}(t,h,x) \equiv \frac{\partial^n}{\partial x^n}\mathcal{E}_n(t,h,x)$$
$$= 2^{-n}\psi^{(n)}\left[\frac{1+x}{2} + \frac{4h}{\pi^2 t}\left(n+\frac{1}{2}\right)\right], \tag{34}$$

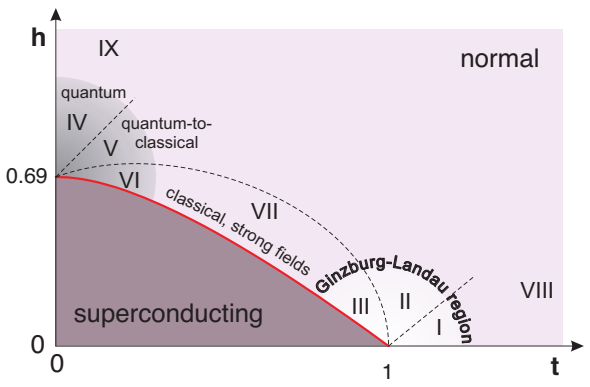

domain	t and h range	description
I	$h = 0,\ \epsilon \ll 1$	zero field, near T_{c0}
II	$\epsilon \ll h \ll 1$	near T_{c0}, above the mirror reflected h_{c2}-line
III	$h - h_{c2}(t) \ll 1,\ \epsilon \ll 1$	near h_{c2}-line
I – III	$h \ll 1,\ \epsilon \ll 1$	GL region
IV	$t \ll \widetilde{h}$	region of quantum fluctuations
V	$t^2/\ln(1/t) \ll \tilde{h} \ll t \ll 1$	quantum-to-classical
VI	$\tilde{h} \ll t^2/\ln(1/t) \ll 1$	classical, near $h_{c2}(t \ll 1)$
VII	$\widetilde{h} \lesssim t \ll h_{c2}(t)$	classical, strong fields
VIII	$\ln t \gtrsim 1, h \ll t$	high temperatures
IX	$h \gg \max\{1, t\}$	high magnetic fields

FIG. 9 *Left:* Schematic representation of the regions of different behavior of superconducting fluctuations in the h-t diagram, following Ref. (Glatz *et al.*, 2011a). *Right:* Classification of domains in terms of different limits for t and h. Here $\epsilon \equiv \ln t$, $\widetilde{h} = (H - H_{c2}(T))/H_{c2}(T); H > H_{c2}(T)$.

plays an important role for the fluctuation contributions discussed in the following sections, as well as its derivatives with respect to the magnetic field:

$$\left(\frac{\partial \mathcal{E}_n}{\partial h}\right) = \frac{8}{\pi^2 t}\left(n+\frac{1}{2}\right)\mathcal{E}_n'\,;\left(\frac{\partial^2 \mathcal{E}_n}{\partial h^2}\right) = \left[\frac{8}{\pi^2 t}\left(n+\frac{1}{2}\right)\right]^2 \mathcal{E}_n''\,. \tag{35}$$

Throughout the review we present asymptotic expressions of fluctuation contributions in nine different domains of the phase diagram, shown and described in Fig. 9. Domains I–III encompass the region of temperatures close to T_{c0} and fields $h \ll 1$, corresponding to the regime of classical thermal fluctuations accessible in the GL approach (with some restrictions for fluctuation diamagnetism). The vicinity of the quantum phase transition at $H = H_{c2}(0)$ is covered by the domains IV–VI: quantum fluctuations in the domain IV gradually acquire thermal nature in domain VI, despite the low temperature ($t \ll 1$). The crossover between the regimes of quantum and classical fluctuations occurs in region V, where $h \sim t$. This part of the phase diagram can be described microscopically in the approximation of the lowest Landau level for the FCP motion. This approach can be extended along the line $H_{c2}(T)$ (domain VII). The high temperature region VIII, $T_{c0} \ll T$, having also relatively weak fields, $H \ll H_{c2}(0)$, accounts for short wave and dynamic fluctuations. The same is true in the strong magnetic field domain IX.

IV. FLUCTUATION DIAMAGNETISM

A. General expression for magnetic susceptibility

The qualitative estimate of the fluctuation diamagnetic susceptibility in section II demonstrates that for $2D$ systems, even at high temperatures $T \gg T_{c0}$, it noticeably exceeds the one-electron diamagnetic contribution (Aslamazov and Larkin, 1974; Bulaevskii, 1974; Maki, 1973).

In order to recognize the role of fluctuation diamagnetism in the entire phase diagram of a superconductor beyond the line $H_{c2}(T)$, let us start from the first order fluctuation correction to the free energy per unit square, graphically represented by the diagram shown in Fig. 10. After integration over electronic momenta and summation over corresponding fermionic frequencies, it can be written in the form (Galitski and Larkin, 2001a; Larkin and Varlamov, 2009)

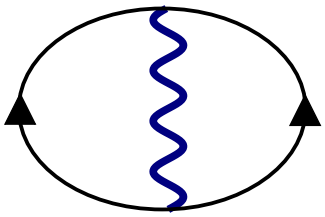

FIG. 10 (Color online) The first order fluctuation correction to the free energy. The wavy line represents the fluctuation propagator, solid lines with arrows are impurity averaged normal state Green's functions.

$$F^{(\mathrm{fl})}(H,T) = -T\sum_{\Omega_k}\frac{H}{s\Phi_0}\sum_{m=0}\ln\mathcal{L}_m^{-1}(\Omega_k)\,, \tag{36}$$

where s is the film thickness. Eq. (36) can be rewritten in dimensionless variables with accuracy up to an irrelevant constant:

$$F^{(\mathrm{fl})}(h,t) = -\frac{T_{c0}}{2\pi s\xi^2}t\sum_{\Omega_k}h\sum_{m=0}\ln\mathcal{E}_m(t,h,|k|)\,. \tag{37}$$

The fluctuation part of the bulk magnetic susceptibility is determined by the negative second derivative of the free energy with respect to magnetic field:

$$\chi^{(\mathrm{fl})}(h,t) = -\frac{32e^2\xi^2 T_{c0}}{\pi^3 s}\sum_{\Omega_k}\sum_{m=0}^{M_t}\left(m+\frac{1}{2}\right)\left[\frac{\mathcal{E}'_m}{\mathcal{E}_m(t,h,|k|)}+\frac{4h}{\pi^2 t}\left(m+\frac{1}{2}\right)\frac{\mathcal{E}''_m\mathcal{E}_m-(\mathcal{E}'_m)^2}{\mathcal{E}_m^2(t,h,|k|)}\right], \tag{38}$$

with the cutoff $M_t = 1/(tT_{c0}\tau)$.

B. Asymptotic analysis

We begin the analysis of the general Eq. (38) with the limit of low temperatures, moving along the line $H_{c2}(T)$ from the point of the quantum phase transition ($T = 0$) to higher temperatures, followed by the limits of high temperatures and high fields away from the $H_{c2}(T)$ line.

1. Region close to the line $H_{c2}(T)$ (domains IV-VII)

In the case of low temperatures, $t \ll h_{c2}(t) = H_{c2}(T)/\widetilde{H}_{c2}(0)$ one can use the lowest Landau level (LLL) approximation, i.e., restrict the summation over Landau levels in Eq. (38) by the lowest one with $m = 0$. Along the line $h_{c2}(t)$, i.e. when $\widetilde{h}(t) \ll 1$, the function $\mathcal{E}_0$, Eq. (33), acquires the simple form

$$\mathcal{E}_0(t,h,|k|) = \widetilde{h}(t) + \frac{\pi^2 t|k|}{4h_{c2}(t)}\,. \tag{39}$$

The limit of low temperatures, also allows to replace the sum over Matsubara frequencies by an integral, which was calculated in Ref. (Galitski and Larkin, 2001b):

$$\chi^{(\mathrm{fl})}(t,h) = \frac{12\chi_{\mathrm{L}}l}{s}\left(\frac{8\gamma_{\mathrm{E}}}{\pi^2}\right)^2 h_{c2}^2(t)\left[\frac{1}{2\gamma_{\mathrm{E}}t}\psi'\left(\frac{\widetilde{h}}{2\gamma_{\mathrm{E}}t}\right)-\frac{\gamma_{\mathrm{E}}t}{\widetilde{h}^2}\right], \tag{40}$$

where $l = v_{\mathrm{F}}\tau$ is the electron mean free path, and $\chi_{\mathrm{L}} = e^2 v_{\mathrm{F}}/12\pi^2$ is the absolute value of Landau diamagnetic susceptibility ($\gamma_{\mathrm{E}} = e^{\gamma_e}$, where γ_e is the Euler-Mascheroni constant).

Using the asymptotic expression for the ψ-function, one obtains the result for the fluctuation magnetic susceptibility close to $H_{c2}(0)$, both in the regimes of quantum and thermal fluctuations (domains `IV` and `VI`, respectively):

$$\chi^{(\mathrm{fl})}(t,h) = 12\chi_{\mathrm{L}}\left(\frac{l}{s}\right)\begin{cases}\frac{1}{\widetilde{h}}, & t \ll \widetilde{h}\,,\\ \frac{\gamma_{\mathrm{E}}t}{\widetilde{h}^2}, & \widetilde{h} \ll t\,.\end{cases} \tag{41}$$

In the region of quantum fluctuations, $\chi^{(\mathrm{fl})}(t \ll h)$ is temperature independent and describes the diamagnetism generated by clusters of rotating FCPs. Its positive sign and strong dependence of $\widetilde{h}$ indicates a rapid decrease of this fluctuation effect as the distance from the critical field increases. Let us stress that the microscopically obtained Eq. (40) is in complete agreement with the above evaluation of the contribution of quantum fluctuations to the magnetic susceptibility, Eq. (8).

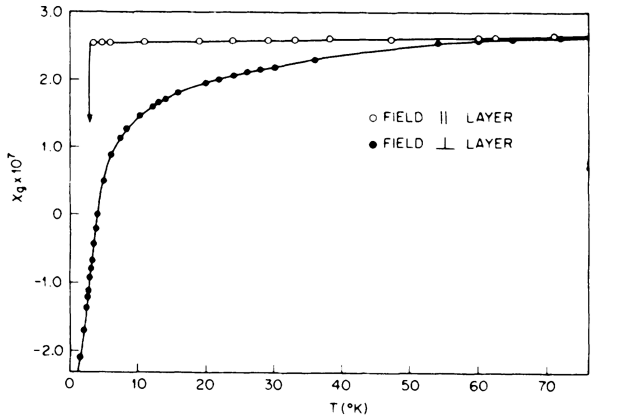

FIG. 11 Magnetic susceptibility per gram of $TaS_2(\mathrm{pyridine})_{1/2}$ as a function of temperature (Geballe *et al.*, 1971). $\chi_\perp(\chi_\parallel)$ was measured with the applied field perpendicular(parallel) to the layers. The points above 5K were taken from several samples and field values between 1 and 8 kOe. No magnetic field dependence within experimental errors (size of the dots) was observed. *Reprinted figure with permission from (Geballe* et al., *1971). Copyright (1971) by the American Physical Society.*

Taking the factor $h_{c2}(t)$ in Eq. (40) in account, allows to obtain the diamagnetic susceptibility in domain `VII`:

$$\chi^{(\mathrm{fl})}(\widetilde{h} \ll t \lesssim h_{c2}(t)) = \frac{3\cdot 2^9\chi_{\mathrm{L}}\gamma_{\mathrm{E}}^3}{\pi^4}h_{c2}^2(t)\left(\frac{l}{s}\right)\frac{t}{\widetilde{h}^2}\,. \tag{42}$$

One can see that the fluctuating contribution to magnetic susceptibility remains positive along the line $H_{c2}(T)$ and exceeds the conventional Landau diamagnetism in a very large region of the phase diagram.

2. Limit of weak fields (domains `I`–`III` and `VIII`)

Moving along the line $H_{c2}(T)$ to the region of weak fields, one finds that the summation over Landau levels in the general formula for fluctuation diamagnetic susceptibility, Eq. (38), leads to a divergent result. The problem can be resolved in the case of weak fields by separating the magnetic field-dependent part of the free energy from the temperature background (the meaning of 'weak fields' depends on the domain of the phase diagram under consideration). In order to do this, one can

apply the Euler-Maclaurin formula

$$\lambda \sum_{m=0}^{\infty} f\left[\lambda\left(m+\frac{1}{2}\right)\right] = \lambda \int_{-\frac{1}{2}}^{\infty} f\left[\lambda\left(m+\frac{1}{2}\right)\right] dm - \frac{\lambda^2}{24}\left[f'(\infty) - f'(0)\right]$$

to Eq. (37), which gives

$$\frac{4h}{\pi^2 t}\sum_{m=0}^{\infty} \ln \mathcal{E}_m = \int_0^{\infty} \ln \mathcal{E}_\xi \, d\xi - \frac{1}{12}\left(\frac{4h}{\pi^2 t}\right)^2 \frac{\mathcal{E}_0'(t,0,|k|)}{\mathcal{E}_0(t,0,|k|)}\,.$$

The first term does not dependent on magnetic field, and one finds for the diamagnetic susceptibility in the approximation of weak fields

$$\chi^{(\mathrm{fl})}(h,t) = -\chi_{\mathrm{L}}\left(\frac{l}{s}\right)\sum_{\Omega_k}\frac{\mathcal{E}_0'\,(t,0,|k|)}{\mathcal{E}_0\,(t,0,|k|)}\,. \tag{43}$$

a. Vicinity of T_{c0} (domains I–III) In the case of temperatures close to T_{c0} and small magnetic fields, $h \ll \epsilon \ll 1$ (domain I of the phase diagram), the zero Matsubara frequency in Eq. (43) gives the most singular contribution, leading to the following asymptotic behavior:

$$\chi^{(\mathrm{fl})}(h \ll \epsilon) = -\frac{\pi^2}{4}\chi_{\mathrm{L}}\left(\frac{l}{s}\right)\frac{1}{\epsilon}\,. \tag{44}$$

At higher magnetic fields, when h exceeds the reduced temperature ϵ, Eq. (43) becomes no longer applicable. Yet, the GL approach (Larkin and Varlamov, 2009), valid in the vicinity of T_{c0}, allows to obtain an expression for the fluctuation susceptibility applicable in the vicinity of the critical temperature (domains I–III):

$$\chi^{(\mathrm{fl})}(\epsilon, h \ll 1) = -\frac{3\pi^2}{4}\chi_{\mathrm{L}}\left(\frac{l}{s}\right)\frac{\epsilon}{h^2}\left[1-\frac{\epsilon}{2h}\psi'\left(\frac{1}{2}+\frac{\epsilon}{2h}\right)\right]. \tag{45}$$

Its asymptotic expression in the weak-field domain I reproduces Eq. (44). At higher fields, in domain II the expansion of Eq. (45) gives

$$\chi^{(\mathrm{fl})}(\epsilon \ll h \ll 1) = -\frac{3\pi^2}{4}\chi_{\mathrm{L}}\left(\frac{l}{s}\right)\frac{\epsilon}{h^2}\,. \tag{46}$$

Finally, in domain III one obtains

$$\chi^{(\mathrm{fl})}(\epsilon + h \ll 1) = \frac{3\pi^2}{2}\chi_{\mathrm{L}}\left(\frac{l}{s}\right)\frac{h}{(\epsilon+h)^2}\,. \tag{47}$$

One can see that the magnetic susceptibility changes its sign between domains II and III as the line $H_{c2}(T)$ is approached.

Eq. (47) can be rewritten as the function of the reduced field $\widetilde{h}$, which characterizes the distance from the line $h_{c2}(t)$. Indeed, the value $\epsilon + h$ is nothing else, but the reduced temperature $\epsilon(H) = (T - T_c(H))/T_c(H)$, with respect to $T_c(H)$. The latter can be expressed in terms of the reduced field: $\epsilon(H) = \tilde{h}/h_{c2}(t)$. It is therefore evident that Eq. (47) at $t \sim h_{c2}(t)$ (middle of the domain VII) is in full agreement with Eq. (42), up to a numerical factor. The latter was obtained in the LLL approximation, i.e., using a set of approximations very different from the GL approach.

b. High temperatures (domain VIII) In the domain of high temperatures, $T_{c0} \ll T \ll \tau^{-1}$, one can replace the summation over Matsubara frequencies by an integration. In the 2D case, the integration in Eq. (43) can be performed exactly:

$$\chi^{(\mathrm{fl})}_{(2)}(T,H) = -2\chi_{\mathrm{L}}\left(\frac{l}{s}\right)\left(\ln\ln\frac{1}{T_{c0}\tau} - \ln\ln\frac{T}{T_{c0}}\right). \tag{48}$$

Here the weak double logarithmic ultraviolet divergence of Eq. (43) was cut off by the applicability limit of the dirty superconductor approximation, $\Omega_k \sim \tau^{-1}$. This expression was first obtained by Maki and Bulaevski (Bulaevskii, 1974; Maki, 1973). The extremely slow decrease of the fluctuation diamagnetism explains the long tales in the diamagnetic susceptibility observed in intercalated dichalcogenides TaS_2 and $NbSe_2$ in the early 1970s (Geballe *et al.*, 1971; Morris and Coleman, 1973) (see Fig. 11). The weak magnetic field limit is not restrictive here: $H \ll H_{c2}(0)\ln(T/T_{c0})$. In the 3D case, the ultraviolet divergence is even stronger, yet it can be eliminated by subtracting the corresponding quantity taken at $T \sim T_{c0}$. This yields

$$\chi^{(\mathrm{fl})}_{(3)}(T) = -2\chi_{\mathrm{L}}\frac{\sqrt{T\tau}}{\ln(T/T_c)}\,. \tag{49}$$

3. Limit of very strong fields (domain IX)

The remaining region of very strong fields is the domain of dynamic and short-wavelength fluctuations. It is beyond the limits of applicability of all three approximations used above: neither the GL approach nor the LLL approximation, nor the Euler-Maclaurin weak-field expansion is valid there. Following Maki and Takayama (Maki and Takayama, 1971), Lev Bulaevskii, Ref. (Bulaevskii, 1974), transformed the sum over Matsubara frequencies into the contour integral and then applied the generalized Euler-Maclaurin transformation for the summation over Landau levels valid for arbitrary fields. As a result, he obtained the expression for fluctuation magnetization in strong fields $H > H_{c2}(0)$ at zero temperature:

$$M(h,T=0)=-\frac{8\gamma_{\rm E}e^2\mathcal{D}H_{c2}(0)}{\pi^4 s}\,h\left[\ln\frac{\ln\frac{1}{T_{c0}\tau}}{\ln\left(\frac{8\gamma_{\rm E}}{\pi^2}h\right)}-\frac{2}{\pi}\int_0^\infty dx\frac{\ln\left(1-e^{-\pi x}\right)\left[\ln\left(\frac{8\gamma_{\rm E}}{\pi^2}h\right)+\frac{1}{2}\ln\left(1+x^2\right)\right]}{\left[\ln\left(\frac{8\gamma_{\rm E}}{\pi^2}h\right)+\frac{1}{2}\ln\left(1+x^2\right)\right]^2+\arctan^2 x}\right]. \tag{50}$$

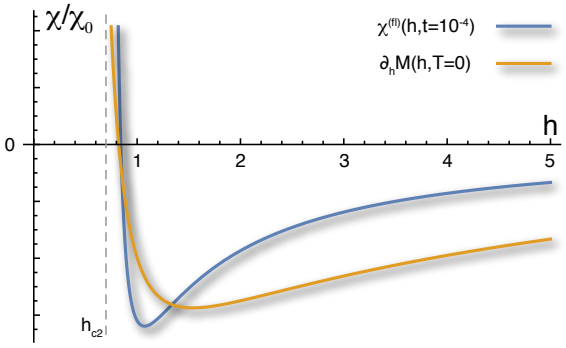

FIG. 12 (Color online) Fluctuation contribution to susceptibility of a 2D impure superconductor at low temperatures as a function of magnetic field above h_{c2}. The solid, blue [darker] line shows the behavior of Eq. (38) at $t=10^{-4}$, while the solid orange [lighter] line the approximate expression at zero temperature obtained from (50) as $\partial_h M(h,T=0)$. Both curves show similar asymptotic behavior in domains IV and IX. The units of χ are arbitrary.

One can see that when magnetic field approaches $H_{c2}(0)$, the corresponding magnetic susceptibility is determined by the first term in Eq. (50), it is positive, and reproduces the first line of Eq. (41), obtained in the LLL approximation. Domain IX corresponds to the fields $H_{c2}(0)\ll H\ll(e\mathcal{D}\tau)^{-1}$, where $\ln h\gg 1$. Here the magnetic susceptibility changes its sign [7]:

$$\chi^{(\rm fl)}(h,0)=-\frac{e^2\mathcal{D}}{\pi^2 s}\left[\ln\ln\frac{1}{T_{c0}\tau}-\ln\ln h\right]. \tag{51}$$

A comparison of the susceptibilities obtained from Bulaevski's approximation (50) and the full expression (38) at very low temperatures is shown in Figure 12.

It is necessary to note that Maki *et al.* (Maki, 1973; Maki and Takayama, 1971) already obtained the large, weakly temperature dependent, divergent contribution to the fluctuation magnetization in weak fields and they identified it with zero-point oscillations of the FCPs. Bulaevskii demonstrated its occurrence at zero temperature above the second critical field. The question whether such oscillations exist, generated lively discussions in the 1970s; today their existence is commonly accepted, they are quantum fluctuations which appear when the system approaches the quantum phase transition.

The above consideration demonstrates that quantum fluctuations give a noticeable contribution to the diamagnetism of two-dimensional impure superconductor placed in perpendicular field in a very wide range of magnetic fields and temperatures.

[7] With logarithmic accuracy we omitted the factor $8\gamma_{\rm E}/\pi^2=1.45$ under the logarithm in the high-field asymptotic expressions.

domain	$\chi^{(\rm fl)}_{(2)}/\left(\chi_{\rm L}\frac{l}{s}\right)$
I–III	$-\frac{3\pi^2}{4}\frac{\epsilon}{h^2}\left[1-\frac{\epsilon}{2h}\psi'\left(\frac{1}{2}+\frac{\epsilon}{2h}\right)\right]$ $=\frac{\pi^2}{4}\begin{cases}-\frac{1}{\epsilon}, & \text{I}\\ -\frac{3\epsilon}{h^2}, & \text{II}\\ \frac{6h}{(\epsilon+h)^2}, & \text{III}\end{cases}$
IV–VII	$12\left(\frac{8\gamma_{\rm E}}{\pi^2}\right)^2 h_{c2}^2(t)\left[\frac{1}{2\gamma_{\rm E}t}\psi'\left(\frac{\tilde{h}}{2\gamma_{\rm E}t}\right)-\frac{\gamma_{\rm E}t}{\tilde{h}^2}\right]$ $=12\begin{cases}\frac{1}{\tilde{h}}, & \text{IV}\\ \frac{\gamma_{\rm E}t}{\tilde{h}^2}, & \text{VI}\\ 0.252\,h_{c2}^2(t)\frac{t}{\tilde{h}^2}, & \text{VII}\end{cases}$
VIII	$-2\left(\ln\ln\frac{1}{T_{c0}\tau}-\ln\ln t\right)$
IX	$-2\left(\ln\ln\frac{1}{T_{c0}\tau}-\ln\ln h\right)$

TABLE III Asymptotic expressions in the different domains, shown in Fig. 9.

C. Fluctuation spectroscopy: analysis of the isothermal magnetization curves

As an example of successful application of fluctuation spectroscopy in characterization of specific superconducting systems, one can cite the Ref. (Bernardi *et al.*, 2006), in which the authors addressed a particular case of the fluctuation contribution to the diamagnetic response of an assembly of lead nano-particles of size d, smaller than the coherence length, placed in an insulating matrix at above the superconducting critical temperature.

For the fluctuation magnetization of an effectively 0D-granule in the GL region, $\mathrm{Gi}_{(0)}\lesssim\epsilon$, one can write the expression valid for a wide range of magnetic fields, $H\ll H_{c2}(0)$ (Larkin and Varlamov, 2009):

$$M_{(0)}(\epsilon,H)=-\frac{6\pi T\xi^2}{5\Phi_0^2 d}\frac{H}{\left(\epsilon+\frac{\pi^2\xi^2}{10\Phi_0^2}H^2d^2\right)}. \tag{52}$$

In accordance with Eq. (52), the fluctuation magnetization turns out to be negative and linear in magnetic field up to some crossover temperature-dependent upper critical field of the granule, $H_{c2(0)}(\epsilon)\sim\frac{\Phi_0}{d\xi(\epsilon)}\sim\frac{\xi}{d}H_{c2}(0)\sqrt{\epsilon}$, at which it reaches a minimum. At higher fields, $H_{c2(0)}(\epsilon)\lesssim H\ll H_{c2}(0)$, the fluctuation magnetization of the 0D granule is inversely proportional to the magnetic field.

In Fig. 13, we present isothermal magnetization curves from Ref. (Lascialfari and Rigamonti, 2017). The average

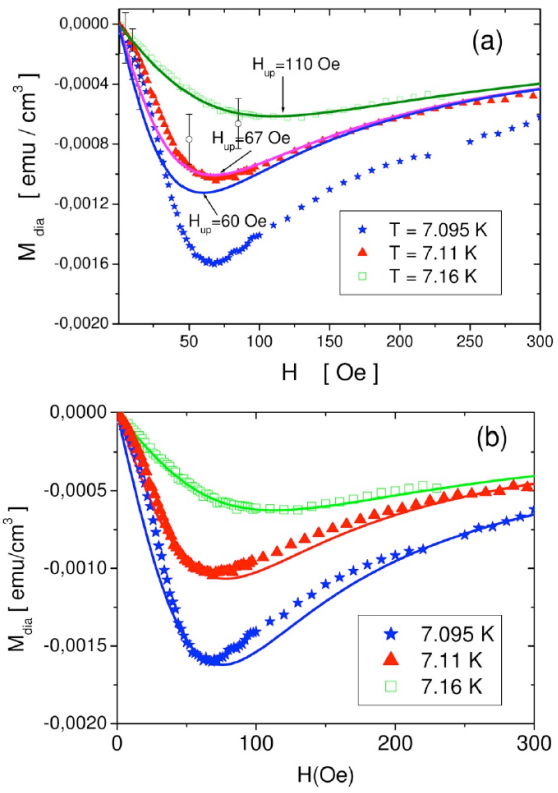

FIG. 13 (Color online) Magnetization curves above $T_c(0) = 7.09 \pm 0.005^\circ K$, for the Pb sample with average particles diameters $d = 75\ nm$. In panel (a) the experimental data are compared to the theoretical curves obtained in the GL quadratic approximation (see Eq. (52)). In the panel (b) the same experimental data are compared with the predictions done using the complete GL functional. *Reprinted with permission by author, see Ref. (Lascialfari and Rigamonti, 2017).*

size of the particles, calculated based on the analysis of the up-turn field, was found to be in excellent agreement with direct experimental measurements. In the immediate vicinity of the transition, the authors have observed a deviation of the experimental curves from the predictions of the quadratic GL approximation. Yet, this data (even the curve corresponding to $T = 7.095$K) turned out to be in a good agreement with the curves of fluctuation magnetization obtained using the complete GL functional including the fourth order term (see Ref. (Larkin and Varlamov, 2009)).

V. FLUCTUATION CONDUCTIVITY

A. General expression for fluctuation conductivity

In the standard Kubo formalism, the electric current is related to the vector potential by means of the electromagnetic response operator:

$$j_\alpha = -\int Q_{\alpha\gamma}(\mathbf{r},\mathbf{r}',t,t')\mathbf{A}_\gamma(\mathbf{r}',t')d\mathbf{r}'dt' \,. \qquad (53)$$

In the framework of the diagrammatic technique at finite temperatures, the latter is graphically represented by a loop diagram comprised of two electron Green's functions connected through electromagnetic vertices.

Taking fluctuation pairing into account, leads to a renormalization of the Green's functions and the vertices by interactions in the Cooper channel (see Fig. 7), with additional averaging over impurity positions. This results in ten leading-order corrections to the electromagnetic response operator shown in Fig. 14, each containing a small parameter of the fluctuation theory (Ginzburg-Levanyuk number, Eq. (28)) as a prefactor.

The fluctuation correction to conductivity is determined by the imaginary part of the sum of all these diagrams:

$$\sigma^{(\mathrm{fl})}(T,H) = -\lim_{\omega\to 0}\frac{\mathrm{Im}Q^{(\mathrm{fl})}(\omega,T,H)}{\omega} \,. \qquad (54)$$

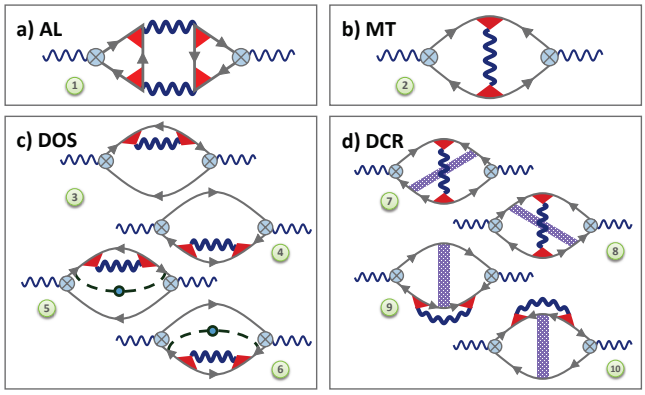

FIG. 14 (Color online) Feynman diagrams for the leading-order contributions to the electromagnetic response operator. Wavy lines correspond to fluctuation propagators (Eq. (32)), solid lines with arrows represent impurity-averaged normal state electron Green's functions, crossed circles are electric field vertices, dashed lines with a circle represent additional impurity renormalizations, and triangles and dotted rectangles are impurity ladders accounting for the electron scattering at impurities (Cooperons, see Eqs. (30), (31)). After Ref. (Glatz *et al.*, 2011a).

As mentioned above, the effect of SF on conductivity close to the superconducting critical temperature T_{c0} is typically discussed in terms of three major contributions: the Aslamazov-Larkin (AL) process, corresponding to the opening of a new channel for the charge transfer (Aslamasov and Larkin, 1968), the anomalous Maki-Thompson (MT) process, which describes single-particle quantum interference at impurities in the presence of SFs (Maki, 1968; Thompson, 1970), and the change of

the single-particle DOS due to their involvement in the pairing of FCPs (Dorin *et al.*, 1993; Ioffe *et al.*, 1993). The AL and MT processes result in the appearance of positive singular contributions to conductivity (diagrams 1 and 2 in Fig. 14). In contrast, the DOS process depletes single-particle excitations at the Fermi level and leads to a decrease of the Drude conductivity (diagrams 3–6 in Fig. 14). The latter contribution is less singular in temperature than the first two and can compete with them only if the AL and MT processes are suppressed (for example in the case of c-axis transport in layered superconductors). Diagrams 7–10 represents the renormalization of the diffusion coefficient (*DCR* diagrams) due to the presence of fluctuations, which are nonsingular close to T_{c0} in two and three dimensions.

These results were first obtained for the vicinity of T_{c0} and later generalized to temperatures far from the transition, see Refs. (Altshuler *et al.*, 1983; Aslamasov and Varlamov, 1980; Larkin, 1980)), and to high magnetic fields, see Ref. (Lopes dos Santos and Abrahams, 1985). In 2D superconductors the slowly (double-logarithmically) decreasing contributions described by diagrams 3–10 starts to dominate far from the critical temperature ($T \gg T_{c0}$). Later, the effect of quantum fluctuations on conductivity was studied. In Refs. ((Beloborodov and Efetov, 1999; Beloborodov *et al.*, 2000)) it was found that in granular superconductors at very low temperatures and close to $H_{c2}(0)$, the singular AL contribution decays as T^2, while the fluctuation suppression of the quasiparticle DOS at zero temperature results in a negative contribution to conductivity, which grows logarithmically in magnitude for $H \to H_{c2}(0)$. In subsection X.D, we come back to the case of granular superconductors.

The effects of quantum fluctuations on the magnetoconductivity of 2D superconductors, close to zero temperatures, were studied in Ref. (Galitski and Larkin, 2001a). In this work, all ten diagrams shown in Fig. 14, were analyzed in lowest Landau level (LLL) approximation, which is valid close to the critical line $H_{c2}(T)$. A nontrivial non-monotonic temperature dependence of the fluctuation conductivity at fields close to $H_{c2}(0)$ was found and, analogously to the situation in granular SCs close to zero temperature, the fluctuation contribution is shown to be negative, i.e., QFs increase *resistivity*, and not conductivity – in contrast to the behavior close to T_{c0}.

The problem of calculating the fluctuation conductivity of a disordered 2D superconductor placed in a perpendicular magnetic field was revisited ten years later in the frameworks of two different approaches in Refs. (Glatz *et al.*, 2011b) (Matsubara diagrammatic technique) and (Tikhonov *et al.*, 2012) (quantum transport equation). In these papers exact calculations (without the use of the LLL approximation) were performed in first order of perturbation theory, valid in the entire H-T phase diagram beyond the superconducting region, i.e., for fields and temperature obeying $H \geq H_{c2}(T)$ or, equivalently, $T \geq T_{c0}(H)$[8].

The complete expression for the fluctuation correction to in-plane conductivity $\sigma_{xx}^{(fl)}(T,H)$ of a disordered 2D SC in a perpendicular magnetic field that holds in the T-H phase diagram beyond the line $H_{c2}(T)$ has the form (Glatz *et al.*, 2011a,b):

$$\sigma_{xx}^{(fl)}(t,h) = \underbrace{\frac{e^2}{\pi}\sum_{m=0}^{M_t}(m+1)\int_{-\infty}^{\infty}\frac{dx}{\sinh^2\pi x}\left\{\underbrace{\frac{\left[\mathrm{Re}^2\left(\mathcal{E}_m-\mathcal{E}_{m+1}\right)-\mathrm{Im}^2\left(\mathcal{E}_m-\mathcal{E}_{m+1}\right)\right]\mathrm{Im}\,\mathcal{E}_m\,\mathrm{Im}\,\mathcal{E}_{m+1}}{\left|\mathcal{E}_m\right|^2\left|\mathcal{E}_{m+1}\right|^2}}_{\sigma_{xx}^{(AL)}}+\right.}$$
$$\underbrace{\left.-\frac{\mathrm{Re}\left(\mathcal{E}_m-\mathcal{E}_{m+1}\right)\mathrm{Im}\left(\mathcal{E}_m-\mathcal{E}_{m+1}\right)\left(\mathrm{Im}\,\mathcal{E}_m\,\mathrm{Re}\,\mathcal{E}_{m+1}+\mathrm{Im}\,\mathcal{E}_{m+1}\,\mathrm{Re}\,\mathcal{E}_m\right)}{\left|\mathcal{E}_m\right|^2\left|\mathcal{E}_{m+1}\right|^2}\right\}}_{+\,\sigma_{xx}^{(AL)}}$$
$$+\underbrace{\frac{e^2}{\pi}\left(\frac{h}{t}\right)\sum_{m=0}^{M_t}\frac{1}{\gamma_\phi+\frac{2h}{t}(m+1/2)}\int_{-\infty}^{\infty}\frac{dx}{\sinh^2\pi x}\frac{\mathrm{Im}^2\,\mathcal{E}_m}{\left|\mathcal{E}_m\right|^2}}_{\sigma_{xx}^{(MT,an)}+\sigma_{xx}^{(MT,reg2)}}+\underbrace{\frac{e^2}{\pi^4}\left(\frac{h}{t}\right)\sum_{m=0}^{M_t}\sum_{k=-\infty}^{\infty}\frac{4\mathcal{E}_m''(t,h,|k|)}{\mathcal{E}_m(t,h,|k|)}}_{\sigma_{xx}^{(MT,reg1)}}$$
$$+\underbrace{\frac{4e^2}{\pi^3}\left(\frac{h}{t}\right)\sum_{m=0}^{M_t}\int_{-\infty}^{\infty}\frac{dx}{\sinh^2\pi x}\frac{\mathrm{Im}\,\mathcal{E}_m\,\mathrm{Im}\,\mathcal{E}_m'}{\left|\mathcal{E}_m\right|^2}}_{\sigma_{xx}^{(DOS)}}+\underbrace{\frac{4e^2}{3\pi^6}\left(\frac{h}{t}\right)^2\sum_{m=0}^{M_t}(m+\frac{1}{2})\sum_{k=-\infty}^{\infty}\frac{8\mathcal{E}_m'''(t,h,|k|)}{\mathcal{E}_m(t,h,|k|)}}_{\sigma_{xx}^{(7-10)}}. \qquad (55)$$

[8] Obviously, the calculations were done within the model constrains specified in section III and beyond the critical region.

where $\gamma_\phi = \pi/(8T_{c0}\tau_\phi)$.

This complete expressions allows for a straightforward numerical evaluation and to derive asymptotic expressions in all its qualitatively different domains. A typical example of the surface $\sigma_{xx}^{(fl)}(T,H)$ is plotted in Fig. 15. It demonstrates the important fact that the fluctuation conductivity is positive only in the domain bound by the lines $H_{c2}(T)$ and $\sigma_{xx}^{(fl)}(T,H)=0$, and negative throughout the rest of the phase diagram (see Fig. 5, showing the domains of different overall signs of $\sigma_{xx}^{(fl)}(T,H)$ and contours of constant $\sigma_{xx}^{(fl)}$ in the whole phase diagram). Contrary to a common perception, the fluctuation correction to conductivity is only positive in weak fields. The region in which $\sigma_{xx}^{(fl)}$ is positive depends on the (positive) anomalous MT contribution (i.e. on the value of the phase-breaking time τ_ϕ). With increasing magnetic field, the temperature interval where $\sigma_{xx}^{(fl)}(T,H) > 0$ shrinks and vanishes close to $H_{c2}(0)$. As a result, the fluctuation conductivity exhibits a highly non-trivial behavior at low temperatures. Near the QPT, the surface $\sigma_{xx}^{(fl)}(T,H)$ has a trough-shaped structure with a "sink" at the point $(H = H_{c2}(0), T = 0)$ and the dependence $\sigma_{xx}^{(fl)}(T, H = \text{const})$ is non-monotonic. This feature is also observed in experiments, which we review below.

Fig. 5 gives an overview of the entire phase diagram where the leading fluctuation contributions to magnetoconductivity are indicated. In particular near T_{c0} the singular contributions (paraconductivity, anomalous MT, and DOS) determine the overall behavior, while in the QF region they become zero as $\sim T^2$ (compare to Refs. (Beloborodov and Efetov, 1999; Beloborodov *et al.*, 2000; Mineev and Sigrist, 2001)) and the leading contribution comes from the sum of diagrams 7-10 and the regular part of the MT diagram (Glatz *et al.*, 2011a), which are usually ignored. [9]

B. Asymptotic analysis

Asymptotic expressions of Eq. (55) for fluctuation conductivity throughout the entire h-t phase diagram are summarized in table IV.

We begin their discussion with domains I–III, corresponding to the Ginzburg-Landau region of fluctuations close to T_{c0} and in zero magnetic field (domain I). The contribution of diagrams 7-10 was analyzed in Ref. (Glatz *et al.*, 2011a) and is also discussed here. It was usually ignored in literature, since it does not diverge close to T_{c0}. Nevertheless, its constant contribution $\sim \ln\ln(T_{c0}\tau)^{-1}$ is necessary for matching the GL results with the neighboring domains VIII & IX. Domains II & III are still described by the GL theory in weak magnetic fields and Eq. (55) reproduces all asymptotic expressions found in literature.

In the domain of quantum fluctuations (IV) (see Fig. 5), the AL paraconductivity term (which is the leading, singular contribution close to T_{c0}) decays with decreasing temperature as T^2. The same happens with the anomalous MT contribution, which in that domain is equal to the AL contribution. Moreover, it is exactly canceled by the negative contribution of the four DOS-like diagrams 3-6:

$$\sigma_{xx}^{(AL)} = \sigma_{xx}^{(MT,an)} = -\sigma_{xx}^{(DOS)} = \frac{4e^2\gamma_E^2 t^2}{3\pi^2\widetilde{h}^2}\,. \qquad (56)$$

The total fluctuation contribution to conductivity $\sigma_{xx}^{(fl)}$ in this important region ($t \ll \widetilde{h}$) turns out to be negative and at zero temperature diverges logarithmically when the magnetic field approaches $H_{c2}(0)$. The nontrivial fact following from Eq. (55) is that an increase of temperature at a fixed magnetic field mainly results in a further decrease of conductivity in this domain

$$\sigma_{xx}^{(fl)} = -\frac{2e^2}{3\pi^2}\ln\frac{1}{\widetilde{h}} - \frac{2\gamma_E e^2}{3\pi^2}\frac{t}{\widetilde{h}} + O\left[\left(\frac{t}{\widetilde{h}}\right)^2\right]. \qquad (57)$$

Only at the boundary with domain V, when $t \sim \widetilde{h}$, the fluctuation conductivity $\sigma_{xx}^{(fl)}$ passes through a minimum and starts to increase. Such non-monotonic behavior of the conductivity close to $H_{c2}(0)$ was observed multiple times in experiments (Caprara *et al.*, 2009; Gantmakher *et al.*, 2003; Jin *et al.*, 2008; Leridon *et al.*, 2007).

Domain V describes the transition regime between quantum and classical fluctuations, while in domains VI–VII, (along the line $H_{c2}(T)$) superconducting fluctuations have already classical character and can be considered in a generalized TDGL scheme, see Ref. (Mineev and Sigrist, 2001).

Finally, in the peripheral domains VIII-IX, the direct positive contribution of fluctuation Cooper pairs (AL) to conductivity decays faster than all the others: $\sim \ln^{-3}(T/T_{c0})$. We stress, that this result differs from the evaluation of the AL paraconductivity far from the transition of Ref. (Aslamasov and Varlamov, 1980), but is in complete agreement with the high temperature asymptotic expression for the paraconductivity of a clean 2D superconductor, see Ref. (Reggiani *et al.*, 1991). This agreement seems natural: FCP transport is insensitive

[9] Here we note, that there is some controversy regarding the origin of the logarithmic singularity in $\sigma_{xx}^{(fl)}(t \ll \tilde{h})$, see (Galitski and Larkin, 2001a; Glatz *et al.*, 2011a; Tikhonov *et al.*, 2012). The asymptotic expression for the fluctuation conductivity in the QF region is the same in all three works. However, in Refs. (Galitski and Larkin, 2001a; Tikhonov *et al.*, 2012) all 10 diagrams of Fig. 14 contribute to the logarithm, while Ref. (Glatz *et al.*, 2011a) states that the quantum phase transition in conductivity is governed only by the sum of diagrams 7-10 and the regular part of the MT diagram and all other contributions in this domain cancel out.

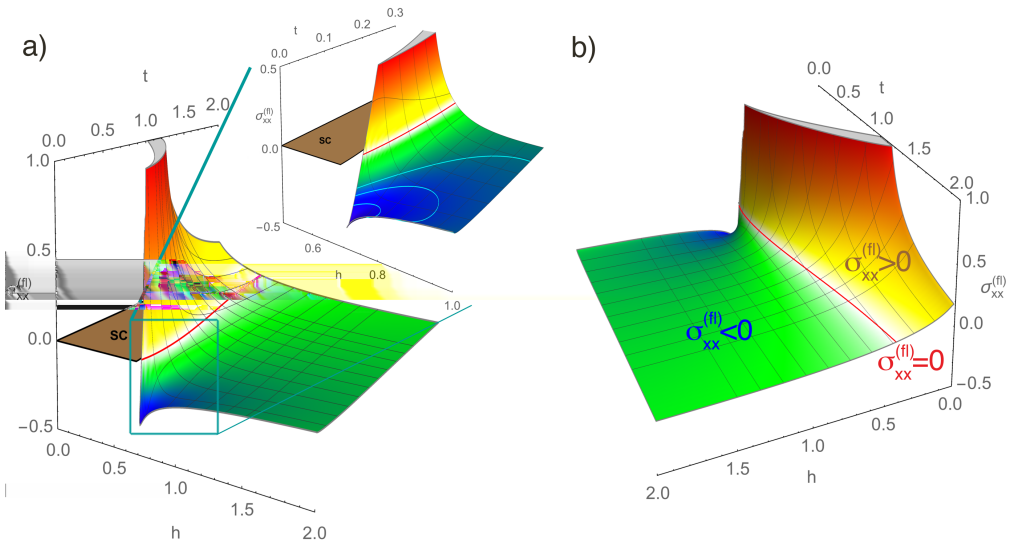

FIG. 15 (Color online) Fluctuation correction to conductivity $\sigma_{xx}^{(fl)}(t,h)$ as function of the reduced temperature $t = T/T_{c0}$ and magnetic field $h = 0.69H/H_{c2}(0)$ plotted as surface. The FC changes its sign along the thick red [black] line ($\sigma_{xx}^{(fl)}(t,h) = 0$). The superconducting region is marked by "SC". Here $\sigma_{xx}^{(fl)}$ is plotted for constant $\tau T_{c0} = 10^{-2}$ and $\tau_\phi T_{c0} = 10$. (a) shows a view at the quantum region at low temperatures, the inset a close-up of the trough with a few negative contour lines (cyan [light gray]). (b) shows a view at the high temperature region.

domain	$\sigma_{xx}^{(fl)}$
I–III	$\underbrace{\frac{e^2}{2\epsilon}\left(\frac{\epsilon}{2h}\right)^2\left[\psi\left(\frac{1}{2}+\frac{\epsilon}{2h}\right)-\psi\left(\frac{\epsilon}{2h}\right)-\frac{h}{\epsilon}\right]}_{\sigma_{xx}^{(AL)}}+\underbrace{\frac{e^2}{8}\frac{1}{\epsilon-\gamma_\phi}\left[\psi\left(\frac{1}{2}+\frac{\epsilon}{2h}\right)-\psi\left(\frac{1}{2}+\frac{\gamma_\phi}{2h}\right)\right]}_{\sigma_{xx}^{(MT,an)}}-\underbrace{\frac{28\zeta(3)\,e^2}{\pi^4}\left[\psi\left(\frac{1}{2h}\right)-\psi\left(\frac{1}{2}+\frac{\epsilon}{2h}\right)\right]}_{\sigma_{xx}^{(MT,reg)}+\sigma_{xx}^{(DOS)}}+\underbrace{\frac{e^2}{3\pi^2}\ln\ln\frac{1}{T_{c0}\tau}}_{\sigma_{xx}^{(DCR)}}$ $= \begin{cases} \frac{e^2}{16\epsilon}+\frac{e^2}{8(\epsilon-\gamma_\phi)}\ln\frac{\epsilon}{\gamma_\phi}-O\left[\ln\left(\frac{1}{\epsilon}\right)\right]+\frac{e^2}{3\pi^2}\ln\ln\frac{1}{T_{c0}\tau}, & \text{I} \\ \left(1+\frac{\pi^2}{4}\right)\frac{e^2}{8h}-O\left[\ln\left(\frac{1}{h}\right)\right]+\frac{e^2}{3\pi^2}\ln\ln\frac{1}{T_{c0}\tau}, & \text{II} \\ \frac{e^2}{2h(\epsilon+h)}+\frac{e^2}{3\pi^2}\ln\ln\frac{1}{T_{c0}\tau}, & \text{III} \end{cases}$
IV–VII	$\begin{cases} -\frac{2e^2}{3\pi^2}\ln\frac{1}{h}-\frac{2\gamma_E e^2}{3\pi^2}\frac{t}{h}+O\left[\left(\frac{t}{h}\right)^2\right], & \text{IV} \\ \frac{4\gamma_E e^2}{3\pi^2}\frac{t}{h}, & \text{V} \\ \frac{e^2}{6}\frac{t}{\tilde{h}(t)}, & \text{VI}-\text{VII} \end{cases}$
VIII	$-\frac{2e^2}{3\pi^2}\left(\ln\ln\frac{1}{T_{c0}\tau}-\ln\ln t\right)+\frac{0.05e^2\ln\frac{\pi^2}{2\gamma_\phi}}{\ln^2}+\frac{0.12e^2}{\ln^3 t}$
IX	$-\frac{2e^2}{3\pi^2}\left(\ln\ln\frac{1}{T_{c0}\tau}-\ln\ln h\right)-\frac{0.11e^2}{\ln^2\frac{2h}{\pi^2}}\left(\frac{t}{h}\right)^2+\frac{0.03e^2}{\ln^3\frac{2h}{\pi^2}}\left(\frac{t}{h}\right)^2$

TABLE IV Asymptotic expressions for the fluctuation corrections to conductivity in different domains of the phase diagram.

to impurity scattering. The anomalous MT contribution decays as $\sim \ln\gamma_\phi^{-1}/\ln^{-2}(T/T_{c0})$, in complete agreement with Refs. (Aslamasov and Varlamov, 1980; Larkin, 1980). The contribution of diagrams 3-6 also decays as $\ln^{-2}(T/T_{c0})$, but without the large factor $\ln\gamma_\phi^{-1}$. Finally, the regular MT contribution together with the ones from diagrams 7-10 decay extremely slow, in fact double logarithmically:

$$\sigma_{xx}^{(DCR)} = -\frac{2e^2}{3\pi^2}\left(\ln\ln\frac{1}{T_{c0}\tau}-\ln\ln\frac{T}{T_{c0}}\right). \qquad (58)$$

Up to the numerical prefactor this expression coincides with the results of Refs. (Altshuler *et al.*, 1983; Aslamasov and Varlamov, 1980).

C. Fluctuation spectroscopy: analysis of the conductivity

1. Manifestation of different contributions to conductivity

Eq. (55) provides a basis for a *fluctuation spectroscopy* of superconductors. This means the extraction of microscopic parameters of a measured sample based on the analysis of fluctuation corrections. In the case of $\sigma_{xx}^{(fl)}$

one can extract four parameters; T_{c0}, $H_{c2}(0)$, the elastic scattering time τ, and the (temperature dependent) phase-breaking time $\tau_\phi(T)$. In particular the critical temperature T_{c0} and critical field $H_{c2}(0)$ can be determined precisely as opposed to the often used rule "half width of transition" for T_{c0}, while the elastic scattering time can also be obtained from the normal state properties of the superconductor. In case of phase-breaking time $\tau_\phi(T)$, an analysis of the fluctuation correction is an invaluable tool for the study of its temperature dependence.

In general, the total conductivity of the disordered system is the sum of the bare Drude conductivity σ_0, corrections due to quantum interference of the electron waves [weak localization (WL)] which impede the electrons' propagation, corrections from the interaction between particles with close momenta [diffusion channel (ID)], and superconducting fluctuations:

$$\sigma = \sigma_0 + \sigma^{(\mathrm{WL})} + \sigma^{(\mathrm{ID})} + \sigma_{xx}^{(\mathrm{fl})}\,, \tag{59}$$

where the fluctuation part itself consists of the contributions from diagrams shown in Fig. 14. Drude conductivity, ID & WL corrections are subtracted from the measured conductivity, such that Eq. (55) can then be used to fit the fluctuation corrections.

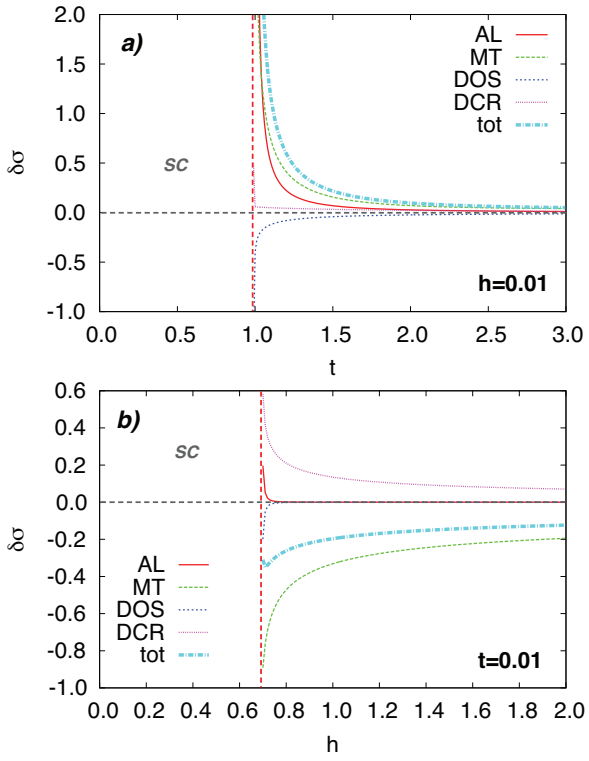

FIG. 16 (Color online) Fluctuation conductivity contributions: AL, MT, DOS, DCR, and total (tot) for $T_{c0}\tau = 10^{-3}$ and $T_{c0}\tau_\phi = 5$. a) shows the temperature dependence at low field $h = 0.01$, and b) the field dependence at low temperature $t = 0.01$. After Ref. (Glatz *et al.*, 2011a).

The exemplary surface of $\sigma_{xx}^{(\mathrm{fl})}(T,H)$ presented in Fig. 15 for $T_{c0}\tau = 10^{-2}$ and $T_{c0}\tau_\phi = 10$ shows that the value of τ_ϕ determines the behavior of fluctuation corrections only in the region of low fields. It is convenient to analyze Fig. 15 side-by-side with Fig. 5 where contour lines $\sigma_{xx}^{(\mathrm{fl})}(T,H) = \text{const}$ throughout the phase diagram are shown. It is interesting to note that the numerical analysis of Eq. (55) shows that the logarithmic asymptotic Eq. (57) is valid only within an extremely narrow field range $\widetilde{h} \lesssim 10^{-6}$.

Fig. 16 shows detailed plots of two particular curves of $\sigma_{xx}^{(\mathrm{fl})}(T,H)$, which illustrate the different contributions from diagram groups a)-d) of Fig. 14. These are curves for $T_{c0}\tau_\phi = 5$ at lowest magnetic field $h = 0.01$ [in a)] and temperature $t = 0.01$ [in b)]. Curve a) reproduces the asymptotic expressions near T_{c0} given in table IV, and one can see that the contribution from diagrams 7-10 is negligible. However, in the quantum regime the latter becomes the dominating contribution [see b)], rendering the total fluctuation conductivity negative. It is only canceled very close to the QPT by the MT contribution.

Despite Eq. (55) being a closed expression, its specific evaluation in the most general case requires sophisticated numerical summation and integration. We describe the more technical aspect of *fluctuation spectroscopy* at the end of this review in section XI.

2. Observation of fluctuation conductivity in experiments

The usefulness of the fluctuation spectroscopy approach was shown for several experimental systems. Below, we review a few of them in some detail.

a. Indium oxide films In (Glatz *et al.*, 2011a) resistivity measurements of thin disordered indium oxide films, presented in Ref. (Steiner and Kapitulnik, 2005), were fitted by Eq. (55). Figure 17 shows the low temperature data for one sample (referred to as "Weak" in Ref. (Steiner and Kapitulnik, 2005)) of a film with thickness 30nm, transition temperature $T_{c0} = 3.35$K, and critical magnetic field $B_{c2}(0) = 13$T. The resistivity was measured, depending on magnetic field, for low temperature values $T = 200, 300, 400, 500$mK. The theoretical expression for $\sigma_{xx}^{(\mathrm{fl})}$ is plotted using fitting parameter values $B_{c2}(0) = 13.7$T, $T_{c0}\tau_\phi = 5 \pm 1$, and the experimentally found value of $T_{c0} = 3.35$K. Overall, the fitted $\sigma_{xx}^{(\mathrm{fl})}$ curves show good agreement with the results of the measurements.

As mentioned above, τ_ϕ usually depends on temperature, such that for a better fit one needs first to analyze FC data at constant temperatures to extract $\tau_\phi(T)$ and then fit temperature dependent data. This way one can obtain precise values for the parameters T_{c0}, $H_{c2}(0)$, and

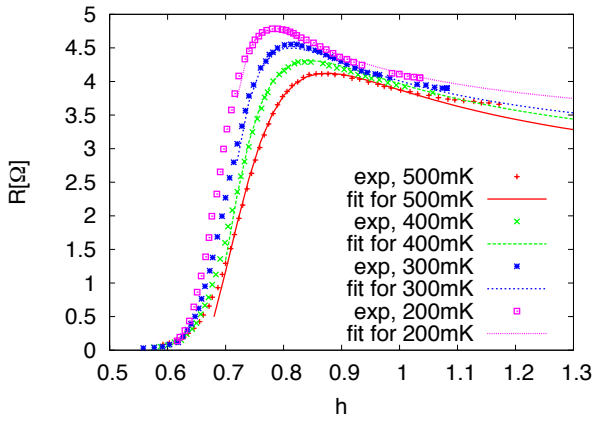

FIG. 17 (Color online) Comparison to resistivity measurements in thin indium oxide films. The experimental data was taken from Fig. 4a of (Steiner and Kapitulnik, 2005) for the "Weak" sample with thickness 30nm, $T_{c0} = 3.35$K, and $B_{c2}(0) = 13$T. The resistivity R for temperatures 0.2, 0.3, 0.4, and 0.5K was fitted using (55) with the experimentally found T_{c0}. For $B_{c2}(0)$ a slightly larger value of 13.7T and $T_{c0}\tau_\phi = 5 \pm 1$ were used. After Ref. (Glatz *et al.*, 2011a).

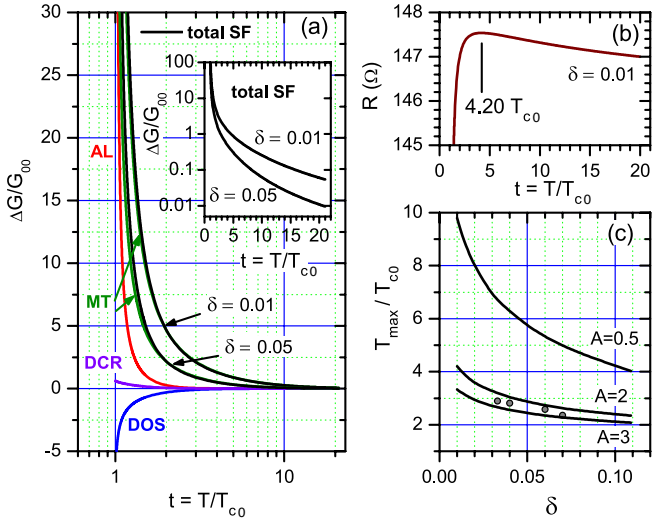

FIG. 18 (Color online) (a) Temperature dependences of superconducting fluctuation contributions to conductance [in units of $G_{00} = \sigma_{00} = e^2/(2\pi^2\hbar)$]. The curves for AL, DOS, and DCR processes are universal functions of reduced temperature $t = T/T_c$, the MT contribution is presented for $\delta = 0.01$ and 0.05. The black solid lines are the sum of all SF contributions Eq. (55). The inset shows the same total SF contribution on logarithmic scale. (b) Resistance vs. reduced temperature (see details in the text). (c) The set of the curves T_{max}/T_c vs. δ for different coefficients A from Eq. (61). The circles represent the measured T_{max}, T_c, and δ obtained by fitting the experimental data. After Ref. (Baturina *et al.*, 2012).

$\tau_\phi(T)$, which would be difficult to determine otherwise. In many cases it is useful to choose the parameter

$$\delta = \pi\hbar/(8k_B T\tau_\phi) \tag{60}$$

as fitting parameter, since often $\tau_\phi \propto T^{-1}$, such that δ becomes temperature independent. This parameter is related to γ_ϕ in Eq. (55) by $\gamma_\phi = t\delta$.

b. Fluctuations in ultrathin TiN films A rather detailed fluctuation spectroscopy study was presented in Ref. (Baturina *et al.*, 2012), showing how one can extract the real BCS critical temperature from a measurement. In particular, it was demonstrated how an omission of the Maki-Thompson contribution leads to incorrect values of T_c. In that work, the conductivity measured in thin (≤ 5 nm) TiN films was analyzed and we review this work here to some depth.

In thin films, σ in Eq. (59) refers to the conductance rather than to conductivity and the WL and ID corrections can be written as:

$$\sigma^{(\mathrm{WL})} + \sigma^{(\mathrm{ID})} = \sigma_{00} A \ln\left[k_B T\tau/\hbar\right] , \tag{61}$$

with $A = ap + A^{(\mathrm{ID})}$. Here, $\sigma_{00} = e^2/(2\pi^2\hbar)$, $a = 1$ if spin-orbit scattering is neglected ($\tau_\varphi \ll \tau_{so}$) or $a = -1/2$ when scattering is relatively strong ($\tau_\varphi \gg \tau_{so}$), p is the exponent in the temperature dependence of the phase coherence time $\tau_\varphi \propto T^{-p}$, and A_{ID} is a constant depending on the Coulomb screening and which in all cases remains of the order of unity (Finkelshtein, 1983). At low temperatures where electron-electron scattering dominates one gets $p = 1$ and at higher temperatures, where the electron-phonon interaction becomes relevant, $p = 2$. This is in agreement with experimental observations (Bergmann, 1984; Brenig *et al.*, 1986; Bruynseraede *et al.*, 1983; Gershenzon *et al.*, 1983; Gordon and Goldman, 1986; Gordon *et al.*, 1984; Raffy *et al.*, 1983; Santhanam and Prober, 1984; Wu and Lin, 1994) where $1 \leq p \leq 2$, with $p = 1$ at $T < 10$ K.

In Fig. 18c the ratio T_{max}/T_c as function of δ (see Eq. (60)) is plotted for three most common experimental situations where $A = 3$, 2 and 0.5, corresponding to three sets of parameters (a, p, A_{ID}) in Eq. (61): (1,2,1), (1,1,1), and (-1/2,1,1). It is noteworthy that the maximum lies in the domain where the SF are dominated by the Maki-Thompson contribution and that the maximum itself arises from the competition between the WL+ID and MT processes. In general, T_{max}/T_c vs. δ curves relate the quantity T_{max}, which is the only characteristic point in the $R(T)$ dependence, to the transition temperature T_c and as such can serve as a set of calibrating curves for an easy determination of T_c, since A can be estimated from the analysis of the resistance behavior at high temperatures.

In Figure 19a, the temperature dependences of the resistance per square for four TiN films with different room temperature resistances is shown and in panel b) the tem-

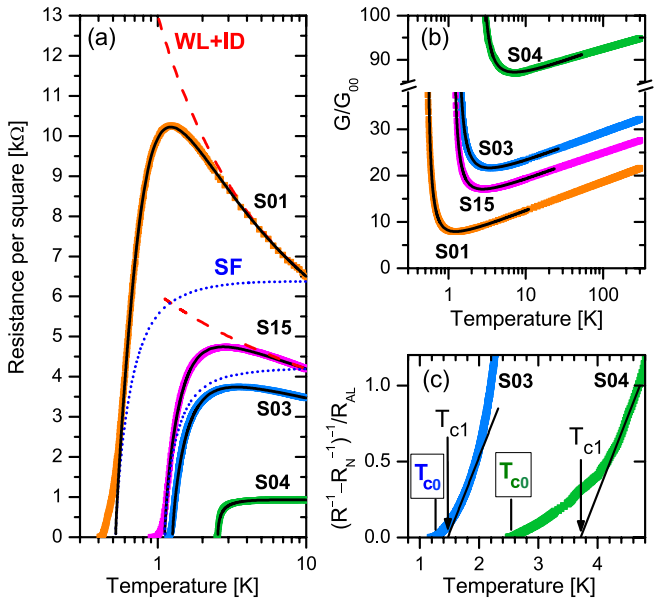

FIG. 19 (Color online) (a) Resistance per square vs. temperature for four different TiN film samples, labeled Sxx. *Solid lines*: fits accounting for all corrections. *Dashed lines* (marked as WL+ID): separate contribution of the sum of weak localization and interaction in the diffusion channel to the resistance of the samples S01 and S15. *Dotted lines* (SF): contribution of superconducting fluctuations. (b) The same data as in (a), but extended to room temperatures and re-plotted as the dimensionless conductance ($G/G_{00} = \sigma/\sigma_{00}$). The semi-logarithmic scale representation reveals a logarithmic decrease of the conductance with temperature due to the WL and ID effects. (c) Reduced conductance $(R^{-1} - R_N^{-1})^{-1}/R_{\rm AL}$ ($R_{\rm AL}^{-1} = e^2/(16\hbar)$ and $R_N = R_{\rm max}$) vs. T. The linear fit to the AL expression (solid lines) are often used for the determination of T_c and generally gives incorrect (much too high) values of the critical temperature, shown here for samples S03 and S04 (marked by arrows). The correct values of T_c obtained through fluctuation spectroscopy are framed and marked by vertical bars. After Ref. (Baturina *et al.*, 2012).

perature behavior of the conductance. Solid fitting lines in Fig. 19a,b account for all quantum contributions.

The fitting captures all major features of the observed dependences: their non-monotonic behavior, the position and the height of $R_{\rm max}$, and the graduate decrease in the resistance matching perfectly the experimental points down to values $R \ll R_{\rm max}$ (without any additional assumptions about mesoscopic inhomogeneities (Caprara *et al.*, 2011; Ioffe and Larkin, 1981)). In this study three fitting parameters, δ, A, and, T_c were used. It is noteworthy that while varying δ and A significantly shifts the temperature position and the value of $R_{\rm max}$, it does not change the position of T_c noticeably. It demonstrates the fact that $\sigma_{xx}^{(\hbar)}$ does not depend on the pair-breaking parameter δ in the close vicinity of T_c (see inset to Fig. 18a where the curves for different δ merge).

At this point it is instructive to review the approaches for inferring T_c from the experimental data that were frequently used in the past. From Fig 19c) one sees that T_c lies at the "foot" of the $R(T)$ curve where $R(T) \simeq (0.08 \div 0.13)R_{\rm max}$. Therefore, the determination of T_c as the temperature where $R(T)$ drops to $0.5R_N$ (let alone to $0.9R_N$) significantly overestimates T_c. Another frequently used procedure (Fiory *et al.*, 1983) is based on the assumption that the effect of quantum corrections can be reduced to the AL term only, i.e., that the resistance obeys the relation $R^{-1} = R_N^{-1} + R_{\rm AL}^{-1}/(T/T_c - 1)$, where $R_{\rm AL}^{-1} = e^2/(16\hbar) = 1.52 \cdot 10^{-5}\,\Omega^{-1}$. This implies that a range of temperatures near T_c exists, where the plot $[(R^{-1} - R_N^{-1})^{-1}/R_{\rm AL}]$ vs. T can be approximated by a straight line with slope one. The intersection of this line with the T-axis would have defined T_c. Utilizing this approach for the data of the two samples plotted in Fig. 19c, yields temperatures of the intersections marked as T_{c1}. One sees, however, that this procedure gives also too high values for the superconducting critical temperatures.

We remark that the used fluctuation spectroscopy does not explain all features of the measured conductance curves, e.g., possible effects of Berezinskii-Kosterlitz-Thouless (BKT) physics (Beasley *et al.*, 1979; Halperin and Nelson, 1979) even above T_{c0}, glassy behavior (Feigel'man *et al.*, 2010; Sacepe *et al.*, 2011), or spatial inhomogeneities in the films (Caprara *et al.*, 2013) are not taken into account. In fact, the BKT transition was studied as well in Ref. (Baturina *et al.*, 2012) and it was shown that in the analyzed samples the BKT transition temperature follows the universal relation found by Beasley, Mooij, and Orlando in Ref. (Beasley *et al.*, 1979). However, the effect of the BKT transition on corrections to conductivity above T_c is negligible in this case.

In conclusion, Ref. (Baturina *et al.*, 2012) shows that the real microscopic parameters for thin superconducting films obtained by fluctuation spectroscopy can be significantly different than qualitative estimations.

c. Transverse magneto-resistance above $H_{c2}(0)$ Fluctuation spectroscopy can also be used to analyze the transverse magneto-resistance observed in the *layered* organic superconductor κ-(BEDT-TTF)$_2$X above $H_{c2}(0)$ at low temperatures (Kartsovnik *et al.*, 1999; Pratt *et al.*, 1993; Zuo *et al.*, 1999) and explain its non-monotonic behavior. The motion of FCPs in z-direction in such a system has hopping character and the quasiparticle spectrum can be assumed to have the form of a corrugated cylinder. Close to T_{c0} the fluctuation magneto-conductivity tensor in this model was already studied in detail in Ref. (Dorin *et al.*, 1993). In this work it was demonstrated that the transverse paraconductivity in that case is suppressed by the square of the small anisotropy parameter $(\xi_z/\xi_x)^2$, while the dependence on the reduced temperature ϵ is considerably more singular than that of the in-plane paraconduc-

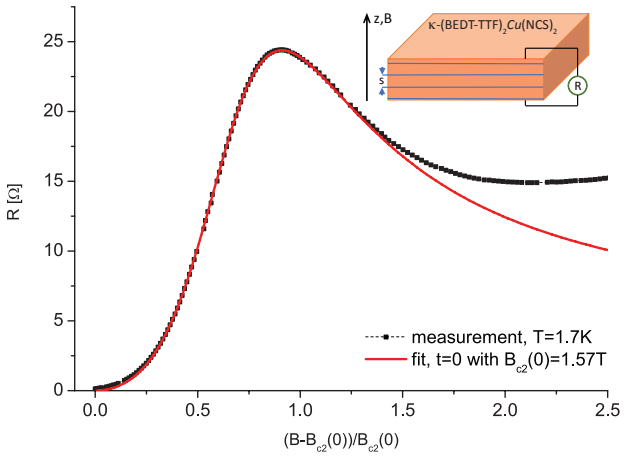

FIG. 20 (Color online) Comparison to resistivity measurements of the layered organic superconductor κ-(BEDT-TTF)$_2$Cu(NCS)$_2$. The material has a transition temperature of $T_{c0} \approx 9.5$K, $B_{c2}(0) \approx 1.57$T, and $\tau = 1.7$ps. This experimental curve is taken at $T = 1.7$K and fitted by expression in Eq. (63), which is in perfect agreement with the experiment. The inset shows a sketch of the measurement setup. After Ref. (Glatz *et al.*, 2011a).

tivity. In terms of the Ginzburg-Landau FCP life-time (1), it can be written as

$$\sigma_{zz}^{(AL)}(\epsilon) = \frac{4e^2\xi_z^4}{\pi^2\xi_{xy}^2 s^3} T_{c0}^2 \tau_{GL}^2(\epsilon)\,, \qquad (62)$$

where s is the interlayer distance. In principle this result could be obtained, even from the Drude formula applied to the FCP charge transfer [see above, how Eq. (62) for $\sigma_{xx}^{(AL)}(\epsilon)$ was obtained] combined with the above speculations regarding the hopping of FCPs along z-axis (Lerner *et al.*, 2008). This general approach, which does not involve the GL scheme, allows to map Eq. (62) on the case of the QPT by just replacing $\tau_{GL}(\epsilon) \to \tau_{QF}\left(\widetilde{h}\right)$:

$$\sigma_{zz}^{(AL)}\left(\widetilde{h}\right) = \frac{4e^2\xi_z^4}{\xi_x^2 s^3} T_{c0}^2 \tau_{QF}^2\left(\widetilde{h}\right) = \frac{4e^2\xi_z^4}{\xi_x^2 s^3}\left(\frac{\gamma_E}{\pi}\right)^2 \frac{1}{\widetilde{h}^2}\,.$$

The negative contribution appearing from the diffusion coefficient renormalization competes with the positive $\sigma_{zz}^{(AL)}\left(\widetilde{h}\right)$. The only difference between the in-plane [see Eqs. (57) & (58)] and z-axis components of this one-particle contribution consists in the anisotropy factor $\langle v_z^2\rangle / v_x^2 = \xi_z^2/\xi_x^2$. As a result one gets:

$$\sigma_{zz}^{(DCR)} = -\frac{2e^2}{3\pi^2 s}\frac{\xi_z^2}{\xi_x^2}\ln\frac{1}{\widetilde{h}}$$

and the total fluctuation correction to the z-axis magneto-conductivity at zero temperature above $H_{c2}(0)$ can be written as

$$\sigma_{zz}^{(fl)} = \frac{2e^2\xi_z^2}{3\pi^2\xi_x^2 s}\left[1.94\left(\frac{\xi_z}{s}\right)^2\frac{1}{\widetilde{h}^2} - \ln\frac{1}{\widetilde{h}}\right]. \qquad (63)$$

In Ref. (Glatz *et al.*, 2011a), Eq. (63) was used for the analysis of data taken from Ref. (Kartsovnik *et al.*, 1999) on the magneto-resistance of the layered organic superconductor κ-(BEDT-TTF)$_2$Cu(NCS)$_2$ at temperature $T = 1.7$K, much below $T_{c0} \approx 9.5$K, but at magnetic fields above $B_{c2}(0) \approx 1.57$T. In this measurement the magnetic field and current were applied perpendicular to the layers. The experimental curve was fitted by $0.23\left(0.18/\widetilde{h}^2 + \ln\widetilde{h}\right)$, see Fig. 20. For the material parameters of this compound, the author reports $\tau = 1.7$ps, $\xi_z = 0.3 - 0.4$ nm, and $s = 1$ nm. The fitting shown in Fig. 20 corresponds to the ratio $\xi_z/s = 0.32$ and looks rather convincing.

The discrepancy appearing between the theoretical and experimental curves in the high field region, was attributed to the large normal-state magneto-resistance, reflecting the specifics of the cyclotron orbits on the multi-connected Fermi surface of the compound (due to the low crystal symmetry it is quite difficult to fit).

VI. FLUCTUATION HALL CONDUCTIVITY

A. Fluctuation Hall effect and the special role of particle-hole asymmetry

It is known that interacting electronic systems with simple band structure do not exhibit the Hall effect without impurity scattering (Aronov *et al.*, 1995). So how does the presence of superconducting fluctuations lead to a non-zero Hall resistance?

The FCP contribution to the Hall effect was first mentioned in Ref. (Abrahams *et al.*, 1971), where the effect of the magnetic field on fluctuations above T_{c0} was studied in the framework of the time-dependent GL theory. The authors recognized that the non-zero fluctuation correction to the Hall conductivity appears only if an additional term proportional to frequency is included in the non-stationary GL equation. They have introduced an imaginary part of the diffusion coefficient without going into a detailed discussion about its origin. Ullah and Dorsey (Ullah and Dorsey, 1991) extended the phenomenological consideration of the effect of fluctuations on the Hall conductivity for the wide range of magnetic fields by applying the Hartree approximation. They attributed the imaginary part, which is responsible for particle-hole asymmetry, to the coefficient in front of the time derivative in the time-dependent GL equation, which is mathematically equivalent to the approach taken in Ref. (Abrahams *et al.*, 1971). Later, Aronov and Rapoport (Aronov and Rapoport, 1992) expressed

the parameter characterizing particle-hole asymmetry of superconducting fluctuations through the derivative of the critical temperature with respect to the quasiparticle chemical potential, $\frac{\partial T_{c0}}{\partial \mu}$ at the Fermi level, without any assumptions concerning the microscopic nature of superconductivity.

Simultaneously with Abrahams *et al.*, Fukuyama and coauthors (Fukuyama *et al.*, 1971) approached the problem of the fluctuation Hall conductivity in the framework of a microscopic theory. They found that the fluctuation correction to σ_{xy}, like in the case of the intrinsic effect in a normal metal, is proportional to $\frac{\partial \rho_e}{\partial E}\Big|_{E=\mu}$, i.e. it differs from zero only when the electron-hole asymmetry is taken into account.

Finally, Aronov *et al.* (Aronov *et al.*, 1995) demonstrated that, due to the requirement of the gauge invariance of the time-dependent GL theory, the only form in which the particle-hole asymmetry can manifest itself in the fluctuation propagator (32) is through the appearance of the term $\frac{i\Omega_k}{\pi^2}\frac{\partial \ln T_{c0}}{\partial \mu}$ side by side with the modulus of the boson frequency $|\Omega_k|$.

In addition to the small particle-hole asymmetry factor, the fluctuation correction to the Hall conductivity contains the small parameter $\mathrm{Gi}_{(\mathrm{d})}$ related to the weakness of superconducting fluctuations. This explains why the first experimental evidence of the pronounced effect of fluctuations on the Hall conductivity were reported only when high-temperature superconductors came into the focus of investigations (Artemenko *et al.*, 1989; Forro and Hamzić, 1989; Galffy and Zirngiebl, 1988; Hagen *et al.*, 1990; Iye *et al.*, 1989). In these materials, the Ginzburg-Levanyuk number can be as large as 10^{-2} due to their effectively two-dimensional structure. Moreover, the fluctuation Hall conductivity acquires a stronger singularity upon approaching T_{c0} ($\propto \epsilon^{-2}$ (Ullah and Dorsey, 1991; Varlamov and Livanov, 1990) instead of $\propto \epsilon^{-3/2}$ (Fukuyama *et al.*, 1971) for 3D superconductors). As a result, the Hall resistance exhibits a distinct deviation from the linear temperature dependence expected in the normal state, up to temperatures of about $2T_{c0}$ (Graybeal *et al.*, 1994; Hagen *et al.*, 1993; Kokubo *et al.*, 2001; Lang *et al.*, 1995; Liu *et al.*, 1997; Paalanen *et al.*, 1992; Samoilov, 1994; Smith *et al.*, 1994). At temperatures near T_{c0}, a sign reversal of the Hall conductivity was observed.

Note, that the electron-hole asymmetry in the band structure is not the only effect that can lead to the appearance of a nonzero fluctuation correction to Hall conductivity. It has been shown (Angilella *et al.*, 2003) that its sign and the value can depend on the topological structure of the Fermi surface. Evidence for a universal behavior of the Hall conductivity as a function of doping, which can change the topology of the Fermi surface, has been reported in the cuprate superconductors (Nagaoka *et al.*, 1998).

B. Microscopic theory of fluctuation Hall effect

Formally, similar to the diagonal component of conductivity, the fluctuation correction to the Hall conductivity is described by the same ten diagrams depicted in Fig. 14, but with one of the vertices being $e\hat{v}_y$ instead of $e\hat{v}_x$. Historically, the AL process, corresponding to an independent channel of charge transfer, was studied themost, since it is the dominant contribution in the GL regime, domains I–III near T_{c0} (Abrahams *et al.*, 1971; Aronov and Rapoport, 1992; Fukuyama *et al.*, 1971; Inoue *et al.*, 1979; Ullah and Dorsey, 1990, 1991; Varlamov and Livanov, 1990).

First, we discuss of the physical meaning of the Hall resistivity ρ_{xy}. In the case of only one type of carriers, it depends on their concentration n and turns out to be independent of the electron diffusion coefficient: $\rho_{xy} = H/(en)$. The fluctuation processes of MT and DCR types contribute to the diffusion coefficient, so their expected contribution to the Hall resistivity is zero. For the Hall conductivity in a weak field one can write

$$\begin{aligned}\sigma_{xy} &= \rho_{xy}\sigma_{xx}^2 = \rho_{xy}\sigma_{xx}^{(n)2} + 2\rho_{xy}\sigma_{xx}^{(n)}\sigma_{xx}^{(\mathrm{fl})} \\ &= \sigma_{xy}^{(n)}\left(1 + 2\frac{\sigma_{xx}^{(\mathrm{fl})}}{\sigma_{xx}^{(n)}}\right). \end{aligned} \tag{64}$$

This means, the relative fluctuation correction to the Hall conductivity is twice as large than the fluctuation correction to the diagonal component. This qualitative consideration is confirmed by a direct calculation of the MT diagram (Fukuyama *et al.*, 1971).

A complete theory of the fluctuation Hall effect was recently developed by Michaeli *et al.* (Michaeli *et al.*, 2012). In agreement with the statement of Ref. (Aronov *et al.*, 1995), the authors introduced the particle-hole asymmetry parameter $\varsigma = -\frac{1}{2}\frac{\partial \ln T_{c0}}{\partial \mu}$ in the propagator of superconducting fluctuations as follows:

$$\tilde{L}_n^{-1}(\Omega_k) = \tag{65}$$
$$-\rho_e\left[\ln\frac{T}{T_{c0}} + \psi\left(\frac{1}{2} + \frac{|\Omega_k| + \Omega_H(n+\frac{1}{2})}{4\pi T}\right) - \psi\left(\frac{1}{2}\right) + \varsigma\Omega_k\right].$$

The fact that the term linear in Ω_k appears outside the argument of the polygamma-function is related to the smallness of ς and the condition $|\Omega_k| \leq \tau^{-1}$ which allows to expand the ψ-function with respect to $\varsigma\Omega_k$ and to arrive at Eq. (65), which results in the total contribution from the aforementioned ten diagrams being proportional to $\varsigma\Omega_H$.

The authors of Ref. (Michaeli *et al.*, 2012) support the above qualitative statement and demonstrated that the sum of the contributions of the two DOS diagrams, 5 and 6 in Fig. 14, the MT diagram and all DCR diagrams is equal to zero for all H and T above the transition line $H_{c2}(T)$ (their combined effect can be reduced to a renormalization of the diffusion coefficient). It is therefore

sufficient to consider only the AL contribution and the two remaining DOS contributions, 3 and 4.

Michaeli *et al.* also considered two usually disregarded diagrams, shown in Fig. 21, which also contribute a leading-order correction to the Hall conductivity. This additional contribution is proportional to the cyclotron frequency of quasiparticles, $\omega_c^{(qp)}$. It turns to be dominant at high temperatures $T \gg T_{c0}$. Note that the correction to the diagonal component of fluctuation conductivity $\sigma_{xx}^{(fl)}$ from these two diagrams contains an additional small prefactor $T\tau$ and does not contribute to the leading order.

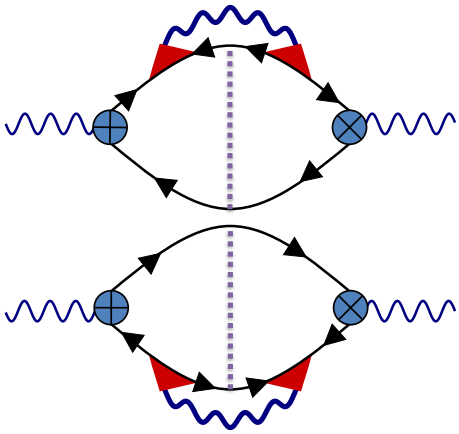

FIG. 21 (Color online) Two additional Feynman diagrams giving leading-order contributions to the Hall conductivity. The solid lines represent the electron Green's function, wavy lines the fluctuation propagator, and red [dark gray] triangles electron scattering at impurities. In addition, the dotted purple [gray] lines takes into account the flux enclosed by the paths of all charged excitations. The x- and y-vertices are maked by "+" and "x", respectively. All other diagrams are similar to the conductivity diagrams 14, but with different vertices.

C. Asymptotic analysis and comparison to experiments

1. Region close to the line $H_{c2}(T)$

In the vicinity of the superconducting phase transition line at small enough magnetic fields, $h \ll t$, the leading correction to σ_{xy} is produced by the AL diagram:

$$\sigma_{xy}^{(fl)}(h,t) = \frac{2e^2 \varsigma T_{c0}\rho_{(0)}}{\pi}\,\mathrm{sgn}(h)t\sum_n (n+1)\frac{\left[\tilde{L}_n(0)-\tilde{L}_{n+1}(0)\right]^3}{\left[\tilde{L}_{n+1}(0)+\tilde{L}_n(0)\right]^2} \tag{66}$$

This correction is negative due to the fact that $\varsigma < 0$ for a superconducting film with three-dimensional electrons and a simple electron spectrum, and has a non-monotonic

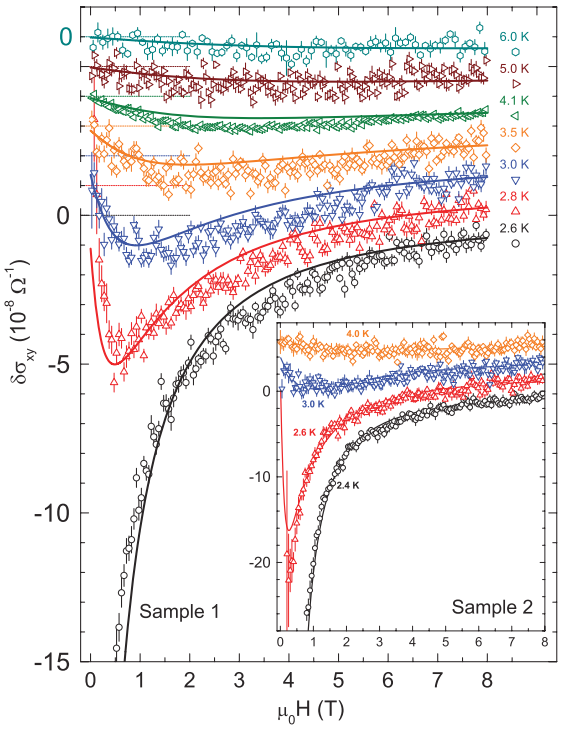

FIG. 22 (Color online) Experimental results for fluctuation Hall conductivity in two samples of TaN_x as a function of applied magnetic field for a range of temperatures near $T_c(H)$. The fitting is done in accordance with Eq. (66). *Reprinted figure with permission from Ref. (Breznay* et al., *2012). Copyright (2012) by the American Physical Society.*

dependence on the applied magnetic field, reaching a peak at $h^* = 1.3\epsilon$ in the close vicinity of T_{c0}.

The experimental results of (Breznay *et al.*, 2012) for the fluctuation correction to the Hall conductivity in ultrathin disordered films of TaN_x, calculated by subtracting the normal (linear in magnetic field) component from the total measured conductivity, are in excellent agreement with a fitting based on the AL correction, Eq. (66), which is dominant over a wide range of magnetic fields and temperatures in a region around the transition, as shown in Fig. (22).

In another recent experimental study (Breznay and Kapitulnik, 2013), the authors have also observed a significant fluctuation contribution to the Hall resistance (less the normal linear contribution) at $T > T_c(H)$. The results indicate the existence of a peak Hall resistance due to superconducting fluctuations observed at some H^* above the $H_c(T)$ line, see Fig. (23). This peak at H^*, as a function of temperature above the transition, starts to form at T_{c0} and shifts towards larger fields until at a temperatures $\sim T \sim 2T_{c0}$ the Hall effect from superconducting fluctuations becomes too weak and the peak is smeared out.

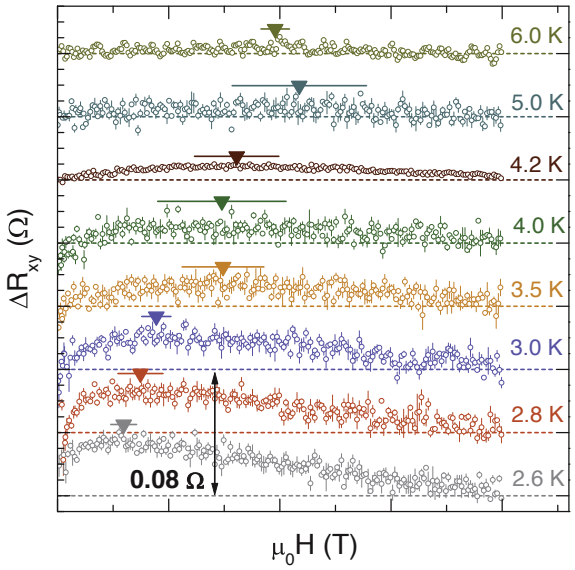

FIG. 23 (Color online) Experimental results for fluctuation Hall resistance in a TaN thin film as a function of applied magnetic field for a range of temperatures above $T_c(H)$ with marked peak at H^*. The normal-state contribution has been subtracted from R_{xy}. The curves are offset vertically for clarity, and a vertical scale bar of 0.08Ω is indicated. *Reprinted figure with permission from Ref. (Breznay and Kapitulnik, 2013). Copyright (2013) by the American Physical Society.*

2. Limit of weak fields

In the GL domains I–II, the sum over Landau levels in Eq. (66) can be replaced by a continuous integral, yielding the following complete correction to Hall conductivity:

$$\sigma_{xy}^{(fl)} = \frac{\varsigma\Omega_H e^2}{96}\frac{\mathrm{sgn}(h)}{(\epsilon+h)^2}. \tag{67}$$

Notice, that the divergence of the Hall conductivity near T_{c0}, $\sigma_{xy}^{(fl)} \sim 1/(\epsilon+h)^2$, is stronger than the one for the contribution to longitudinal conductivity, $\sigma_{xx}^{(fl)} \sim 1/(\epsilon+h)$.

Close to the $H_{c2}(0)$ line, in domain III, it is sufficient to consider only the contribution of the lowest Landau level, which yields:

$$\sigma_{xy}^{(fl)} = \frac{2\varsigma T_{c0}e^2}{\pi}\frac{\mathrm{sgn}(h)}{\epsilon+h}. \tag{68}$$

In the region of high temperatures and low fields, domain VIII, $t \gg 1 \gg h$, the contribution from the two diagrams shown in Fig. 21 dominates over the AL and DOS corrections, resulting in:

$$\sigma_{xy}^{(fl)} = \frac{\varsigma\omega_c^{(qp)}e^2}{4\pi^2}\,\mathrm{sgn}(h)\left[\ln\ln\frac{1}{T_{c0}\tau} - \ln\ln t\right]. \tag{69}$$

3. Limit of strong fields

In the vicinity of $H_{c2}(0)$, all of the above terms produce comparable contributions to the Hall conductivity. In the regime of classical fluctuations and classical-to-quantum transition (domains V–VI), the complete correction takes form

$$\sigma_{xy}^{(fl)} = \frac{2e^2}{\pi}\frac{\mathrm{sgn}\,(h)}{\tilde{h}}\left(\varsigma T - \frac{21T}{8\varepsilon_F}\right). \tag{70}$$

Notice, that the first term in Eq. (70) is in full agreement with Eq. (68), where $1/(\epsilon+h)$ in domain III turns into $1/\tilde{h}$ in domain VI. The second term in Eq. (70) comes from the anomalous MT contribution and does not contribute to the leading-order correction at weak fields.

In the quantum regime (domain IV), the fluctuation correction to Hall conductivity becomes:

$$\sigma_{xy}^{(fl)} = \frac{e^2}{2\pi^2}\,\mathrm{sgn}(h)\ln\tilde{h}\left(\frac{2\varsigma\Omega_H}{3} - \omega_c^{(qp)}\tau\right). \tag{71}$$

The results for the different domains of the phase diagram are summarized in Table V.

domain	$\sigma_{xy}^{(fl)}$
I-II	$\frac{\varsigma\omega_H e^2}{96}\frac{\mathrm{sgn}(h)}{(\epsilon+h)^2}$
III	$\frac{2\varsigma T_{c0}e^2}{\pi}\frac{\mathrm{sgn}(h)}{\epsilon+h}$
IV	$\frac{e^2}{2\pi^2}\,\mathrm{sgn}(h)\ln\tilde{h}\left(\frac{2\varsigma\Omega_H}{3} - \omega_c^{(qp)}\tau\right)$
V-VI	$\frac{2e^2}{\pi}\frac{\mathrm{sgn}\,(h)}{\tilde{h}}\left(\varsigma T - \frac{21T}{8\varepsilon_F}\right)$
VIII	$\frac{\varsigma\omega_c^{(qp)}e^2}{4\pi^2}\,\mathrm{sgn}\,(h)\left[\ln\ln\frac{1}{T_{c0}\tau} - \ln\ln t\right]$

TABLE V Asymptotic expressions for fluctuation corrections to the Hall conductivity in different domains of the phase diagram.

VII. FLUCTUATION NERNST-ETTINGSHAUSEN EFFECT

A. General expression for the fluctuation Nernst-Ettingshausen coefficient

The theoretical description of fluctuation contributions to the thermoelectric and thermomagnetic coefficients remains complex and controversial. Initially, the fluctuation contribution to the Seebeck coefficient in 3D superconductor was studied by Maki (Maki, 1973) in the framework of the time dependent Ginzburg-Landau equation, and it was found to be non-singular and negligibly small. After the discovery of an anomaly in the Seebeck coefficient behavior close to T_c in monocrystals of $YBa_2Cu_3O_{7-\delta}$ (Howson *et al.*, 1990) the problem was revisited both phenomenologically (Ullah and Dorsey, 1991) and microscopically (Reizer and Sergeev, 1994). Both papers confirmed Maki's conclusion that

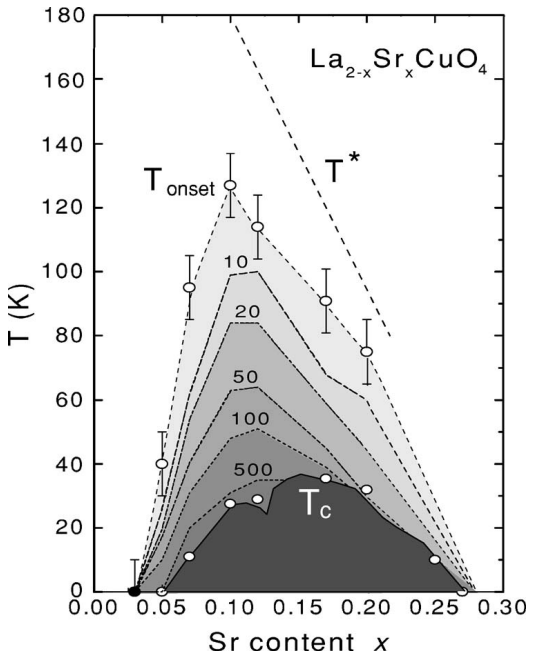

FIG. 24 The phase diagram of LSCO showing the Nernst region between T_c and $T_{\rm onset}$ (numbers on the contour curves indicate the value of the Nernst coefficient ν in nV/KT). The curve of $T_{\rm onset}$ vs. x has end points at $x = 0.03$ and $x = 0.26$ and peaks conspicuously near 0.10. The dashed line is T^* estimated from heat-capacity measurements. *Reprinted figure with permission from (Wang* et al.*, 2006). Copyright (2006) by the American Physical Society.*

the fluctuation correction to the Seebeck coefficient is proportional to the degree of particle-hole asymmetry. Yet, the authors found that in the 2D case it logarithmically depends on the closeness to T_{c0}: $S^{(\rm fl)}_{(2)} \sim (T/E_{\rm F}) \ln\left[T_{c0}/\left(T - T_{c0}\right)\right]$.

The fluctuation Nernst-Ettingshausen (NE) effect was initially studied in the framework of the GL approach in Ref. (Ullah and Dorsey, 1991). The authors demonstrated that the FCP contribution to the NE coefficient, despite being very similar to the thermoelectric coefficient, does not contain the smallness induced by the particle-hole asymmetry $(T/E_{\rm F})$ and close to the transition exhibits a much stronger temperature dependence: $\nu^{(\rm fl)}_{(2)} \sim T_{c0}/\left(T - T_{c0}\right)$.

The discovery of the giant Nernst signal in underdoped phases of high temperature superconductor LSCO (Wang *et al.*, 2006; Xu *et al.*, 2000), see Fig. 24, (with critical temperatures around 30K) triggered great interest, both, of theorists and experimentalists. The authors reported an anomalously enhanced Nernst signal at temperatures as high as 150K and attributed this phenomenon to the specific physics of HTS. Since the NE effect in type II superconductors below $T_{\rm c}$ is related to the entropy transport by moving vortices they hypothesized the presence of strong phase fluctuations in the pseudogap phase. Such fluctuations do not destroy the pseudogap but the Meissner effect. Later this idea was supported theoretically by Refs. (Podolsky *et al.*, 2007; Raghu *et al.*, 2008; Tan and Levin, 2004), while in Ref. (Hartnoll *et al.*, 2007) the anomalously large NE effect was attributed to the proximity of the system to a quantum critical point.

Being inspired by the new experimental findings by Ong's group, Ussishikin et al. (Ussishkin, 2003; Ussishkin and Sondhi, 2004; Ussishkin *et al.*, 2002) revisited the problem of the calculation of the NE coefficient in the fluctuation regime. In these papers the authors, besides reproducing the linear response theory results of Ref. (Ullah and Dorsey, 1991), emphasized importance of the fluctuation magnetization currents flowing in the sample subject of applied magnetic field and gradient of temperature. Taking into account their contribution to the heat flow, they demonstrated that this results in a thrice lower value of the NE coefficient compared to what was predicted in the vicinity of T_{c0} by Ullah and Dorsey (Ullah and Dorsey, 1991).

Later, giant Nernst signals were also discovered in superconducting films (Pourret *et al.*, 2006a, 2007), which are well-described by the usual BCS model. Therefore, they provide an indication that superconducting fluctuations are likely to be a key to understanding the underlying physics of the giant thermomagnetic response. Below we will concentrate on the properties of conventional type-II superconductor, abstaining from the specifics of underdoped phases of HTS.

The complete microscopic analysis of the fluctuation NE signal through the whole phase diagram was performed by Serbyn *et al.* (Serbyn *et al.*, 2009) in the framework of the Matsubara diagrammatic technique, while the quantum kinetic approach was developed by Michaeli and Finkel'stein (Michaeli and Finkel'stein, 2009a,b). It was shown in these papers that the role of magnetization currents turns out to be even more important in the regime of quantum fluctuations. Indeed, the restriction of the straightforward calculus of the Kubo-like response contribution to the heat flow (Mahan, 2013) results in the violation of the third law of thermodynamics which can only be rectified by taking into account the fluctuating Meissner magnetization above $H_{c2}(0)$.

1. Definition of the NE coefficient

Let us review the definition of transport coefficients and consider a conductor placed in magnetic field $\mathbf{H}$, subjected to an applied temperature gradient ∇T. The electric and heat transport currents in it are related to the applied weak-enough electric field and temperature gradient by means of the relations:

$$\mathbf{j}^{(e)}_{{\rm tr},\alpha} = \sigma^{\alpha\delta}(\mathbf{H})\mathbf{E}_\delta + \beta^{\alpha\delta}(\mathbf{H})\nabla_\delta T\,, \qquad (72)$$

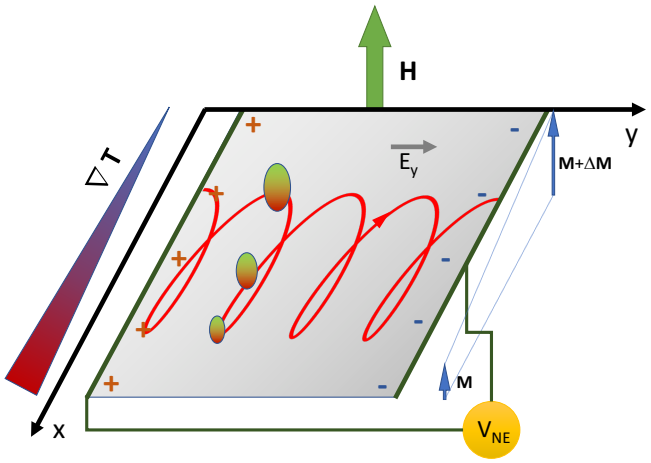

FIG. 25 (Color online) Schematic representation of the FCP motion in a superconducting film subjected to a temperature gradient along its x-axis. The concentration and size of FCPs vary with temperature. The local magnetization parallel to the external magnetic field varies along x-axis as well. The spatial inhomogeneity of the magnetization leads to a transformation of the FCP trajectories from circular to trochoidal, which is why the magnetization currents appear. To compensate these currents a voltage is induced in y-direction that provides a sizable contribution to the fluctuation NE coefficient.

$$\mathbf{j}^{(h)}_{\mathrm{tr},\alpha} = \gamma^{\alpha\delta}(\mathbf{H})\mathbf{E}_\delta - \kappa^{\alpha\delta}(\mathbf{H})\nabla_\delta T\,, \tag{73}$$

where $\beta^{\alpha\beta}(\mathbf{H}), \gamma^{\alpha\beta}(\mathbf{H})$ and $\kappa^{\alpha\beta}(\mathbf{H})$ are thermoelectricity and heat conductivity tensors (here we use two superscripts for tensors and subscripts for vector components). Thermoelectric tensors $\beta^{\alpha\beta}$ and $\gamma^{\alpha\beta}$ are connected by the Onsager relation: $\gamma^{\alpha\beta}(\mathbf{H}) = -T\beta^{\alpha\beta}(-\mathbf{H})$. Let us mention, that the validity of the Onsager relation follows from the principle of the symmetry of transport coefficients, which is based on the invariance of the quantum mechanical equations with respect to time-reversal.

The off-diagonal components of the tensor $\beta^{\alpha\beta}$ in the absence of a magnetic field are equal to zero. If besides a temperature gradient ∇T, also a magnetic field $\mathbf{H}$ is applied to the sample, a potential difference $V^{(\mathrm{NE})}$ along y axis appears. The circuit in this direction is supposed to be broken. The corresponding open circuit conditions are: $\nabla_x T \neq 0$, $\mathbf{j}^{(\mathrm{h})}_{\mathrm{tr,x}} = \mathbf{j}^{(\mathrm{e})}_{\mathrm{tr,x}} = \mathbf{j}^{(\mathrm{e})}_{\mathrm{tr,y}} = 0$, see Fig. 25. This, so called Nernst-Ettingshausen (or Nernst) effect, [10] is well pronounced in semiconductors but is usually small in good metals. It is characterized by the NE coefficient which can be expressed by means of the conductivity and thermoelectric tensors [11]:

$$\nu = \frac{E_y}{(-\nabla_x T)\,H} = \frac{1}{H}\frac{\beta^{\mathrm{xy}}\sigma_{\mathrm{xx}} - \beta^{\mathrm{xx}}\sigma_{\mathrm{xy}}}{(\sigma_{\mathrm{xx}})^2 + (\sigma_{\mathrm{xy}})^2}\,. \tag{74}$$

Usually, when the Hall component of conductivity $\sigma_{\mathrm{xy}} \ll \sigma_{\mathrm{xx}}$, while both β^{xx} and β^{xy} are of the same order, Eq. (74) relates directly the NE coefficient to the off-diagonal component of the thermoelectric tensor

$$\nu(T,H) = R_\square \beta^{\mathrm{xy}}(T,H)/H\,, \tag{75}$$

where $R_\square = (\sigma_{\mathrm{xx}})^{-1}$ is the sheet resistance of the film. In the case under consideration, the validity of approximation (75) is even more justified, considering the excess of the off-diagonal thermoelectricity compared to the diagonal one.

2. Onsager relations and magnetization currents

It is well known that the absence of free electron magnetism in the classical theory is explained by the compensation of the total current created by the electrons moving along closed trajectories in the bulk of the sample by the current of the electrons moving along the open "hopping" trajectories close to its surface. In quantum theory such a compensation does not occur (Teller, 1931) and Landau diamagnetism (Landau, 1930) takes place. In the middle of the 20th century a lively debate concerning the fulfillment of reciprocal Onsager relations in metals and semiconductors subjected to a magnetic field and gradient of temperature was taking place (see Ref. (Obraztsov, 1964) and references therein). Yu.N. Obraztsov demonstrated that microscopic surface currents inducing electron magnetization can contribute considerably to the density of the macroscopic current when a temperature gradient is applied to the sample. Taking corresponding contributions to the heat and electric currents flowing in the system into account, restores the fulfillment of the reciprocal Onsager relations and validity of the third low of thermodynamics.

The contribution to the electric current can be easily expressed using Ampere's law as

$$\mathbf{j}^{\mathrm{mag}} = \frac{c}{4\pi}\nabla \times \mathbf{B}\,,$$

where $\mathbf{B} = \mathbf{H} + 4\pi\mathbf{M}$, $\mathbf{H}$ is the spatially homogeneous external magnetic field, $\mathbf{M}$ is the local value of magnetization. In the presence of a temperature gradient $\nabla_x T$ one can express the magnetization current as (Obraztsov, 1964; Ussishkin *et al.*, 2002)

$$j^{\mathrm{mag}}_y = -c\,(dM_z/dT)\,\nabla_x T\,,$$

[10] The Nernst-Ettingshausen effect is closely related to the Ettingshausen effect, which is just the opposite: it consists in the appearance of a temperature gradient in a conductor placed in a magnetic field, when an electric current is applied.

[11] The Nernst signal is related to the NE coefficient through the simple relation $\mathfrak{N} = \nu H$.

and the thermoelectric tensor $\beta^{\alpha\delta}(\mathbf{H})$ in Eq. (72) acquires besides its kinetic part $\widetilde{\beta}^{\alpha\delta}(\mathbf{H})$ also a magnetization contribution $\beta^{\alpha\delta}_{\rm M} = \epsilon^{\alpha\beta\zeta} c dM_\zeta/dT$:

$$\beta^{\alpha\delta}(\mathbf{H}) = \widetilde{\beta}^{\alpha\delta}(\mathbf{H}) + \epsilon^{\alpha\beta\zeta} c \frac{dM_\zeta}{dT} \tag{76}$$

with $\epsilon^{\alpha\beta\zeta}$ being the Levi-Civita symbol. In the case of NE geometry the above mentioned open circuit condition holds: $\mathbf{j}^{(e)}_{\rm tr,y} = 0$ and in full analogy to the classical Hall effect, the magnetization current in y direction is compensated by the current induced through the Nernst-Ettingshausen voltage: $E^{\rm NE}_{\rm y} = R_\square j^{\rm mag}_{\rm y}$.

The transport heat current (73) is also affected by magnetization currents. In the presence of a magnetic field, the measurable transport heat current $\mathbf{j}^{(h)}_{\rm tr}$ differs from the microscopic heat current $j^{(h)}$ by the circular magnetization current $\mathbf{j}^{(h)}_{\rm M} = c\mathbf{M}\times\mathbf{E}$, see (Larkin and Varlamov, 2009). As a result, the thermoelectric tensor $\gamma^{\alpha\delta}$ relating $\mathbf{j}^{(h)}_{\rm tr}$ with the applied electric field can be found as the sum of the kinetic, $\widetilde{\gamma}^{\alpha\delta}$, and thermodynamic, $\gamma^{\alpha\delta}_{\rm M} = \epsilon^{\alpha\delta\zeta} c M_\zeta/T$ contributions:

$$\gamma^{\alpha\delta} = \widetilde{\gamma}^{\alpha\delta} + \epsilon^{\alpha\delta\zeta} c M_\zeta/T\,. \tag{77}$$

The reciprocal Onsager relations in this interpretation acquire the form:

$$\widetilde{\gamma}^{\alpha\delta}(H) + \epsilon^{\alpha\delta\zeta}\frac{cM_\zeta(H)}{T} = -T\left[\widetilde{\beta}^{\alpha\delta}(-\mathbf{H}) + \epsilon^{\alpha\delta\zeta} c\frac{dM_\zeta(-\mathbf{H})}{dT}\right]. \tag{78}$$

Hence, in order to find the NE coefficient (see Eq. (75)) one can calculate $\widetilde{\gamma}^{\alpha\delta}(-H)$ instead of $\widetilde{\beta}^{\alpha\delta}(\mathbf{H})$ and obtain

$$\nu(T,H) = -R_\square \frac{\widetilde{\gamma}^{\rm xy}(H) + cM_z(H)/T}{TH}\,. \tag{79}$$

This way turns out to be much more straight-forward using the microscopic approach.

3. Microscopic expression for fluctuation NE coefficient

Here we review the microscopic calculation of the NE coefficient. In the spirit of the Kubo formalism one can relate the electron heat current $\mathbf{j}^{(h)}_{\rm tr}$ to the value of the heat current operator averaged over quantum and thermal states applied to the one-electron Green's function. Expansion of the latter in the electric field relates the tensor $\gamma^{\alpha\delta}(\mathbf{H})$ to the loop of two electron Green functions separated by the heat and electromagnetic field vertexes (analogously to the loop for electro-magnetic field operator for the conductivity tensor):

$$\tilde{\gamma}^{\alpha\delta} = -\lim_{\omega\to 0}\frac{{\rm Im}\widetilde{Q}^R_{\alpha\delta}(-i\omega+0)}{\omega}\,.$$

The electric – heat current correlation function $\widetilde{Q}_{\alpha\delta}(\omega_k)$ is calculated first at bosonic Matsubara frequencies $\omega_k = 2\pi T k$ and then analytically continued to real frequencies.

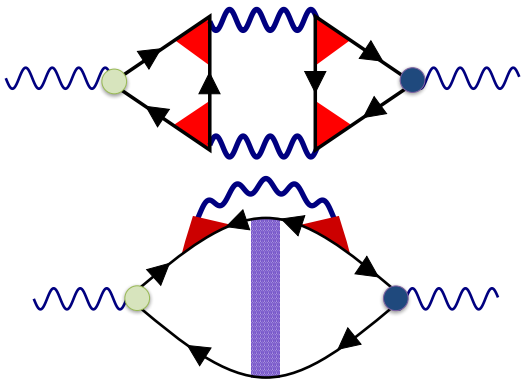

FIG. 26 (Color online) The Aslamazov-Larkin (top) and diffusion coefficient renormalization (DCR, bottom) diagrams for the thermoelectric response $\tilde{\gamma}^{\rm xy}$. The DCR diagram has a symmetric counterpart. The green and blue [light and dark gray] circles correspond to the different heat and electric vertexes, the triangular and rectangular blocks represent impurity interaction, and wavy lines denote the fluctuation propagator. After Ref. (Glatz and Varlamov, 2017).

The fluctuation part of the electric – heat current correlation function $\widetilde{Q}^{(\text{fl})}_{\alpha\delta}(\omega_k)$ is graphically represented by the same ten diagrams of Fig. 14, but taken with vertices as in Fig. 26. These were analyzed in detail in Ref. (Serbyn *et al.*, 2009). The authors found that in the case of the NE effect, the Maki-Thompson contribution exactly becomes zero. The contribution of the DOS diagrams turns out to be less singular than that one corresponding to the diagrams containing three Cooperons (DCR, see Fig. 26). The positive Aslamazov-Larkin (AL) term dominates in the GL region and competes with the negative DCR contribution everywhere else. The fluctuation magnetization has been discussed above. Finally, the general expression for the NE coefficient of 2D superconductors, valid beyond the line $H_{c2}(T)$ takes form:

$$\nu^{(\mathrm{fl})}=\frac{\beta_0 R_\square}{8H}\left[\eta\sum_{m=0}^{M_t}(m+1)\sum_{k=0}^{\infty}\left\{\left(\frac{3}{\mathcal{E}_m}+\frac{1}{\mathcal{E}_{m+1}}\right)\left(\mathcal{E}'_m-\mathcal{E}'_{m+1}\right)+\left[\eta\left(2m+1\right)+k\right]\frac{\mathcal{E}''_m}{\mathcal{E}_m}+\left[\eta(2m+3)+k\right]\frac{\mathcal{E}''_{m+1}}{\mathcal{E}_{m+1}}\right\}\right. \tag{80}$$

$$+4\pi^2\sum_{m=0}^{M_t}(m+1)\int_{-\infty}^{\infty}\frac{dx}{\sinh^2\pi x}\left\{\frac{\eta\,\mathrm{Im}\,\mathcal{E}_m\,\mathrm{Im}\left(\mathcal{E}_m+\mathcal{E}_{m+1}\right)+\left[\eta(m+1/2)\,\mathrm{Im}\,\mathcal{E}_m+x\,\mathrm{Re}\,\mathcal{E}_m\right]\mathrm{Im}\left(\mathcal{E}_{m+1}+\eta\mathcal{E}'_m-\mathcal{E}_m\right)}{|\mathcal{E}_m|^2}\right.$$

$$\left.+\frac{\eta\,\mathrm{Im}\,\mathcal{E}_{m+1}\,\mathrm{Im}\left(\mathcal{E}_m+\mathcal{E}_{m+1}\right)+\left[\eta(m+3/2)\,\mathrm{Im}\,\mathcal{E}_{m+1}+x\,\mathrm{Re}\,\mathcal{E}_{m+1}\right]\mathrm{Im}\left(\mathcal{E}_{m+1}+\eta\mathcal{E}'_{m+1}-\mathcal{E}_m\right)}{|\mathcal{E}_{m+1}|^2}+4x\,\mathrm{Im}\ln\frac{\mathcal{E}_m}{\mathcal{E}_{m+1}}\right.$$

$$\left.\left.-2\frac{\mathrm{Im}\left(\mathcal{E}_m+\mathcal{E}_{m+1}\right)\left(\mathrm{Im}\,\mathcal{E}_m\,\mathrm{Im}\,\mathcal{E}_{m+1}+\mathrm{Re}\,\mathcal{E}_m\,\mathrm{Re}\,\mathcal{E}_{m+1}\right)}{|\mathcal{E}_{m+1}|^2|\mathcal{E}_m|^2}\left[\eta\left(m+\frac{3}{2}\right)\mathrm{Im}\,\mathcal{E}_{m+1}-\eta\left(m+\frac{1}{2}\right)\mathrm{Im}\,\mathcal{E}_m+x\,\mathrm{Re}\left(\mathcal{E}_{m+1}-\mathcal{E}_m\right)\right]\right\}\right],$$

where $\eta=\frac{4h}{\pi^2 t}$ and $\beta_0=k_{\mathrm{B}}e/\pi\hbar=6.68$ nA/K is the quantum of thermoelectric conductance.

B. Asymptotic analysis

The effect of SF on the Nernst-Ettingshausen coefficient is demonstrated in Fig. 27, where a surface plot of $\nu^{(\mathrm{fl})}(T,H)$ according to Eq. (80) is shown. We start discussion with its asymptotic expressions, which are summarized in table VI.

domain	$\frac{H}{\beta_0 R_\square}\nu^{(\mathrm{fl})}$
I	$\frac{2eH\xi^2_{\mathrm{GL}}(T)}{3c}=\frac{2eH\xi^2}{3c}\frac{1}{\epsilon}$
II	$1-(\ln 2)/2$
III	$\frac{1}{\epsilon+h}$
IV	$-\frac{2\gamma_{\mathrm{E}}}{9}\frac{t}{\tilde{h}}$
V	$\ln\frac{t}{\tilde{h}}$
VI	$\frac{8\gamma^2_{\mathrm{E}}}{3}\frac{t^2}{\tilde{h}(t)}$
VII	$\frac{1}{\tilde{h}(t)}\left[1+\frac{2h_{c2}(t)}{\pi^2 t}\frac{\psi''(\frac{1}{2}+\frac{2h_{c2}(t)}{\pi^2 t})}{\psi'(\frac{1}{2}+\frac{2h_{c2}(t)}{\pi^2 t})}\right]$
VIII	$\frac{4e\xi^2 H}{3\pi^2 c}\frac{1}{t\ln t}$
IX	$\frac{\pi^2}{48}\frac{t}{\tilde{h}\ln\tilde{h}}$

TABLE VI Asymptotic expressions for fluctuation corrections to the NE coefficient in different domains of the phase diagram.

Close to the critical temperature T_{c0}, where fluctuations have thermal character (GL domains I-III), only the AL contribution is essential, which takes magnetization currents into account. In the limit of vanishingly small magnetic fields $h\ll\epsilon$ (domain I), the numerical factor in the coefficient of the NE signal slightly varies in Refs. (Michaeli and Finkel'stein, 2009b; Reizer and Sergeev, 1994; Serbyn *et al.*, 2009; Ussishkin, 2003; Ussishkin *et al.*, 2002). This difference between GL and microscopic approaches may signal, e.g. a problem with the definition of the heat currents within the time-dependent Ginzburg-Landau theory and diagrammatics. The exact origin of this discrepancy presently remains unclear. In the limit of relatively strong fields in the GL region $\epsilon\ll h$ (domain II) and approaching the transition line $(H-H_{c2}(T)\ll H_{c2}(T)$ (domain III), the NE signal diverges.

Next, we look at the low-temperature regime close to the upper critical field $H_{c2}(0)$ (domains IV–VI in Fig. 9). Here the role of the magnetization term becomes crucial: The cancellation of the $1/T$-divergence by magnetization currents ensures that the third law of thermodynamics holds, and the total NE coefficient remains finite in the $T\to 0$ limit. In the purely quantum limit of vanishing temperature and away from $H_{c2}(0)$ ($t\ll\tilde{h}$, domain IV), $\nu^{(\mathrm{fl})}$ is negative, linear in temperature and diverges as $\tilde{h}^{-1}$ approaching the transition point. One can see from table VI that it coincides with our qualitative estimation Eq. (22). This change of sign in the thermoelectric response is similar to the negative fluctuation conductivity close to the quantum phase transition in the vicinity of $H_{c2}(0)$ found in Ref. (Galitski and Larkin, 2001a) (compare inserts in Figs. 15 and 27). The sign change is due to the DCR contribution, which is larger than the positive AL term in this region. In the quantum-to-classical crossover region, where H approaches $H_{c2}(T)$ but remains finite ($t^2/\ln(1/t)\ll\tilde{h}\ll t$, domain V), the NE coefficient becomes positive and less singular. Increasing the temperature one goes over into the region of thermal fluctuations. Moving further along the line $H_{c2}(T)(\tilde{h}\ll t^2/\ln(1/t)$ (domain VI), one sees that the NE signal grows. Eq. (80) allows for to study the full classical region just above the transition line, which covers a wide range of temperatures and magnetic fields ($\tilde{h}\ll 1$, domain VII). Close to T_c, the expression obtained matches that one valid in domain III (here $\tilde{h}(t)=\epsilon+h$), while in the limit $T\to 0$ it matches the asymptotic expression, provided that $\tilde{h}\ll t^2/\ln(1/t)$.

Finally, we address the "non-singular" domains VIII and IX far from the transition line. In these limits, the Kubo contribution $\tilde{\gamma}^{\mathrm{xy}}$ diverges as $[\ln\ln(1/T_{c0}\tau)-\ln\ln\max(h,t)]$, with $1/\tau$ playing the role of an ultraviolet cutoff of the Cooperon modes. Remarkably, the same divergence with opposite sign occurs in the magnetization contribution $\gamma^{\mathrm{xy}}_{\mathrm{M}}$. Hence, the total expression for $\nu^{(\mathrm{fl})}$ remains finite (see table VI). We see that even far from the transition, the fluctuation Nernst signal can be

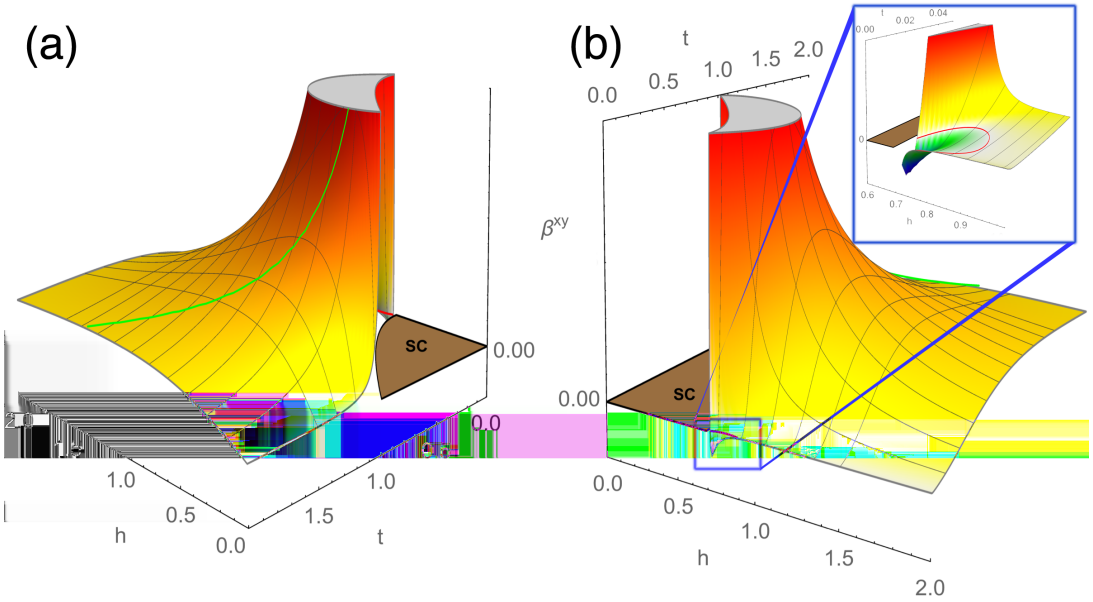

FIG. 27 (Color online) The magnetic field and temperature dependence of the fluctuation part of the Nernst coefficient. (a) shows a view from the $h = 0$ plane with ghost field line in green [light gray] indicating the maximum of Nernst coefficient for constant t. (b) shows a view from the $t = 0$ plane with a zoom close to the quantum fluctuation region at $h = h_{c2}$. The red [dark gray] line indicates the contour where the Nernst coefficient becomes zero. After Ref. (Glatz and Varlamov, 2017).

comparable or even parametrically larger than the Fermi liquid terms. In fact, it is conceivable that in some materials the Cooper channel contribution to thermal transport dominates even in the absence of any superconducting transition (e.g., if it is "hidden" by another order).

C. Fluctuation spectroscopy: analysis of Nernst signal measurements

As mentioned above, numerous experimental studies of the last two decades have revealed an anomalously strong thermomagnetic signal, both, in the normal state of high-temperature superconductors (HTS) (Capan *et al.*, 2002; Li and Greene, 2007; Tafti *et al.*, 2014; Wang *et al.*, 2006, 2002, 2001; Wen *et al.*, 2003; Xu *et al.*, 2000, 2005) and conventional superconducting films (Pourret *et al.*, 2006a, 2007), see Fig. 28. In experiments on $La_{2-x}Sr_xCuO_4$ HTS compounds, the Nernst-Ettingshausen (NE) signal, $\mathfrak{N}$, exceeded the background value a hundred times close to the superconducting transition and a sizable effect remained even up to 130 K, well above the transition temperature, T_{c0}. Surprisingly, in experiments on conventional superconductor $Nb_{0.15}Si_{0.85}$ (Pourret *et al.*, 2006a, 2007) the value of the excess signal transcended the expected magnitude according to the classical Sondheimer theory (Sondheimer, 1948) not by a hundred but a few thousand times. Such observations were especially striking in view of the previously recorded data on the magnitude of the Seebeck coefficient in the normal state of superconductors, undergoing a weak singular decrease close to T_{c0} but remaining on the same order of magnitude as in the normal phase (Howson *et al.*, 1990; Lowe *et al.*, 1993; Ri *et al.*, 1994). These and further similar experiments have sparked the interest in thermomagnetic phenomena beyond the superconducting state.

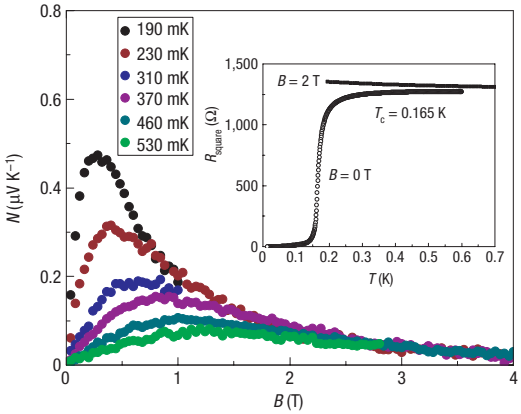

FIG. 28 (Color online) Nernst signal (labeled N in the figure, $\mathfrak{N}$ in the text) measured in a $Nb_{0.15}Si_{0.85}$ film as a function of magnetic field for temperatures ranging from 0.19K to 5.8K, for a sample with $T_c = 0.165$K (Pourret *et al.*, 2006a). A finite Nernst signal is present for $T > T_c$. With increasing temperature, this signal decreases in magnitude and becomes more linear in field. *Reprinted by permission from Macmillan Publishers Ltd: Nature Physics (Pourret* et al., *2006a), copyright (2006).*

One of the reasons of this interest is that the mea-

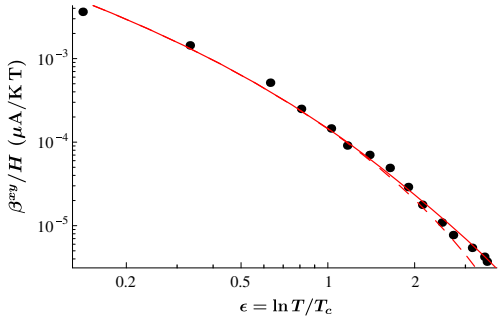

FIG. 29 (Color online) Comparison with experiment. Circles: experimental data for the fluctuation part of the NE coefficient vs. $\epsilon = \ln T/T_c$ obtained for the 12.5-nm-thick $Nb_{0.15}Si_{0.85}$ film (Pourret *et al.*, 2006a). Dashed line: theoretical prediction for the strictly 2D geometry. Solid line: theoretical prediction for the sample with 2D-3D crossover taken into account. The only adjustable parameter in this fit is the diffusion coefficient – here 0.087 cm^2/s. After Ref. (Serbyn *et al.*, 2009).

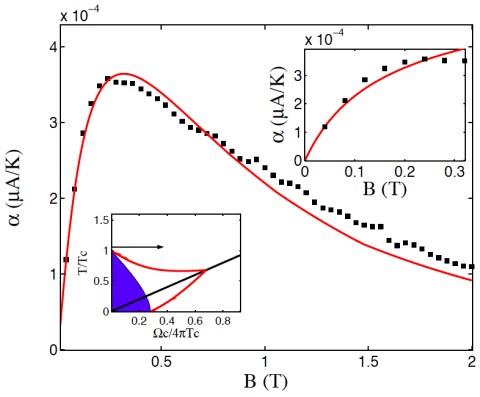

FIG. 30 (Color online) Comparison with experiment. The Nernst signal (labeled α, $\mathfrak{N}$ in the text) as function of the magnetic field measured at $T = 410mK$. The black squares correspond to the experimental data of Ref. (Pourret *et al.*, 2006a) while the solid line describes the theoretical result of Ref. (Michaeli and Finkel'stein, 2009a). The arrow on the phase diagram illustrates the direction of the measurement. In the insert the low magnetic field data are fitted with the theoretical curve. *Reprinted by permission from IOP Publishing: Europhysics Letter (Michaeli and Finkel'stein, 2009a), Fig. 5, copyright (2009).*

sured fluctuation effects exceed Sondheimer's evaluation of the normal phase quasiparticle contribution by orders of magnitude. Close to the critical temperature and in sufficiently weak magnetic fields the experimental findings are in a good agreement – see Ref. (Behnia and Aubin, 2016) – with results obtained in the simple GL approximation (Ullah and Dorsey, 1991; Ussishkin *et al.*, 2002). Moreover, since the fluctuation Nernst signal can be observed in a wide temperature range, one can compare experimental data with the predictions of the microscopic theory (Michaeli and Finkel'stein, 2009a; Serbyn *et al.*, 2009) in detail.

1. Giant Nernst signal in NbSi

In Fig. 29 a comparison between the theory of Ref. (Serbyn *et al.*, 2009) and the magnitude of the experimentally measured Nernst coefficient (Pourret *et al.*, 2006a) in weak fields is plotted for a $Nb_{0.15}Si_{0.85}$ film of thickness $d = 12.5$ nm in a wide range of temperatures up to $30\,T_{c0}$. The dashed line corresponds to the theoretically calculated Nernst coefficient (Ref. (Serbyn *et al.*, 2009)). A diffusion coefficient of 0.087 cm^2/s, which is 60% of that reported in Ref. (Pourret *et al.*, 2006a) is used for the fitting. Far from the transition temperature ($\epsilon > 2$), the superconducting coherence length $\xi(T)$ becomes shorter than d and the 3D nature of the diffusion manifests itself. Taking this fact into account, noticeably improves the fitting (see the solid line in Fig. 29).

In Fig. 30 an excellent agreement between the theory of Ref. (Michaeli and Finkel'stein, 2009a) and the measurements of the Nernst signal (performed on the same $Nb_{0.15}Si_{0.85}$ film) as a function of the magnetic field is demonstrated.

2. Analysis of the ghost critical field

The characteristic feature of the fluctuation Nernst signal is its non-monotonic behavior as a function of the magnetic field. One can see from the first row of Table VI that close to T_{c0}, the Nernst signal is proportional to the magnetic field and quadratically dependent on the GL coherence length. As long as the magnetic field is relatively small, the effective size of FCPs remains to be determined by $\xi_{GL}(\epsilon)$ and is fixed by temperature. However, when the magnetic field increases and consequently the magnetic length $\ell_H = \sqrt{c/2eH}$ of the FCPs becomes comparable to $\xi_{GL}(\epsilon)$, the former gradually takes on the role of the characteristic size of FCP. Such field-induced shrinking of the fluctuations characteristic scale is well-known since the early studies of fluctuating diamagnetism (Behnia and Aubin, 2016; Gollub *et al.*, 1973; Prange, 1970; Schmid, 1969; Skocpol and Tinkham, 1975). As a result, the Nernst signal reaches its maximum at some field $H^*(T)$ and decreases when the magnetic field further increases.

Pourret et al. (Pourret *et al.*, 2006a) were the first who measured such isothermal curves (see Fig. 31) and also determined the temperature dependence $H^*(T)$ for the temperatures several times exceeding T_{c0}. They identified $H^*(T)$ with the field when $\ell_H = \sqrt{c/(2eH^*)} \sim \xi_{GL}(\epsilon)$ and, following Kapitulnik et al (Kapitulnik *et al.*, 1985), called the curve $H^*(\epsilon)$ as the "mirror field" (other authors call it the "ghost critical field"; in the vicinity of T_{c0} it is indeed symmetrical to the line $H_{c2}(\epsilon)$).

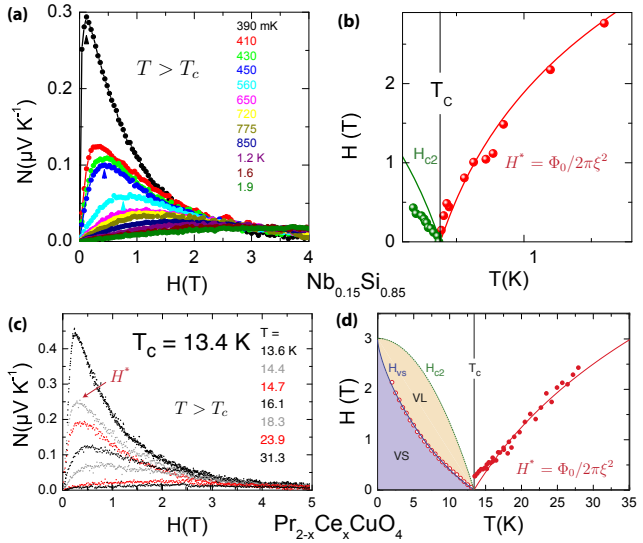

FIG. 31 (Color online) Nernst signal (labeled N in the plots, $\mathfrak{N}$ in the text) (a) in the conventional superconductor $Nb_{0.15}Si_{0.85}$ and (c) in the HTS $Pr_{2-x}Ce_xCuO_4$ measured above critical temperature (taken from the Refs. (Pourret *et al.*, 2006a; Tafti *et al.*, 2014)) and the related temperature dependencies of the corresponding maxima, labeled H^* (the "ghost critical field") in panels (b) and (d), respectively. *Reprinted by permission from IOP Publishing: Reviews of Progress in Physics (Behnia and Aubin, 2016), Fig. 7, copyright (2016).*

Moreover, recalling that ϵ in the microscopic theory is the asymptotic expression of the $\ln T/T_{c0}$, the authors of Ref. (Pourret *et al.*, 2006a) extended their fitting also to temperatures beyond the GL region.

The study of temperature dependence of $H^*(T)$ acquired special significance for HTS compounds. Recently, the authors of Ref. (Tafti *et al.*, 2014; Yamashita *et al.*, 2015) have proposed using it for the precise determination of the second critical field $H_{c2}(0)$, often unaccessible for direct measurements because of its huge value. The analysis of the experimental data obtained on the HTS compound $Pr_{2-x}Ce_xCuO_4$ led the authors of Ref. (Tafti *et al.*, 2014) to propose for the temperature dependence of the "ghost critical field" a phenomenological expression:

$$H^*(T) = H_{c2}(0) \ln \frac{T}{T_{c0}} \,. \tag{81}$$

The prefactor $H_{c2}(0)$ was chosen as a single empirical parameter that characterizes the strength of superconductivity. The authors stated that "the characteristic field scale encoded in superconducting fluctuations above T_c", is equal to the field needed to kill superconductivity at $T = 0$K. I.e. a straightforward empirical procedure for measuring of the fundamental field scale for superconductivity from superconducting fluctuations above T_{c0} was proposed.

The complete expression, Eq. (80), unfortunately does not allow one to extract the temperature dependence of the ghost field, $H^*(T)$, analytically. Nevertheless, due to its specific scaling form, the temperature dependence of the magnetic field corresponding to the maximum of the Nernst signal can be expressed in the very generic way (Kavokin and Varlamov, 2015):

$$H^*(T) = H_{c2}(0) \left(\frac{T}{T_{c0}}\right) \varphi\left(\ln \frac{T}{T_{c0}}\right) , \tag{82}$$

where $\varphi(x)$ is some smooth function which satisfies the condition $\varphi(0) = 0$.

We note that Eq. (82) coincides with Eq. (81) only in the particular case of $\varphi(x) = x \exp(-x)$. In the case of any other analytical function $\varphi(x)$, the magnetic field corresponding to the maximum of the NE signal, $H^*(T)$, would increase mainly linearly with the growth of temperature.

Let us recall, that the heuristic justification of Eq. (81) is based on the statement that the maximum in the NE signal magnetic field dependence occurs where the FCP size $\xi_{GL}(T)$ is of the order of its magnetic length $\ell_{H^*} = (c/2|e|H^*)^{1/2}$. Close to the critical temperature, this indeed yields $H^* \sim H_{c2}(0)\,(T - T_{c0})\,/T_{c0} \approx H_{c2}(0) \ln \frac{T}{T_{c0}}$. Far from T_{c0} the authors of (Pourret *et al.*, 2006a; Tafti *et al.*, 2014; Yamashita *et al.*, 2015) extend the GL expression as $\xi_{GL}(T) = \xi_{BCS}/\sqrt{\ln \frac{T}{T_{c0}}}$, which brings them to Eq. (81). We believe that this extension misses some justification, and the microscopically obtained Eq. (80) has to be investigated for its extrema.

However, it is possible to extract the ghost field from Eq. (80) numerically. The result is shown in Fig. 32. In addition to this numerically extracted curve, we plotted scaled experimental data from Refs. (Chang *et al.*, 2012) on Eu-LSCO and from (Tafti *et al.*, 2014) on doped PCCO. The latter is in fact fitted better by the maximum of Eq. (80) than the phenomenological curve (81) in its lower temperature range. The former data set also shows a rather linear behavior at higher temperatures with a slope of 0.35.

VIII. FLUCTUATION PSEUDOGAP AND LOW BIAS ANOMALY

A. Fluctuation depletion of the electron DOS

According to the microscopic BCS theory (Bardeen *et al.*, 1957a,b), the superconducting state is characterized by a gap in the quasiparticle spectrum centered around the Fermi level, which vanishes along the transition line $H_{c2}(T)$. However, it was predicted as early as in 1970 (Abrahams *et al.*, 1970) that thermal fluctuations result in a noticeable suppression of the DOS in a narrow energy range around the Fermi level even in the normal

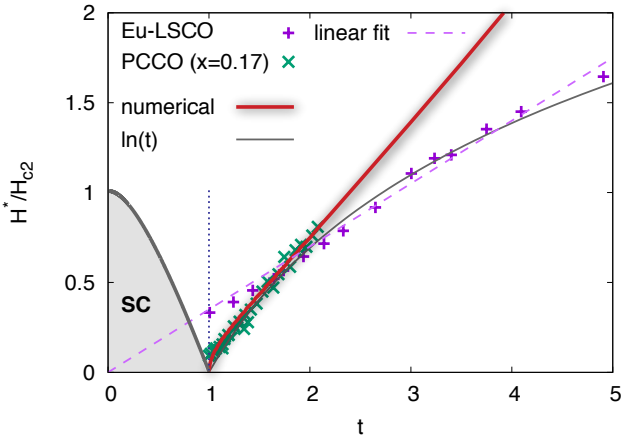

FIG. 32 (Color online) Temperature dependence of the ghost field scaled to H_{c2} from experiments ('+' and '×'), numerically obtained from Eq. (80) (thick solid red [dark gray] line), and $\ln(t)$ (thin gray line). The experimental data on Eu-LSCO (+) is taken from (Chang *et al.*, 2012) (Fig. 3b) and the data on PCCO at doping level $x = 0.17$ (×) from (Tafti *et al.*, 2014) (Figure 10). The data on Eu-LSCO is also fitted to a line through zero (slope 0.35) for comparison (dashed line). After Ref. (Glatz and Varlamov, 2017).

state of a superconductor (see Fig. 33a). More specifically, in the case of a disordered thin film, the fluctuation correction to the DOS assumes the form (Abrahams *et al.*, 1970):

$$\frac{\delta\rho^{(\mathrm{fl})}_{(2)}(E,T)}{\rho_e}=\frac{4.6\mathrm{Gi}_{(2)}k_\mathrm{B}^2T^2}{\left(E-\frac{1}{2}\tau_\mathrm{GL}^{-1}\right)^2}\left[\frac{E-\frac{1}{2}\tau_\mathrm{GL}^{-1}}{E+\frac{1}{2}\tau_\mathrm{GL}^{-1}}-\ln\frac{E+\frac{1}{2}\tau_\mathrm{GL}^{-1}}{\tau_\mathrm{GL}^{-1}}\right], \tag{83}$$

where ρ_e is the electron density of states per one spin of a normal metal at the Fermi level, $\mathrm{Gi}_{(2)} = 1.3\hbar^2/(p_\mathrm{F}^2 ls)$ is Ginzburg-Levanyuk number for a 2D film of thickness s, l is the electron mean free path, τ_GL is Ginzburg-Landau time.

One can see that Eq. (83) is a sign-changing function and its integral over the complete energy range must be equal zero:

$$\int_0^\infty \delta\rho^{(\mathrm{fl})}(E,T)dE = 0\,. \tag{84}$$

Expression (84) is merely the sum rule: superconducting interaction cannot create new states, it just redistributes the existing ones over the energy spectrum. In particular, a sharp dip $(\delta\rho^{(\mathrm{fl})}_{(2)}(0,\epsilon) \sim -\mathrm{Gi}_{(2)}\rho_e/\epsilon^2)$ is formed at the Fermi level, which is a precursor effect of the superconducting gap. At the same time, the electron states corresponding to the fluctuation pairing move to higher energies. Yet, it is clear that these pairings are restricted to energies not much larger than $\Delta E_s \sim k_\mathrm{B}(T - T_{c0})$, where the maximum of Eq. (83) is formed (see Fig. 33a).

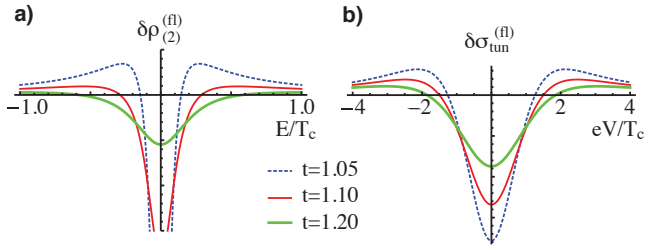

FIG. 33 (Color online) (a) Theoretical curves of the fluctuation correction to the single particle DOS, $\delta\rho^{(\mathrm{fl})}_{(2)}$, versus energy, E, for 2D superconductors above critical temperature ($t = T/T_{c0} = 1.05, 1.1, 1.2$). (b) The pseudogap in the tunneling conductivity obtained by applying Eq. (86) to the fluctuation correction (83). After Ref. (Glatz *et al.*, 2014).

B. Fluctuation pseudogap in tunneling conductivity: phenomenological approach

Tunneling spectroscopy is the tool of choice for investigating the quasiparticle spectrum. Therefore, the ability to analyze voltage-current characteristics obtained by a superconducting electrode in the fluctuation regime (N+SF) is of integral importance, as the domain is key to revealing the microscopic mechanisms of high-temperature superconductivity and the superconductor-insulator transition.

Giaever and Megerle (Giaever and Megerle, 1961) (GM) related the quasiparticle tunneling current to the densities of electron states of the left and right electrodes, and to the difference of the equilibrium distribution functions in both of them:

$$I^{(\mathrm{fl})}(V) = -\frac{\hbar}{eR_N\rho_\mathrm{L}(0)\rho_\mathrm{R}(0)}\times \tag{85}$$
$$\int_{-\infty}^{\infty}\left[n_\mathrm{F}(E+eV)-n_\mathrm{F}(E)\right]\rho_\mathrm{L}(E+eV)\rho_\mathrm{R}(E)dE$$

Here R_N is the tunnel junction resistance, $n_\mathrm{F}(E)$ is the Fermi distribution function, and $\rho_{\mathrm{L,R}}$ is the energy dependent density of states of the left (right) electrode, respectively. Assuming the left electrode is a normal metal with constant density of states ρ_L and the right electrode is a thin superconducting film above its critical temperature, one can write an explicit expression for the excess tunneling conductivity in terms of $\delta\rho^{(\mathrm{fl})}_{(2)}(E,T)$ and the derivative of the Fermi function. Combining the latter with the sum rule (84), one finds

$$\delta\sigma^{(\mathrm{fl,GM})}_{\mathrm{tun}}(V)=\frac{\hbar}{4TeR_N\rho_e}\int_{-\infty}^{\infty}\tanh^2\frac{E+eV}{2k_\mathrm{B}T}\delta\rho^{(\mathrm{fl})}_{(2)}(E)\,dE \tag{86}$$

and arrives at the disappointing conclusion that the predicted strong and narrow singularity in the density of states, Eq. (83), manifests itself in the observable tunnel-

ing conductivity only as a wide ($eV^{(\mathrm{pg})} \sim T_{c0} \sim \Delta_{\mathrm{BCS}}$ instead of $\Delta E_s \sim k_{\mathrm{B}}(T - T_{c0})$) and weak in the magnitude ($\ln(k_{\mathrm{B}} T \tau_{\mathrm{GL}}/\hbar) \sim \ln[T_{c0}/(T - T_{c0})]$ instead of $T_{c0}^2/(T - T_{c0})^2$) pseudogap structure, resembling that one in the superconducting phase (Varlamov and Dorin, 1983) (see Fig. 33b). The strong divergence of Eq. (83) at zero energy in the process of integration in Eq. (86) is completely eliminated due to presence of $\tanh^2(E/2k_{\mathrm{B}}T)$. As a result, only a weakly singular dip as function of temperature at zero voltage and two bumps of $\delta\sigma_{\mathrm{tun}}^{(\mathrm{fl})}(V)$ are reminiscent of the proximity to the superconducting transition.

This kind of pseudogap has been repeatedly observed both in experiments with conventional (Belogolovskii *et al.*, 1986; Sacépé *et al.*, 2010) and high-temperature (Jacobs *et al.*, 2016) superconductors. However, in such non-trivial superconducting systems like HTS materials or strongly disordered superconducting films close to superconductor-insulator transition, multiple other mechanisms of pseudogap formation are possible (Bennemann and Ketterson, 2008; Chen *et al.*, 2005; Palestini *et al.*, 2012; Perali *et al.*, 2002; Sacepe *et al.*, 2011).

C. General expression for the fluctuation tunneling conductivity

The GM phenomenology accounts for the depletion of single-electron DOS due to superconducting fluctuations, but it is not sufficient to uncover quantum coherent effects similar to Andreev reflection of injected electrons on a SF domain in a biased electrode. In order to do correctly describe such effects, one can employ the Matsubara temperature Green function technique. This quantitative theory was developed in Ref. (Glatz *et al.*, 2014) and is capable of adequately describing high resolution STM/STS data side-by-side with the pseudogap, thus uncovering subtle features of the tunneling spectra.

A low-transparency junction can be described by the tunnel Hamiltonian

$$\widehat{\mathcal{H}}_T = \sum_{\mathbf{p},\mathbf{k},\sigma} \left(T_{\mathbf{p},\mathbf{k}} \widehat{a}^+_{\mathbf{p},\sigma} \widehat{b}_{\mathbf{k},\sigma} + T^*_{\mathbf{p},\mathbf{k}} \widehat{b}^+_{\mathbf{k}} \widehat{a}_{\mathbf{p}} \right), \qquad (87)$$

where $\widehat{a}^+_{\mathbf{p},\sigma}$ and $\widehat{b}_{\mathbf{k},\sigma}$ are the creation and annihilation operators in the left and right electrodes, correspondingly. The summations are performed over the electron states $\mathbf{p}$, $\mathbf{k}$ in the corresponding electrodes, and spin components σ, $T_{\mathbf{p},\mathbf{k}}$ is the tunnel matrix element between states $\mathbf{p}$ and $\mathbf{k}$. The transparency of the barrier is determined by the averaged value of $|T_{\mathbf{p},\mathbf{k}}|^2$. The tunneling current can be identified as the time derivative of the particle number operator in one of the electrodes, $\widehat{\mathcal{N}}_{\mathrm{L}} = \sum_{\mathbf{p},\sigma} \widehat{a}^+_{\mathbf{p},\sigma} \widehat{a}_{\mathbf{p},\sigma}$, averaged over the statistical ensemble:

$$I^{(\mathrm{fl})}(V,T) = e \left\langle \frac{d\widehat{\mathcal{N}}_{\mathrm{L}}}{dt} \right\rangle = -\frac{ie}{\hbar} \left\langle \left[\widehat{\mathcal{N}}_{\mathrm{L}}, \widehat{\mathcal{H}}_T \right] \right\rangle . \qquad (88)$$

The procedure of ensemble averaging with the density matrix is described in detail in Ref. (Richardson, 1997). The tunneling current is then determined by the loop (correlator) of two exact one-electron Green's functions G_{L} and G_{R} of the electrodes (Varlamov and Dorin, 1983):

$$K(\omega_k) = 4T \sum_{\varepsilon_n} \sum_{\mathbf{q},\mathbf{p}} |T_{\mathbf{p},\mathbf{q}}|^2 G_{\mathrm{L}}(\mathbf{p}, \varepsilon_n + \omega_k) G_{\mathrm{R}}(\mathbf{q}, \varepsilon_n) \qquad (89)$$

Here the summations are performed over all momenta and fermionic frequencies $\varepsilon_n = 2\pi T(n + 1/2)$. The external bosonic frequency, $\omega_k = 2\pi T k$ ($k = 0, 1, 2...$), accounts for the potential difference between the electrodes, and the factor 4 is due to the summation over the spin degrees of freedom. The current is then given by

$$I^{(\mathrm{fl})}(V) = -e \mathrm{Im} K^R(\omega_k \to -ieV), \qquad (90)$$

where the superscript "R" means that the correlator $K(\omega_k)$ is continued to the plane of complex voltages in such a way that it remains an analytic function in the upper complex half-plane.

The fluctuation correction to the tunneling current is presented graphically by the diagram shown in Fig. 34b). The details of its calculation are reported in Ref. (Glatz *et al.*, 2014), where the complete expression valid for arbitrary temperatures, magnetic fields, and voltages was derived:

$$I^{(\mathrm{fl})}(t,h,v_t) = -\frac{2eT_{c0}Sh}{\pi^3 \sigma_n R_N} \sum_{m=0}^{M_t} \sum_{k=0}^{\infty} \frac{\mathrm{Im}\mathcal{E}'_m(k - iv_t)}{\mathcal{E}_m(k)} + \frac{eT_{c0}Sh}{\pi^3 \sigma_n R_N} \sum_{m=0}^{M_t} \left\{ \frac{\mathrm{Im}\mathcal{E}'_m(-iv_t)}{\mathcal{E}_m(0)} \right. \qquad (91)$$

$$\left. + \sinh\left(\frac{\pi}{2} v_t\right) \oint_{-\infty}^{\infty} dz \frac{\mathrm{Re}\,\mathcal{E}_m(iz) \left[\mathrm{Re}\,\mathcal{E}'_m(iz - iv_t) - \mathrm{Re}\,\mathcal{E}'_m(iz)\right] + \mathrm{Im}\mathcal{E}_m(iz) \left[\mathrm{Im}\mathcal{E}'_m(iz - iv_t) + \mathrm{Im}\mathcal{E}'_m(iz)\right]}{\sinh(\pi z) \sinh\left[\pi(z - v_t/2)\right] \left[\mathrm{Re}^2\mathcal{E}_m(iz) + \mathrm{Im}^2\mathcal{E}_m(iz)\right]} \right\},$$

with the dimensionless voltage $v = 2eV/\Delta_{\mathrm{BCS}}$ used in the parameter

$$v_t = v/(2\gamma_{\mathrm{E}} t) = eV/(\pi T),$$

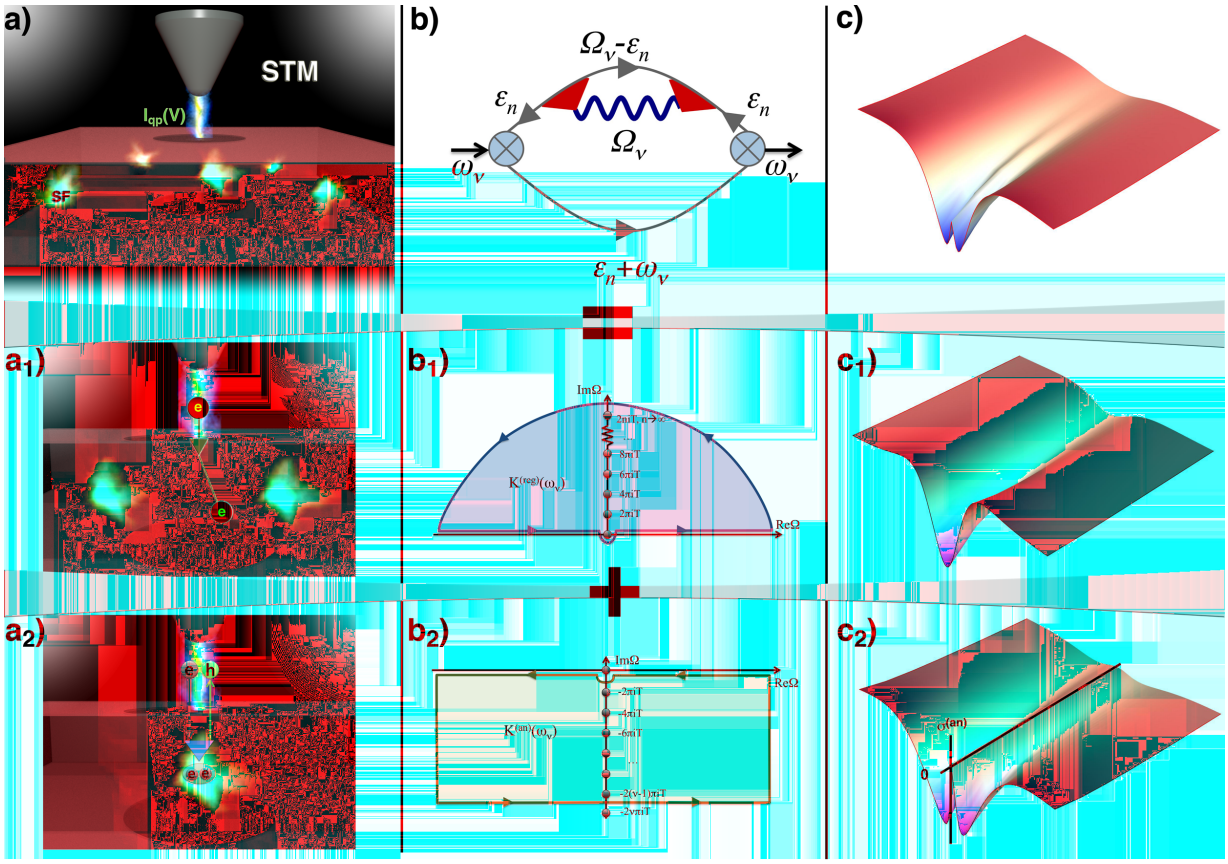

FIG. 34 (Color online) **a**) Schematic STM setup of a N-I-(N+SF) tunnel experiment. $\mathbf{a}_1$) An injected electron pair ($2e$) thermalizes in the electrode, which reduces the density of states due to superconducting fluctuations. $\mathbf{a}_2$) Andreev-like reflections of injected electrons in the region of superconducting fluctuations. **b**) The (Matsubara) diagram describing the fluctuation contribution to tunneling current. $\mathbf{b}_1$)+$\mathbf{b}_2$) Two contours in the plane of complex voltage describing both corresponding tunneling processes shown in a_1) and a_2). **c**) Surface plot of the total tunneling conductivity, Eq. (91) depending on voltage and temperature. The corresponding theoretical expression is valid throughout the whole phase diagram of temperature and magnetic field with a wide pseudogap structure and narrow low-bias anomaly (LBA). $\mathbf{c}_1$) Pseudogap anomaly related to the renormalization of the one-electron density of states due to superconducting fluctuations in the electrode. It directly corresponds to the process pictured in a_1) and contour b_1). $\mathbf{c}_2$) LBA contribution of the tunneling conductivity due to process a_2), resulting from contour b_2). After Ref. (Glatz *et al.*, 2014).

$\Delta_{\rm BCS} = \pi T_{c0}/\gamma_E$ the value of the BCS gap, and cutoff $M_t = 1/(tT_{c0}\tau)$.

Notice, that the AL and MT fluctuation contributions, which are essential for the majority of the phenomena discussed in this review, only manifest themselves in second order $\left(\sim |T_{\mathbf{p},\mathbf{k}}|^4\right)$ in the barrier transparency (see Ref. (Larkin and Varlamov, 2009)).

D. Fluctuation pseudogap: Asymptotic analysis

We start the analysis of Eq. (91) in the strong pair-breaking regime, when its second term is suppressed and the effect of fluctuations is manifested by the pseudo-gap structure in tunnel conductivity, already discussed qualitatively in the framework of phenomenological approach.

1. Tunnel conductivity in weak magnetic filed

Close to T_{c0}, in domains `I-III`, in sufficiently weak magnetic fields $H \ll H_{c2}(0)$, the most singular term in Eq. (91) arises from zero frequency bosonic mode $k = 0$. The summation over Landau levels can be performed in terms of polygamma-functions, $\psi^{(n)}(x)$, and one finds an expression valid for any combination of ϵ and $h \ll 1$:

$$I^{(\rm fl)}(\epsilon, h, v_t) = -\frac{eTS}{2\pi^3\sigma_n R_N}\left[\ln\frac{1}{2h} - \psi\left(\frac{1}{2}+\frac{\epsilon}{2h}\right)\right] \cdot {\rm Im}\psi'\left(\frac{1}{2}(1-iv_t)\right). \quad (92)$$

Eq. (92) reproduces the results of Refs. (Reizer, 1993; Varlamov and Dorin, 1983). The corresponding contri-

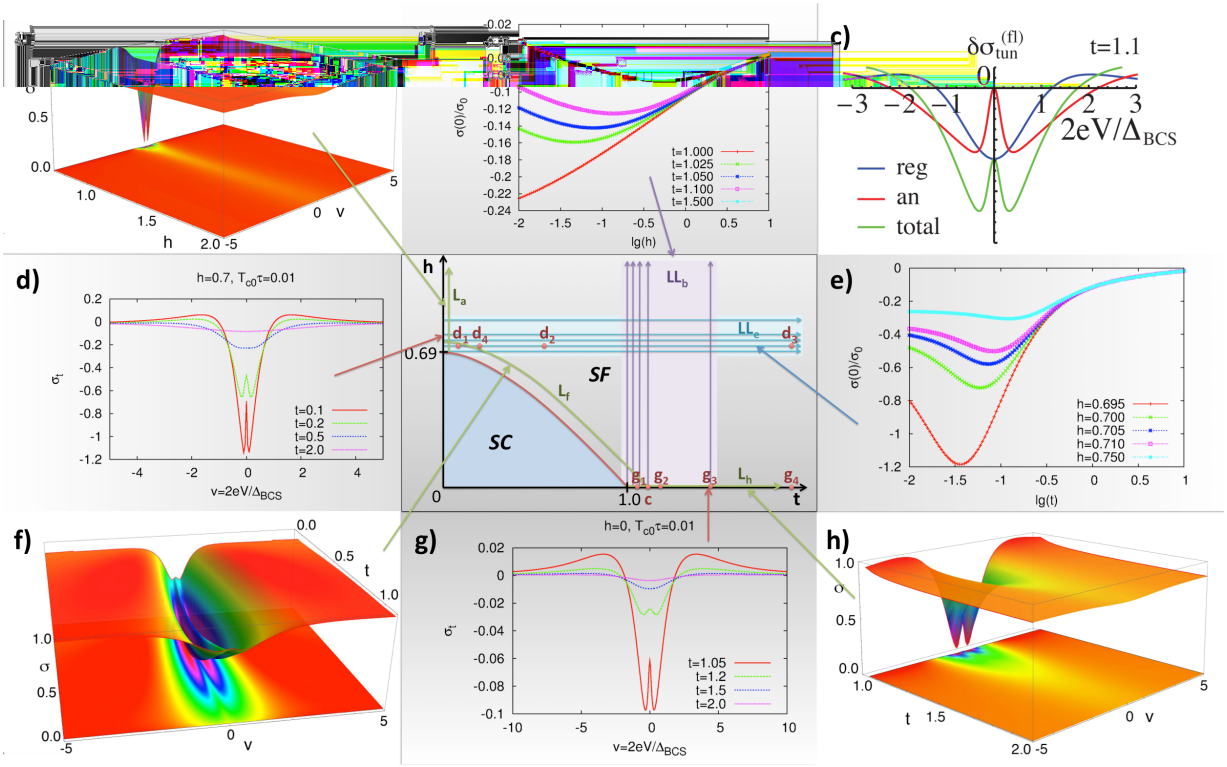

FIG. 35 (Color online) Various plots of the tunneling conductance for different cuts and points in the $t-h$ plane. The cut lines and points are indicated in the $t-H$ phase diagram in the central panel. Points are labeled by the panel letter, lines by "L" and panel letter subscript. **a)** Low temperature ($t = 0.05$) dependence of the conductivity as surface plot depending on voltage, v, and magnetic field, $h > h_{c2}(0) = 0.69$ [cut line L_a]. **b)** Zero-bias conductivity at fixed temperatures as function of $\ln(h)$ [cut lines LL_b]. **c)** $t = 1.1$ plot of the components (pseudo gap, "reg", and LBA, "an") of the tunneling conductivity [point c]. **d)** Tunnel conductance for $h = 0.7$ at different temperatures depending on v [points d_1-d_4]. **e)** Zero-bias conductivity at fixed magnetic field as function of $\ln(t)$ [cut lines LL_e]. **f)** Conductivity as surface plot depending on voltage and closely following the superconducting transition line in the $t-h$ plane [cut line L_f].**g)** Tunnel conductance for $h = 0$ at different temperatures depending on v [points g_1-g_4]. **h)** Zero field ($h = 0$) dependence of the conductivity as surface plot depending on voltage, v, and temperature, $t > t_c = 1$ [cut line L_h] (the same parameters as used for column c) of Fig. 34). After Ref. (Glatz *et al.*, 2014).

bution to the tunneling conductance is

$$\sigma_{\rm tun}^{\rm (fl)}(\epsilon,h,v_t) = \frac{Se^2}{4\pi^4\sigma_n R_N}\left[\ln\frac{1}{2h} - \psi\left(\frac{1}{2}+\frac{\epsilon}{2h}\right)\right] \cdot {\rm Re}\psi''\left(\frac{1}{2}(1-iv_t)\right), \tag{93}$$

which gives the pseudogap structure in the limit of zero field (domain I)

$$\sigma_{\rm tun}^{\rm (fl)}(\epsilon,v_t) = \frac{Se^2}{4\pi^4\sigma_n R_N}\ln\frac{1}{\epsilon}{\rm Re}\psi''\left(\frac{1}{2}(1-iv_t)\right). \tag{94}$$

A corresponding plot for the tunneling resistance is shown in Fig. 38 for different values of ϵ. The value of the pseudogap follows from the maximum of Eq. (94), which appears for $v_t = 1$. This gives

$$eV_{\max}(\epsilon, h=0) = \gamma_{\rm E}\Delta_{\rm BCS}(1+\epsilon). \tag{95}$$

Far from T_{c0}, in domain VIII, one can restrict the consideration to the study of the temperature dependence of the magnitude of the fluctuation contribution to the differential conductivity at zero voltage. When $T \gg T_{c0}$ one can approximate the sums in Eq. (91) by integrals. For the k-integration it was assumed that the main k-dependence is due to the nominator and can it be omitted in the argument of the ψ-function. Cutting off the double logarithm divergence at the upper limit in the usual way, one finds

$$\sigma_{\rm tun}^{\rm (fl)}(t\gg 1, v_t=0) = -\frac{Se^2}{4\pi^2\sigma_n R_N}\left(\ln\ln\frac{1}{T_{c0}\tau} - \ln\ln t\right). \tag{96}$$

which is again in complete agreement with Ref. (Varlamov and Dorin, 1983). This double logarithmic behavior in the wide range of temperatures up to $14T_{c0}$ was observed in Ref. (Sacépé *et al.*, 2010).

2. Vicinity of the line $H_{c2}(t)$

In the vicinity of the line $H_{c2}(t)$, the LLL approximation, Eq. (39), for the $\mathcal{E}_0(k)$ can be applied. It is valid along the line $H_{c2}(t)$ where $t \ll h_{c2}(t)$. The summation in the first term of Eq. (91) can be performed using the relation

$$\sum_{k=0}^{\infty}{}' \frac{1}{k+\alpha}\frac{1}{(k+\beta)^2+\gamma^2} = -\frac{1}{\gamma}\,\mathrm{Im}\,\frac{\psi(\beta+i\gamma)-\psi(\alpha)}{\beta+i\gamma-\alpha} - \frac{1}{2\alpha}\frac{1}{\beta^2+\gamma^2},$$

which gives an expression for the regular part (first term in Eq. (91)) of the fluctuation tunneling current valid for low enough temperatures along the line $h_{c2}(t)$:

$$I^{(\mathrm{fl})}\left[t \ll h_{c2}(t), \widetilde{v}_t\right] = -\frac{2eST_{c0}h}{\pi^3\sigma_n R_N}\frac{\widetilde{v}_t}{1+\widetilde{v}_t^2}\left\{\ln\sqrt{1+\widetilde{v}_t^2} + \left[\ln\left(\frac{4h}{\pi^2 t}\right) - \psi\left(\frac{4h}{\pi^2 t}\widetilde{h}\right)\right] - \frac{\arctan\widetilde{v}_t}{\widetilde{v}_t}\right\}. \tag{97}$$

Here, we introduced the dimensionless voltage

$$\widetilde{v}_t = \frac{V}{V_0\left(t,\widetilde{h}\right)}.$$

The value

$$V_0\left(t,\widetilde{h}\right) = \frac{\Delta_{\mathrm{BCS}}}{2e}\left[1+2\gamma_E t - \widetilde{h}/h_{c2}(t)\right] \tag{98}$$

determines the voltage at which the differential conductivity crosses zero in the considered domain of the phase diagram (see Fig. 35g,h) as we will see below.

Close to $H_{c2}(0)$, in the region of quantum fluctuations $t \ll \widetilde{h}$, the argument of the ψ-function in Eq. (97) becomes large despite the smallness of $\widetilde{h}$, and the ψ-function can therefore be approximated by its logarithmic asymptotic expression:

$$I^{(\mathrm{fl})}\left(\widetilde{h},\widetilde{v}_t\right) = -\frac{e\Delta_{\mathrm{BCS}}S}{4\pi^2\sigma_n R_N}\frac{\widetilde{v}_t}{1+\widetilde{v}_t^2}\ln\frac{\sqrt{1+\widetilde{v}_t^2}}{\widetilde{h}}.$$

The corresponding tunneling conductivity up to logarithmic accuracy is given by

$$\sigma_{\mathrm{tun}}^{(\mathrm{fl})}\left(\widetilde{h},\widetilde{v}_t\right) = \frac{dI}{dV} \approx -\frac{e^2S}{2\pi^2\sigma_n}\frac{1}{\left[1-8\gamma_{\mathrm{E}}\widetilde{h}/\pi^2\right]}\frac{1-\widetilde{v}_t^2}{\left(1+\widetilde{v}_t^2\right)^2}\ln\frac{\sqrt{1+\widetilde{v}_t^2}}{\widetilde{h}}.$$

At zero temperature one just needs to replace $\widetilde{v}_t$ by v above. One sees that this expression has a pseudogap structure similar to Eq. (94). The corresponding value of the pseudogap gap close to H_{c2} is given by

$$eV_{\max}\left(t=0, h=\pi^2/(8\gamma_{\mathrm{E}})\right) = \frac{\sqrt{3}}{2}\Delta_{\mathrm{BCS}}. \tag{99}$$

Comparing this expression to Eq. (95), one notices that the fluctuation pseudogap is determined by Δ_{BCS} in both cases, but the numerical coefficients depend on the shape of the fluctuation correction of tunneling conductivity.

In the region of high fields $H \gg H_{c2}$ and low temperatures, the sums in Eq. (91) can be approximated by integrals, which gives for the value of the differential conductivity at zero voltage:

$$\sigma_{\mathrm{tun}}^{(\mathrm{fl})}(h \gg 1, v=0) = -\frac{e^2S}{4\pi^2\sigma_n R_N}\left(\ln\ln\frac{1}{T_{c0}\tau} - \ln\ln h\right).$$

One can see that this dependence is exactly the same as that one in the case of high temperatures with reversed roles of the reduced temperature and field.

E. Weak pairbreaking: low bias anomaly

The second term in Eq. (91) describes the anomalous process of Andreev reflection of injected, energetically non-relaxed electrons at a fluctuation-induced superconducting domain in the biased electrode, see Fig. 34 $\mathbf{a}_2$. In order to participate in fluctuation Cooper pairing, the injected electron "extracts" an electron-hole pair from vacuum with momentum opposite to its own, and forms a Cooper pair with the electron, while the remaining hole returns along its previous trajectory (see Fig. 34$\mathbf{a}_2$). This quantum coherent contribution cannot be accounted for by the phenomenological method, but can only be derived within the microscopic diagrammatic approach. This anomalous tunneling process gives rise to an additional current, which, like the regular one, is proportional to the first powers of the Ginzburg-Levanyuk number and barrier transparency, and is cubic in voltage V near zero bias. The additional current becomes relevant only sufficiently close to the superconducting transition. As a

result, a peculiar LBA appears near the superconducting transition line $H_{c2}(T)$.

It turns out that the discussed LBA in the I-V characteristics appears only in the case where the energy (or phase) relaxation time τ_ϕ of an electron injected into the explored electrode is long enough: $T_{c0}\tau_\phi \gg \hbar/k_B$. The shape of the LBA close to the critical temperature $[\hbar\tau_\phi^{-1} \lesssim k_B(T-T_{c0}) \ll k_B T_{c0}]$ for low voltages $eV \lesssim k_B(T-T_{c0})$, can be found analytically:

$$\sigma_{tun}^{(fl)} = -\frac{7\zeta(3)e^2 S}{2\pi^4\hbar\sigma_n R_N}\left[\ln\frac{T_{c0}}{T-T_{c0}} + \frac{3\tau_\phi}{8\pi\hbar k_B}\frac{(eV)^2}{(T-T_{c0})}\right]. \quad (100)$$

When $k_B(T-T_{c0})$ decreases to the value $\hbar\tau_\phi^{-1}$, the growth of the LBA ceases. One can show that close to the transition temperature T_{c0}, the dip in the tunneling conductivity develops on the scale $eV_{LBA}^{(th)} \sim \Delta_{BCS}^{1/2}\sqrt{\hbar\tau_\phi^{-1}(T-T_{c0})/T_{c0}} \ll \Delta_{BCS}$. At zero temperature, close to the second critical field $H_{c2}(0)$, fluctuations acquire quantum nature and the corresponding voltage scale becomes $eV_{LBA}^{(QF)} \sim \Delta_{BCS}^{1/2}\sqrt{\hbar\tau_\phi^{-1}[H-H_{c2}(0)]/H_{c2}(0)} \ll \Delta_{BCS}$. From the Eq. (100), one can see that the intensity of the LBA is directly proportional to the energy relaxation length $\ell_\phi = v_F\tau_\phi$, which is in a complete agreement with the physical picture of this non-trivial quantum coherence effect presented above: the anomalous Cooper pair formation only takes place in a volume of size $S\cdot\ell_\phi$ near the contact area, where the injected electrons are non-thermalized.

F. Epilogue of the theoretical analysis

Graphical representations of the full fluctuation contribution to tunneling conductivity as a function of magnetic field, temperature and voltage are presented in Figs. 34**c**&35. One can see that as external parameter values depart from the transition line, the amplitude of the LBA rapidly decays.

Remarkably, both complimentary physical processes shown in panels $\mathbf{a}_1$ and $\mathbf{a}_2$ of Fig. 34 are straightforwardly expressed in terms of a graphic mathematical language: the calculation of the diagram of Fig. 34**b** is reduced to the evaluation of the integrals of the electron Green functions in the linked electrodes along two contours in the complex frequency plane shown in panels $\mathbf{b}_1$ and $\mathbf{b}_2$ of Fig. 34, respectively. The upper contour corresponds to the conventional GM tunneling, while the lower one describes the contribution due to Andreev reflection from superconducting fluctuations. Accordingly, the fluctuation part of the tunneling conductance shown in Fig. 34**c** exhibits both, the pseudogap anomaly due to fluctuation depletion of the one-electron DOS (Fig. 34$\mathbf{c}_1$) coming from the integration over the contour of Fig. 34$\mathbf{b}_1$, and Andreev reflection induced LBA (Fig. 34$\mathbf{c}_2$), arising from the integration over the contour of the panel $\mathbf{b}_2$.

One should remark that the latter contribution is zero at zero bias voltage [see Fig. 35**c**]. An important feature of this novel Andreev process is that it appears in the lowest (first) order approximation with respect to tunneling barrier transparency. Its additional smallness, related to the strength of fluctuations Gi, can be noticeably compensated by the presence of a small factor $(T-T_{c0})$ in denominator of the second term of Eq. (100), which makes the effect strongly temperature dependent close to the transition point.

The LBA, which appears already in first order of the transparency, differs qualitatively from the well known Andreev conductance of a superconducting microconstriction (Blonder *et al.*, 1982). This occurs below the transition temperature and rapidly disappears when going from the metallic towards the tunneling regime. The reason for this discrepancy is that the fluctuation-induced superconducting regions in the biased electrode are not separated by any barrier from the surrounding normal phase and thus the process of Andreev reflection does not involve any additional tunneling process.

Fig. 35 shows the plots of fluctuation contributions to the tunneling conductivity for different parts of the temperature-magnetic field phase diagram of the superconducting film. The central panel – the h-t phase diagram – depicts the parameter combinations or ranges for the 2D graphs or 3D surface plots arranged around it in panels a) - h). In accordance with the above theoretical speculations the strength of the singularity in the low-voltage behavior of the tunneling conductance smears out when moving away from the transition line (panels a-d and g, h). We point out that the LBA is most pronounced roughly halfway between the 'endpoints' of the transition line (see panel f).

G. Fluctuation spectroscopy: analysis of experiments

There have been impressive developments in scanning tunneling microscopy (STM) and scanning tunneling spectroscopy (STS) studies of superconductivity triggered by investigations of the pseudogap state and vortex state in high-temperature cuprates (Micklitz and Norman, 2009; Scherpelz *et al.*, 2013), observations of the pseudogap in 2D disordered films of conventional superconductors (Sacépé *et al.*, 2010), investigations of the superconductor-insulator transition (Sacépé *et al.*, 2008), measurements of the tunneling conductivity close to the superconducting transition in intrinsic Josephson junctions in slightly overdoped $Bi_{2-y}Pb_ySr_2CaCu_2O$ crystals (see Ref. (Jacobs *et al.*, 2016; Krasnov *et al.*, 2011)), and many others.

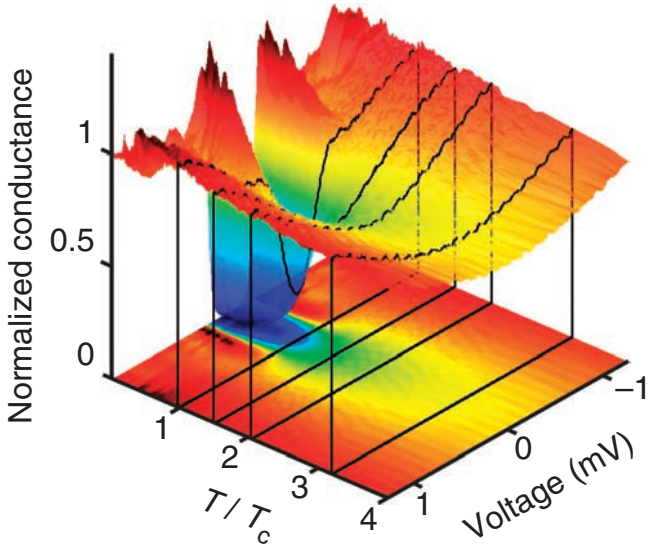

FIG. 36 (Color online) Pseudogap in the density of states. Three-dimensional plot of the tunneling conductance $G(V, T/T_c)$ normalized by the conductance measured at high voltage and low temperature as a function of bias voltage and normalized temperature T/T_c for a superconducting TiN film. Black lines mark the spectra measured at $T/T_c = 1, 1.5, 2$ and 3, illustrating that the pseudogap state grows more pronounced and extends over a wider temperature range as the disorder increases. The suppression of the density of states of the TiN_3 sample remains visible up to $T = 14T_c$. *Reprinted by permission from Macmillan Publishers Ltd: Nature Communications (Sacépé* et al., *2010), copyright (2010).*

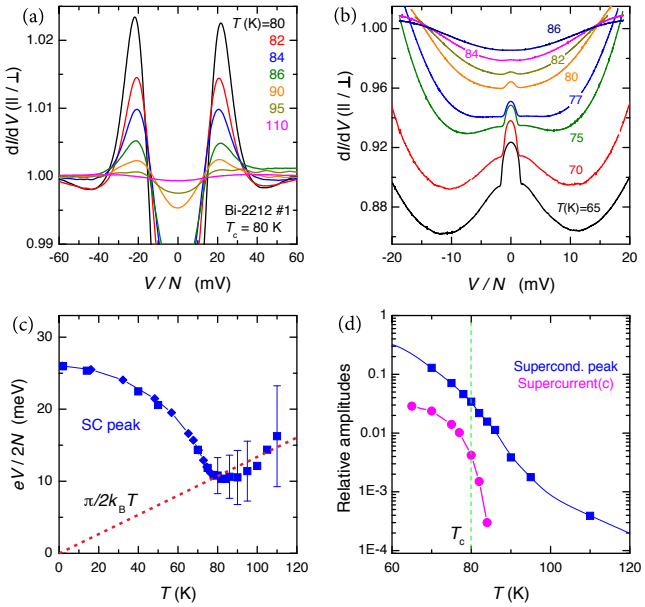

FIG. 37 (Color online) (a) Tunneling curves above T_c at $H = 10$ T for Bi-2212 crystal. (b) Low-bias parts of the curves for the Bi-2212 crystal. The zero-bias maximum which below T_c the authors attribute to an interlayer Josephson current remains also above the critical temperature. (c) Temperature dependencies of the superconducting peak voltage for Bi-2212 crystal. (d) Amplitudes of the SC peak, and the LBA. *Figure printed with permission by V.M. Krasnov. Compare to Figure 2 of Ref. (Jacobs* et al., *2016).*

1. Observation of the fluctuation pseudogap

In the inset of Fig. 38, the result of measurements of the differential resistance in a Al-I-Sn tunnel junction at temperatures slightly above the critical temperature of the Sn electrode is presented. This experiment was conducted (Belogolovskii *et al.*, 1986) to check the proposed theory (Varlamov and Dorin, 1983), plotted as the main graphs in Fig. 38. The nonlinear differential resistance was measured at low voltages, which allowed the observation of the fine structure of the zero-bias anomaly. It is worth mentioning that the experimentally measured positions of the minima are $eV \approx \pm 3T_c$, while the theoretical prediction following from (92) is $eV = \pm\pi T_c$. Similar results on an aluminum film with two regions of different superconducting transition temperatures were reported in Ref. (Park *et al.*, 1995). Observations of pseudogap anomalies in tunneling experiments at temperatures above T_c were reported in (Cucolo *et al.*, 1999; Matsuda *et al.*, 1999; Renner *et al.*, 1998; Suzuki *et al.*, 1998; Tao *et al.*, 1997; Watanabe *et al.*, 1997, 2000) using a variety of experimental techniques.

The pseudogap in the density of states of a superconducting TiN_3 film was thoroughly measured in a wide range of temperatures above T_{c0} in Ref. (Sacépé *et al.*, 2010). The authors observed how the pseudogap state becomes more pronounced and extends over a wider temperature range when increasing the disorder. The suppression of the density of states of the TiN_3 sample remains noticeable up to $T = 14T_{c0}$. The temperature dependence of the minimum of the tunnel conductivity was found to be well described by the double logarithmic behavior described in Eq. (96), which indicates that its origin can be attributed to SF.

A pseudogap, attributed to SFs, was also observed in slightly overdoped high-temperature superconductors (Jacobs *et al.*, 2016). The experimental data presented in this work (see Fig. 37(c)) confirms the prediction of a linear temperature dependence of the pseudogap (Varlamov and Dorin, 1983), see Eq. (95).

2. Observation of the low bias anomaly

At the same time, the LBA gives rise to a new fluctuation spectroscopy tool for determining microscopic material parameters, including the energy relaxation time τ_ϕ, the critical temperature T_{c0}, and magnetic field $H_{c2}(0)$, by measuring the tunneling conductance and fitting the experimental data with the complete expression for the

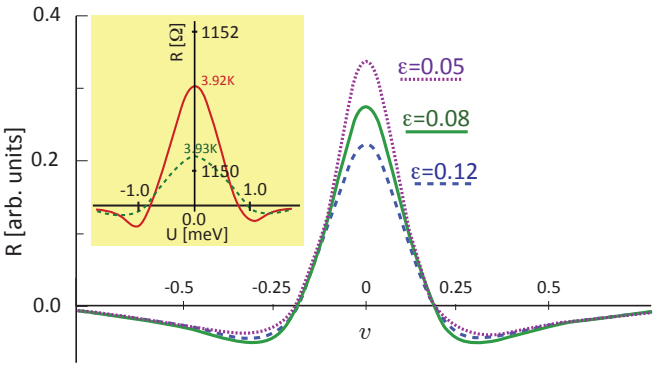

FIG. 38 (Color online) Theoretical prediction for the fluctuation-induced pseudogap structure in the tunnel-junction resistance [see Eq. (92)] as a function of dimensionless voltage v for different reduced temperatures $\epsilon = 0.05, 0.08, 0.12$. The insert shows a fit to experimentally observed differential resistance as a function of voltage in an Al–I–Sn junction ($R_N = 1149.4\Omega$) just above the transition temperature ($T_c = 3.88K$) at two different temperatures $T = 3.92$ (red) and $T = 3.93$ (dashed green) (experimental data used for the fitting from (Belogolovskii *et al.*, 1986)).

fluctuation tunneling current, Eq. (91). Remarkably, all the information about these parameters is encoded in merely the distance between the LBA dips and the height of the central peak in the conductivity curve. An observation of the described LBA in a dc experiment is indicative of the appearance of fluctuation Cooper pairs during the time of the experiment at the point below the STM tip. Recent tunneling current measurements of N-I-S junctions indeed indicate the presence of the LBA (Jacobs *et al.*, 2016) (see Fig. 37(b)). Since the characteristic lifetime of fluctuation Cooper pairs is $\hbar/k_{\rm B}\,(T - T_{\rm c})$, a time-resolved STM measurement utilizing ac currents with frequencies in the range of 1-10 GHz promises to make it possible – in principle – to "visualize" them directly in real time.

IX. EFFECT OF FLUCTUATIONS ON THE NMR RELAXATION RATE

A. General expression for the fluctuation NMR relaxation rate

Nuclear magnetic resonance (NMR) spin-lattice relaxation occurs through the interaction of nuclei with low-frequency excitations (Slichter, 1990). It is an important process for studying dynamics of nuclei in novel materials (Rigamonti *et al.*, 1998). In the vortex phase of type-II superconductors at low temperatures, localized superconducting regions of size $\xi_{\rm BCS}$ separate magnetic flux lines, provided the applied magnetic field is below $H_{\rm c2}$, but well above $H_{\rm c1}$. In the vortex phase the spin-lattice relaxation is mainly due to low-energy intra- and inter-vortex excitations, which are possibly connected by a spin diffusion process (Slichter, 1990). Flux line diffusion can be an additional relaxation mechanism in the vortex liquid phase, see Ref. (Corti *et al.*, 1996) and references therein.

The effect of superconducting fluctuations on the NMR relaxation rate was studied in many works (Carretta *et al.*, 1996; Mitrović *et al.*, 1999, 2002; Eschrig *et al.*, 1999; Gorny *et al.*, 1999; Heym, 1992; Kuboki and Fukuyama, 1989; Maniv and Alexander, 1977; Mosconi *et al.*, 2000; Prando *et al.*, 2011; Randeria and Varlamov, 1994). It can be observed in a wide range of temperatures and magnetic fields beyond the second critical field line $H_{\rm c2}(T)$ It is well-known that the density of quasiparticle excitations, which enters quadratically into the NMR relaxation rate W, is suppressed by SFs (Abrahams *et al.*, 1970; Di Castro *et al.*, 1990). However, a second mechanism of how fluctuations affect spin-lattice relaxation exists. This relaxation process is of quantum nature and consists in fluctuation "self-pairing" of an electron on a self-intersecting trajectory after a spin-flip scattering event on a nucleus (Glatz *et al.*, 2015; Kuboki and Fukuyama, 1989; Larkin and Varlamov, 2009; Maniv and Alexander, 1977), see Fig. 39. This process of Maki-Thompson (MT) type represents a new channel of NMR relaxation and leads to an increase of the relaxation rate W. Note, that the effect of this relaxation process is of opposite sign than that of the DOS contribution.

As described in Section II, a dynamic state with clusters of coherently rotating FCP is formed above the $H_{\rm c2}(T)$ line at low temperatures. Therefore, it is important to analyze the effect of this fluctuation analogue of the vortex state on the magnetic field dependence of the relaxation rate near $H_{\rm c2}(T)$. In Ref. (Lascialfari *et al.*, 2005) the authors studied the ^{11}B NMR relaxation rates in a single crystal of superconducting YNi_2B_2 ($T_{\rm c0} = 15.3$K). They observed an anomalous peak in $W(H)$ at low enough temperatures (2K and 4K) in fields close to $H_{\rm c2}(T)$, which was tentatively attributed to quantum fluctuations of magnetic flux lines. Below we review the effects of superconducting fluctuations, both of thermal and quantum nature, on the NMR relaxation mechanisms.

The NMR relaxation rate W is determined by the imaginary part of the static limit of the dynamic spin susceptibility integrated over all momenta:

$$W = T \lim_{\omega\to 0} \frac{A}{\omega} \,{\rm Im} \int (d\mathbf{k}) \chi^R_{+-}(\mathbf{k}, -i\omega)\,, \qquad (101)$$

where, A is a positive constant involving the gyromagnetic ratio, and $\chi^R_{\pm}(\mathbf{k},\omega) = \chi_{\pm}(\mathbf{k}, \omega_\nu \to -i\omega + 0^+)$ is the dynamic spin susceptibility, calculated as

$$\chi_{\pm}(\mathbf{k},\omega_\nu) = \int_0^{1/T} d\tilde{\tau} e^{i\omega_\nu \tilde{\tau}} \left\langle \hat{T}_{\tilde{\tau}} \left(\hat{S}_+(\mathbf{k},\tilde{\tau}) \hat{S}_-(-\mathbf{k},0) \right) \right\rangle . \qquad (102)$$

Here $\hat{S}_\pm$ are the spin raising and lowering operators, $\tilde{\tau}$ is the imaginary time, $\omega_\nu = 2\pi T\nu$ ($\nu = 0, 1, 2...$) are

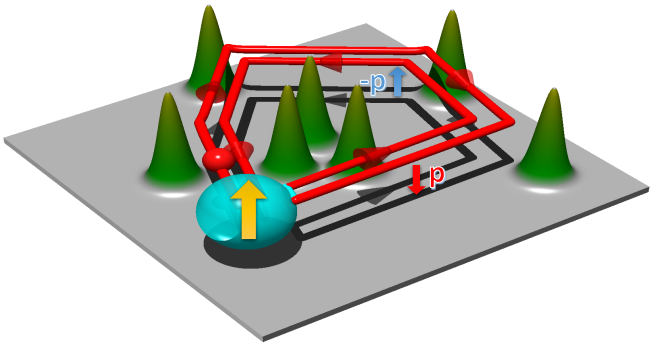

FIG. 39 (Color online) The MT spin-lattice relaxation mechanism is due to self-pairing of electrons on self-intersecting trajectories involving a spin-flip scatterings on the investigated nucleus (cyan [light gray]). Initially, an electron moves along the trajectory $\mathbf{p}$ (clockwise), due to several impurity scattering events (green, Gaussian potential peaks) it returns to the departure point. As a result of the electron's interaction with the nucleus, its spin and momentum flip and it returns along almost the same trajectory $-\mathbf{p}$ (counter-clockwise). During this process, the electron effectively interacts with itself in the past, which is only possible due to "fast" motion of the electron along its trajectory, and the retarded character of electron-phonon interaction.

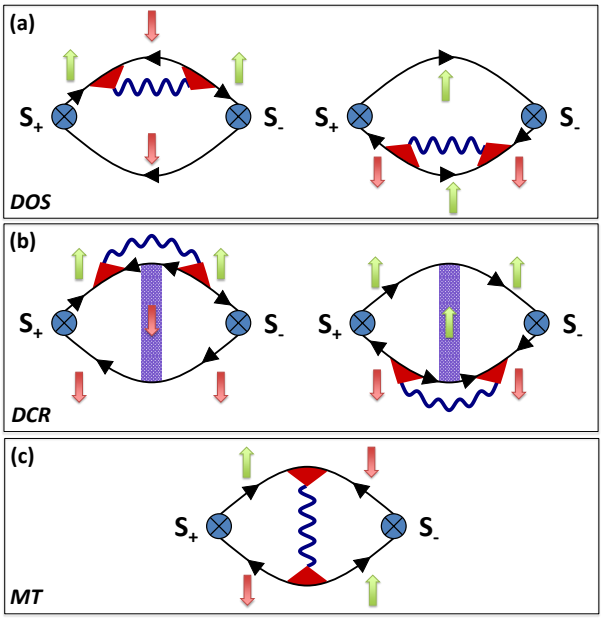

FIG. 40 (Color online) Spin susceptibility diagrams. The solid lines correspond to free electron Green's functions, wavy lines to the fluctuation propagator, dashed triangles and rectangles represent electron scattering at impurities. The two diagrams **(a)** correspond to the DOS correction, the diagrams **(b)** represent the renormalization of the diffusion coefficient (DCR), and the diagram **(c)** corresponds to the MT process. After Ref. (Glatz *et al.*, 2015).

bosonic Matsubara frequencies corresponding to the external field, and the angle brackets denote thermal and impurity averaging in the usual way.

For noninteracting electrons, $\chi_{\pm}^{(0)}(\mathbf{k},\omega_\nu)$ is determined by the usual loop diagram with the $\hat{S}_{\pm}(\mathbf{k},\tilde{\tau})$ operators playing the role of external vertices (electron interaction with the external field), leading to the well-known Korringa law: $W_0 = 4\pi AT\rho_e^2$.

The first-order fluctuation correction to $\chi_{\pm}$ in dirty superconductors at magnetic fields $H > H_{c2}(T)$ can be calculated as the standard loop of two Green's functions "dressed"(see Fig. 40) with a fluctuation propagator (32) and impurity vertices (30–31). Fig. 40 shows the diagrams for fluctuation corrections to spin susceptibility. Two diagrams in the panel (a) represent the effect of fluctuations on the single-particle self-energy, leading to a decrease in corresponding DOS at the Fermi level. Consequently, in accordance with the Korringa law, SFs reduce the relaxation rate W with respect to its normal value. This opens a type of fluctuation spin-gap on approach of the transition line $H_{c2}(T)$ from the normal phase.

The diagrams in the panel (b) contain four-leg Cooperon impurity blocks, which account for the corrections to the NMR relaxation rate due to DCR processes. Analogous contribution is a dominant correction to fluctuation conductivity in the regime of quantum fluctuations (Glatz *et al.*, 2011a). However, in the case of spin susceptibility, these contributions are strongly suppressed due to the additional integration over external momenta(Randeria and Varlamov, 1994), which makes them proportional to the square of the small Ginzburg-Levanyuk number.

The MT process shown in Fig. 40(c) has one important difference from the corresponding diagram for conductivity. Because of the particular spin assignments on the free electron Green's function, the MT diagram for spin susceptibility is a non-planar graph containing a single fermion loop. Yet, the MT diagram for conductivity is a planar graph with two fermion loops, see Ref. (Larkin and Varlamov, 2009). Since the number of loops determines the sign of the fluctuation correction (Abrikosov *et al.*, 1965), the contribution of the MT diagram to spin susceptibility bears the opposite sign to that for conductivity (Kuboki and Fukuyama, 1989). Therefore, MT spin-lattice relaxation processes result in an increase of W with respect to the Korringa value.

The sign of the MT contribution is not the only difference between the first order corrections to fluctuation conductivity and spin susceptibility. Due to the presence of the spin-flip operators $\hat{S}_{\pm}(\mathbf{k},\tilde{\tau})$ as external vertices in the diagram for spin susceptibility, the Aslamazov-Larkin process is completely absent from the corrections to the NMR relaxation rate. It is impossible to consistently assign spin labels to the central fermion lines for spin–singlet pairing (Maniv and Alexander, 1977).

When collecting the DOS and MT contributions in one expression and normalizing the result by the normal Ko-

rringa relaxation rate in metals, one finds (Glatz *et al.*, 2015) the following expression for $W^{(\mathrm{fl})}$ valid in the whole phase diagram (with the restrictions discussed above):

$$\frac{W^{(\mathrm{fl})}(t,h)}{W_0}=\frac{\mathrm{Gi}_{(2)}}{7\zeta(3)}\left(\frac{h}{t}\right)\sum_{m=0}^{M}\left[\sum_{k=-\infty}^{\infty}\frac{8\mathcal{E}_m''(t,h,|k|)}{\mathcal{E}_m(t,h,|k|)}+4\pi\int_{-\infty}^{\infty}\frac{dz}{\sinh^2(\pi z)}\frac{\mathrm{Im}\,\mathcal{E}_m'(t,h,iz)\,\mathrm{Im}\,\mathcal{E}_m(t,h,iz)}{\mathrm{Re}^2\mathcal{E}_m(t,h,iz)+\mathrm{Im}^2\mathcal{E}_m(t,h,iz)}\right.$$
$$\left.+\frac{\pi}{\gamma_\phi/\pi^2+\eta(m+1/2)}\int_{-\infty}^{\infty}\frac{dz}{\sinh^2(\pi z)}\frac{\mathrm{Im}^2\mathcal{E}_m(t,h,iz)}{\mathrm{Re}^2\mathcal{E}_m(t,h,iz)+\mathrm{Im}^2\mathcal{E}_m(t,h,iz)}\right]. \tag{103}$$

B. Asymptotic analysis

1. Vicinity of T_{c0} (domains I-III)

First, we present the limiting behavior of $W^{(\mathrm{fl})}$ in the thermal and quantum regimes in Eq. (103). Close to T_{c0} and for magnetic fields not too high ($h\ll 1$) but arbitrary with respect to reduced temperature $\epsilon=(T-T_{c0})/T_{c0}\ll 1$ and phase-breaking rate $\gamma_\phi\ll 1$, one obtains:

$$\frac{W^{(\mathrm{fl})}(\epsilon,h\ll 1)}{W_0}=-3\mathrm{Gi}_{(2)}\left\{\left[\ln\frac{1}{h}-\psi\left(\frac{\epsilon}{2h}+\frac{1}{2}\right)\right]-\frac{\pi^4}{168\zeta(3)}\frac{1}{\epsilon-\gamma_\phi}\left[\psi\left(\frac{\epsilon}{2h}+\frac{1}{2}\right)-\psi\left(\frac{\gamma_\phi}{2h}+\frac{1}{2}\right)\right]\right\}. \tag{104}$$

As with fluctuation corrections to conductivity discussed in Section V, one can split the limiting cases into nine domains, according to Fig. 9. In the limit of weak field near T_{c0}, $h\ll\epsilon\ll 1$ (domain I), the first term in the corresponding correction (see Table VII) reproduces the zero-field result from Refs. (Heym, 1992; Kuboki and Fukuyama, 1989; Maniv and Alexander, 1977; Randeria and Varlamov, 1994), while the second term provides the magnetic field dependence first calculated in Ref. (Mosconi *et al.*, 2000). One can see that the MT contribution dominates when the pair-breaking is weak, i.e., in weak fields SFs increase the NMR relaxation rate.

As the phase-breaking grows, the role of the first term in domain I of table VII weakens, and the contribution of fluctuations can change sign. The MT trajectories shorten, and the negative contribution of superconducting fluctuations due to the suppression of the quasiparticle DOS becomes the dominant one. Since $\gamma_\phi\lesssim 1$, the effect of magnetic field on $W^{(\mathrm{fl})}$ is always negative.

In the case $1\gg h\gg\max\{\epsilon,\gamma_\phi\}$, domain II, the MT contribution dominates (Mosconi *et al.*, 2000): here, intrinsic pair-breaking is weak while the effect of the magnetic field on the motion of Cooper pairs is not yet strong enough.

2. Region close to the line $H_{c2}(T)$ (domains IV – VII)

Next, we discuss the domain of the phase diagram above the second critical field at relatively low temperatures, where fluctuations manifest themselves in the form of vortex clusters. The general formula (103) allows one to obtain explicit analytical expressions. For instance, the main contribution along the line $H_{c2}(T)$, where $t\ll h_{c2}(t)$, comes from the lowest Landau level of the FCP motion. Performing the summation over bosonic frequencies and the integration in Eq. (103), one finds

$$\frac{W^{(\mathrm{fl})}(t\ll h_{c2}(t))}{W_0}=-\frac{4\pi^2\mathrm{Gi}_{(2)}}{7\zeta(3)}\left\{\ln\frac{1}{\widetilde{h}}+\frac{2\widetilde{h}\gamma_\phi}{\pi^2}\left[\psi'\left(\frac{4h_{c2}(t)\widetilde{h}}{\pi^2 t}\right)-\frac{\pi^2 t}{4h_{c2}(t)\widetilde{h}}-\frac{1}{2}\left(\frac{\pi^2 t}{4h_{c2}(t)\widetilde{h}}\right)^2\right]\right\}. \tag{105}$$

In domain IV, the regime of quantum fluctuations is realized at very low temperatures, $t\ll\widetilde{h}$, and just above $H_{c2}(0)$. Quantum fluctuations suppress the NMR relaxation due to decrease of the quasiparticle density of states. At higher temperatures, $\widetilde{h}\ll t\ll h_{c2}(t)$, superconducting fluctuations become thermal in nature, while the DOS suppression of the NMR relaxation remains dominant.

domain	$\delta W^{(\mathrm{fl})}/W_0$
I	$3\mathrm{Gi}_{(2)}\left[\frac{\pi^4}{168\zeta(3)}\frac{1}{\epsilon-\gamma_\phi}\ln\frac{\epsilon}{\gamma_\phi}-\ln\frac{1}{\epsilon}\right]-\mathrm{Gi}_{(2)}\frac{h^2}{2\epsilon^2}\left[\frac{\pi^4}{168\zeta(3)}\frac{\gamma_\phi+\epsilon}{\gamma_\phi^2}-1\right]$
II	$3\mathrm{Gi}_{(2)}\left[\frac{\pi^6}{672\zeta(3)}\frac{1}{h}-\ln\frac{1}{h}\right]$
III	$3\mathrm{Gi}_{(2)}\left\{\frac{\pi^4}{168\zeta(3)}\frac{2h}{(\epsilon+h)(\gamma_\phi+h)}-\ln\frac{1}{h}\right\}$
I–III	*Eq.* (104)
IV	$-\frac{4\pi^2\mathrm{Gi}_{(2)}}{7\zeta(3)}\left[\ln\frac{1}{\tilde{h}}+\frac{\pi^4t^3\gamma_\phi}{192h_{c2}^3(0)\tilde{h}^2}\right]$
V	$-\frac{4\pi^2\mathrm{Gi}_{(2)}}{7\zeta(3)}\ln\frac{1}{\tilde{h}}$
VI-VII	$-\frac{4\pi^2\mathrm{Gi}_{(2)}}{7\zeta(3)}\left[\ln\frac{1}{\tilde{h}(t)}+\frac{\pi^2t^2\gamma_\phi}{16h_{c2}^2(t)\tilde{h}(t)}\right]$
IV–VII	*Eq.* (105)
VIII	$-\frac{2\pi^2\mathrm{Gi}_{(2)}}{7\zeta(3)}\left[\ln\ln\frac{1}{T_{c0}\tau}-\ln\ln t\right]$
IX	$-\frac{2\pi^2\mathrm{Gi}_{(2)}}{7\zeta(3)}\left[\ln\ln\frac{1}{T_{c0}\tau}-\ln\ln h\right]$

TABLE VII Asymptotic expressions for the total relative correction to the NMR relaxation rate in different domains, see Fig. 9. The first column gives the domain according to that figure and is determined by the t & h regions given in Fig. 9.

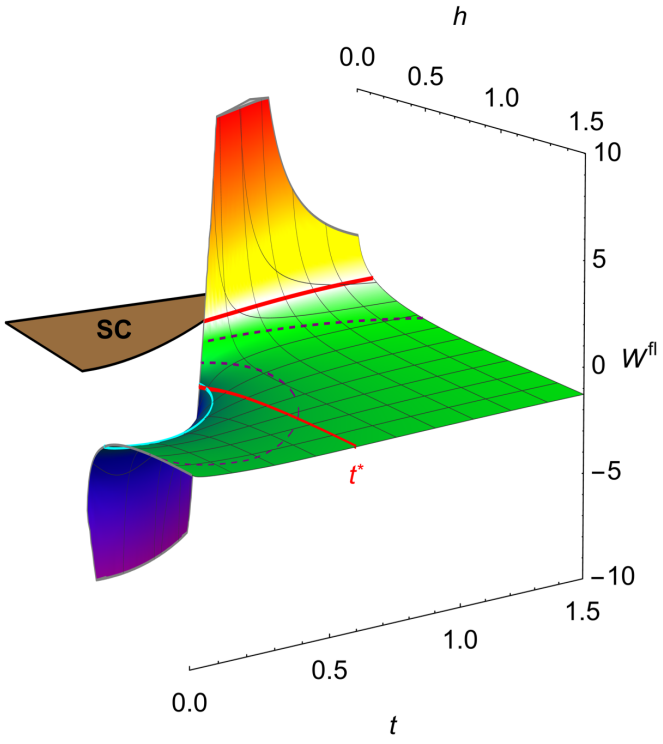

FIG. 41 (Color online) The temperature and magnetic field dependence of the relaxation rate $W^{(\mathrm{fl})}$ in the case of very weak pair-breaking $\gamma_\phi = 0.003$. The thick isoline (red [dark gray]) represents a zero relaxation rate, while the dashed isolines correspond to relaxation rate values of -1 and -2. The mesh-line t^* (red [dark gray]) marks the critical temperature for $\gamma_\phi \to 0$, while the light (cyan [light gray]) contour line indicates the value of $W^{(\mathrm{fl})}$ at $h_{c2}(t^*)$ (-3.04). After Ref. (Glatz *et al.*, 2015).

Fig. 41 presents the results of numerical analysis based on Eq. (103) for different pair-breaking rates γ_ϕ. For small enough pair-breaking, superconducting fluctuations result in the increase of the NMR relaxation rate in a large domain of the phase diagram. Increasing the pair-breaking leads to the suppression of the MT contribution, and for $\gamma_\phi \sim 1$ the effect of quasiparticle DOS suppression on $W^{(\mathrm{fl})}$ dominates in the entire phase diagram.

Note, that even in the absence of pair-breaking, $\gamma_\phi \to 0$, the MT relaxation process is suppressed by strong magnetic fields below some crossover temperature T_0^*, at which point the fluctuation correction $W^{(\mathrm{fl})}$ becomes negative. In the case of a $2D$ superconductor, $T_0^* \approx 0.6T_{c0}$. This results in an opening of a fluctuation spin gap in the magnetic field dependence of W at strong magnetic fields, $H \gtrsim H_{c2}(T_0^*)$.

Above the crossover temperature T_0^*, the field dependence of $W^{(\mathrm{fl})}$ shows a non-monotonic behavior as a result of the two competing contributions, see Fig. 41. The total correction is positive (for not too strong pair-breaking γ_ϕ) close to the line $h_{c2}(t)$; it then decreases rapidly reaching a minimum negative value at some intermediate distance from $h_{c2}(t)$ before increasing up to zero when sufficiently far from the superconducting region.

Below the crossover temperature, the total correction increases monotonically as a function of magnetic field. For $t \ll h_{c2}(t)$, both in the regime of quantum and thermal fluctuations, the numerical analysis is in full agreement with the asymptotic expressions, see Table VII, confirming the negative sign of the total correction.

3. Suppression of the fluctuation contribution to the NMR rate beyond the GL region

The analysis based on Eq. (103) in the entire temperature range along $H_{c2}(T)$ allows to identify the temperature $T^*(\gamma_\varphi)$ at which the DOS and MT relaxation mechanisms fully compensate each other, such that the fluctuation correction $W^{(\mathrm{fl})}$ completely vanishes (in the leading order of perturbation theory). The asymptotic crossover temperature T_0^* is then defined as $T^*(0)$, i.e. the temperature below which the negative DOS contribution always dominates, regardless of the values of γ_φ and h.

C. Fluctuation spectroscopy: analysis of the NMR relaxation rate

At the end of the 1990s and into the 2000s an deep controversy related to the magnetic field dependence of the fluctuation contribution to W existed. The theory predicts, as in the case with magneto-conductivity, that the positive MT contribution is suppressed by magnetic field, while the magnetic-field-dependent part of the negative DOS contribution grows with increasing magnetic field. However, in contrast to the magneto-conductivity, which can be measured extremely precisely, the NMR relaxation rate experiments are much more sophisticated. The result of the competition between these field-dependent corrections to W depends on a number of parameters (γ_φ, τ). The results were found to be qualitatively different in experiments on HTS materials performed by various groups. The reason for this discussion were the absence of a strong positive AL contribution, possible d-pairing, killing the MT contribution (Kuboki and Fukuyama, 1989), small magnitude of the sum of MT and DOS effects even in the case of s-pairing, lack of the precise values of γ_φ, τ leading to contradicting theoretical predictions (Carretta *et al.*, 1996; Eschrig *et al.*, 1999; Mosconi *et al.*, 2000; Randeria and Varlamov, 1994), and the difference in the quality of samples and experimental methods were the reason of this discussion (Brinkmann, 1995; Carretta *et al.*, 2000, 1996; Mitrović *et al.*, 1999; Gorny *et al.*, 1999; Larkin and Varlamov, 2009; Zheng *et al.*, 1999, 2000; Zimmermann *et al.*, 1991).

A first attempt to reveal the role of the SF in the NMR-NQR (nuclear quadrupole resonance) spin lattice relaxation rate was carried out by Carretta *et al.* (Carretta *et al.*, 1996). Since the AL fluctuation correction is zero (for s-wave superconductors), the idea was to focus on the magnetic field dependency on MT and DOS contributions to the relaxation rate. ^{63}Cu NQR (i.e. with zero external magnetic field) measurements of W in YBCO were compared to the corresponding ones in the presence of an external magnetic field. The positive MT contribution to W near T_{c0} was correctly assumed to be strongly

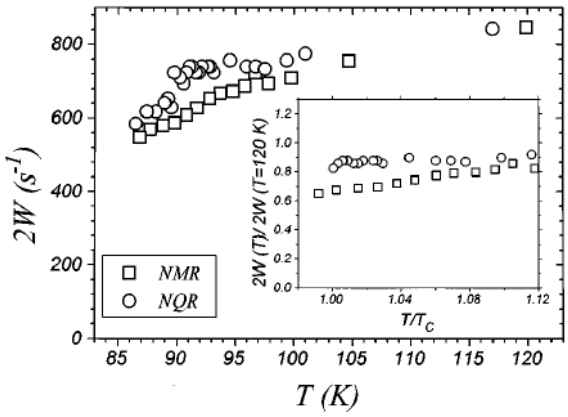

FIG. 42 ^{63}Cu relaxation rates $2W(0)$ in zero field from the NQR relaxation and $2W(H)$ in a field of 5.9 T (from NMR relaxation of the $-1/2 \to 1/2$ line) in the oriented powders of $YBa_2Cu_3O_{7-\delta}$, with $T_{c0}(0) = 90.5$K and $T_c(H) = 87.5$K. The relaxation rates, normalized with respect to $W(H) = W(0)$ for temperatures well above T_c, are reported in the inset as a function of T/T_c. After Ref. (Carretta *et al.*, 1996).

quenched by the field, while the negative DOS term was expected to be more robust. A small dip with respect to the Korringa behavior on approaching T_{c0} from above was observed (see Fig. 42). The studies carried out subsequently by other authors did not confirm the DOS dip, at least not of comparable strength. The role of impurities or defects was suspected to affect the results. Some clarification was provided by the detailed estimate of the effect of external magnetic field on the DOS contribution (Mosconi *et al.*, 2000). Other NMR-NQR studies were carried out for ^{17}O NMR measurements (Mitrović *et al.*, 1999).

Taking into account a non-zero frequency of an a.c. field, the effect of amplitude fluctuations in clean superconductors was considered in (Fay *et al.*, 2001). The results obtained in the limit of zero frequency correspond to that of (Randeria and Varlamov, 1994) in the clean case. Moreover, the authors of (Fay *et al.*, 2001) took the effect of BKT vortex–antivortex fluctuations on the relaxation rate into account.

X. FURTHER DEVELOPMENTS OF FLUCTUATION SPECTROSCOPY

In this review, we focused on a unique approach for the description of the fluctuation phenomena in conventional, dirty 2D superconductors, valid in the wide range of temperatures and magnetic fields beyond the line $H_{c2}(T)$, including the domains of thermal and quantum fluctuations, and the crossover between them. It allows one to study the effect of fluctuations on thermodynamic and transport characteristics of a superconductor both ana-

lytically and numerically. This approach helps to visualize it in the form of 3D surfaces spanning the entire $t-h$ parameter space above the superconducting transition, and to extract from the experimental data such important characteristics as the critical temperature, second critical field, phase-breaking time, etc. In this section we discuss several extensions of the above approach.

A. Extension of fluctuation spectroscopy on quasi-two dimensional superconductors

First, we present an extension of the presented approach to quasi-two dimensional layered superconductors by taking the transverse motion of FCPs into account. Close to T_{c0}, properties of a quasi-two dimensional superconductor can be described well in the framework of the phenomenological Lawrence-Doniach (LD) model (Lawrence and Doniach, 1971), which provides a generalization of the Ginzburg-Landau functional. In the case of a magnetic field applied perpendicular to the coupled superconducting layers, it takes the form:

$$\mathcal{F}^{(\mathrm{LD})}[\Psi]=\sum_l\int d^2r\Big[\alpha T_{c0}\epsilon\left|\Psi_l\right|^2+\frac{b}{2}\left|\Psi_l\right|^4 +\frac{1}{4m}\left|\left(\nabla_\parallel-2ie\mathbf{A}_\parallel\right)\left|\Psi_l\right|^2+\mathcal{J}\left|\Psi_{l+1}-\Psi_l\right|^2\Big]\,.$$

Here Ψ_l is the order parameter of the l-th superconducting layer, and the phenomenological constant $\mathcal{J}$ is proportional to the energy of the Josephson coupling between two adjacent planes. The gauge with $A_z=0$ is chosen. In the immediate vicinity of T_{c0}, the LD functional reduces to the GL one with the effective mass $M=\left(4\mathcal{J}s^2\right)^{-1}$ along the z-direction. One can relate the value of $\mathcal{J}$ to the coherence length along the z-direction, or, more conveniently, with the parameter characterizing the degree of three-dimensionality of the system, $r=4\xi_z^2/s^2$: $\mathcal{J}=\alpha T_{c0}r/2$, see Ref. (Larkin and Varlamov, 2009).

This generalization can also be done in the microscopic approach by accounting for transversal motion in the propagator and Cooperons: $\Omega_H\left(n+\frac{1}{2}\right)\to\Omega_H\left(n+\frac{1}{2}\right)+\frac{\mathcal{J}}{2}(1-\cos q_z s)$ and performing an additional integration over transverse momenta in the final equations. This procedure was performed in Ref. (Glatz *et al.*, 2015) in order to fit the experimental data of Ref. (Lascialfari *et al.*, 2005). It allowed to study the evolution of the crossover temperature $T^*(r)$ as a function of the effective dimensionality of the sample.

B. Fluctuations in two-band superconductors

The specifics of underdoped cuprates attracted the interest to consider fluctuations in these materials in terms of an effective two-gap model (Perali *et al.*, 2000). The latter was motivated by the strong anisotropy of the band dispersion and introduced two weakly coupled bands, in order to preserve a substantial distinction between the superconducting order parameter in different regions of the momentum space. This approach allows for different fluctuation regimes for pairings in different k-space regions. The strongly bound pairs forming at high temperature T^* can experience large fluctuations until the system is stabilized by the coupling with less bound, BCS-like states, leading to a coherent superconducting state at $T_{c0}<T^*$. The temperatures T_{c0} and T^* merge around or above optimum doping. Such a model shares similarities with the fermion-boson models for cuprates (Geshkenbein *et al.*, 1997; Ranninger *et al.*, 1995), to which it reduces in the strong-coupling limit. Important conclusion of Ref. (Perali *et al.*, 2000) was that in the case of two very different but interacting bands, the effective Ginzburg-Levanyuk number, mainly determined by the large band, remains small. As a result, the system is stabilized with respect to fluctuations, allowing for a coherent superconducting phase.

Since the discovery of superconductivity in MgB_2 (see the review (Xi, 2008)), the properties of multi-band superconductors returned to the spotlight of attention after half a century of oblivion (Moskalenko, 1959; Suhl *et al.*, 1959). Further discovery of multi-band high-temperature superconductivity in iron-based materials gave even stronger boost to this field, see the experimental (Johnston, 2010; Paglione and Greene, 2010; Stewart, 2011) and theoretical (Chubukov, 2012; Hirschfeld *et al.*, 2011) reviews.

Superconducting properties of magnesium diboride are strongly influenced by multi-band effects. Among the anomalies found in MgB_2 was the unusually narrow temperature range of applicability of the standard Ginzburg-Landau theory (Komendová *et al.*, 2011; Koshelev and Golubov, 2004; Koshelev *et al.*, 2005). The Cooper pairs of different kinds, formed by electrons of π-band and by electrons of σ-band respectively, behave themselves as the unique condensate only very close to T_{c0}. Due to the large difference in the c-axis coherence lengths of σ and π bands, the condensates of different kinds split already at temperatures parametrically close to T_{c0}: $|T-T_{c0)}|/T_{c0)}\gtrsim\xi_{\sigma z}^2/\xi_{\pi z}^2+S_{\pi\sigma}\ll 1$ (here $S_{\pi\sigma}\ll 1$ is the relative inter-band interaction constant). Evidently, this particularity should manifest itself in fluctuation properties.

The theory generalizing the microscopic theory of fluctuations to a two-band superconductor and deriving the related nonlocal GL functional was developed in Ref. (Koshelev *et al.*, 2005). It was strongly focused on the application to magnesium diboride, in which the main differences between the bands are the strength of intra-band coupling constants and the values of the c-axis coherence length. In result, the very early manifes-

tation of the short wavelength fluctuations in the π band (where superconducting interaction is weaker) was predicted. The predictions of the theory have not been confirmed experimentally, see Ref. (Ferrando *et al.*, 2007), likely because fluctuations in magnesium diboride are extremely weak. The Ginzburg-Levanyuk number for clean MgB_2 can be estimated as $Gi_{(3)} \approx 1.5 \times 10^{-6}$ (see Ref. (Koshelev *et al.*, 2005)).

In contrast, the iron pnictides are multi-band *semimetals* and, as a consequence, are characterized by fairly strong fluctuations. Depending on the compound, the estimates for the Ginzburg-Levanyuk number range from 3×10^{-5} to 5×10^{-3}, see Ref. (Koshelev and Varlamov, 2014). It is likely that behavior of superconducting fluctuations in iron-based superconductors at sufficiently low temperatures is influenced by multi-band effects. Unfortunately, the partial coherence lengths for different bands are not known in present. However, multi-band effects are noticeable in the fluctuation properties of $FeSe_{0.5}Te_{0.5}$ (Klein *et al.*, 2010; Serafin *et al.*, 2010).

The study of short wavelength and dynamic fluctuations in the vicinity of the upper critical field line for a two-band superconductor was performed in Ref. (Koshelev and Varlamov, 2014). As mentioned above, multi-band effects are more pronounced when the bands have significantly different coherence lengths. The transition to the superconducting state is mainly determined by the properties of the rigid condensate of the "strong" band, while the "weak" band with a large coherence length of the Cooper pairs causes the non-locality in fluctuation behavior and break down of the simple Ginzburg-Landau picture. Usually, the effect of a magnetic field on fluctuations becomes essential when the magnetic length ℓ_H reaches the value of the fluctuation Cooper pair size. Since the coherence lengths of different bands together with the gaps in the multiple-band superconductor can differ strongly, one can expect that short wavelength fluctuation modes in them will be excited at very different fields, like it was found in the temperature dependencies of paraconductivity and fluctuation heat capacity for MgB_2 (Koshelev *et al.*, 2005). As expected, the multi-band electronic structure does not change the functional forms of dominating divergences of the fluctuating corrections when the magnetic field approaches the upper critical field. The temperature dependence of the coefficients, however, is modified. Nontrivial consequence of the developed theory consists in the fact that the large in-plane coherence length sets the field scale at which the upper critical field has an upward curvature (see Fig. 43). The authors also observed that the apparent transport transition displaces to lower temperatures with respect to the thermodynamic transition. Even though this effect exists already in the single-band case at sufficiently high fields, it may be strongly enhanced in multi-band materials.

C. Fluctuations in clean superconductors in strong fields

In the limit of a clean superconductor, when the electron mean free path considerably exceeds the BCS coherence length ($T_{c0}\tau \gg 1$), Eqs. (30)–(32) for Cooperons and fluctuation propagator, obtained in the diffusion approximation for the electron motion, are no longer applicable. Moreover, it is known that in the ultra-clean case, when the electron mean free path considerably exceeds the coherence length of FCPs, $\xi_{GL}(\epsilon)$, the DOS and MT contributions cancel each other, see Ref. (Livanov *et al.*, 2000).

The AL contribution for the case of a clean 2D superconductor in the absence of a magnetic field was analyzed in a wide range of temperatures in Ref. (Reggiani *et al.*, 1991). The authors demonstrated that in the temperature dependence of $\sigma_{(2)}^{(AL)} = \frac{e^2}{\hbar} f(\ln t)$ the low temperature ($\ln t \ll 1$) asymptotic $f(x) = x^{-1}/16$ is replaced at high temperatures ($\ln t \gg 1$) by $f(x) = 0.12x^{-3}$. This statement was checked experimentally multiple times and it was found, that the high-temperature regime already starts at an argument value of $x = 0.25$, see Refs. (Caprara *et al.*, 2005; Cimberle *et al.*, 1997).

The compensation of the MT, DOS and DCR contributions in a clean superconductor occurs at the level of the Green's function blocks, i.e., before the integration over FCP momentum, or, more generally, the summation over its quantum numbers. This suggests that in the clean limit, the AL diagram is the only remaining one, even in the case of a strong magnetic field (Galitski and Larkin, 2001a). This is why in order to study the effect of fluctuations on physical properties of a clean superconductor in entire phase diagram, the required elements of the Feynman diagrams have to be found for arbitrary temperatures and in presence of the magnetic field, while taking into account their nonlocal structure.

The role of the magnetic field here in two-fold. First, the superconducting transition itself is governed by the magnetic field. The other effect are the De Haas-van Alphen (in thermodynamic properties) and Shubnikov–de Haas oscillations (in transport coefficients) due to the quantization of the energy levels. However, if $\omega_c\tau \ll 1$ and $T \gg \omega_c \sim T_{c0}^2/E_F$, the oscillation terms are exponentially small and can be neglected.

The method for the analysis of fluctuation effects in the clean case, requiring to deal with non-local operators, is based on the Helfand-Werthamer theory. In the seminal paper (Helfand and Werthamer, 1966), Helfand and Werthamer evaluated the matrix element λ_0 for the Cooperon in a magnetic field, which determines the upper critical field $H_{c2}(T)$. They proved the following mathematical statement, which is referred to as the Helfand-Werthamer theorem. Let us consider an operator $\mathcal{O}$ and suppose that its kernel in coordinate representation has

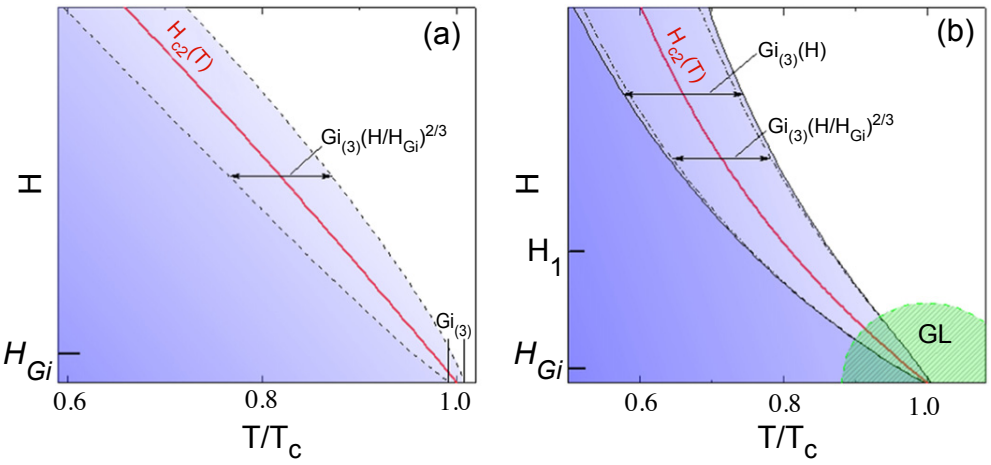

FIG. 43 (Color online) Field dependences for fluctuation region for (a) single-band and (b) two-band superconductors. $H_{\rm Gi} \equiv \tilde{H}_{c2}(0)\mathrm{Gi}_{(3)}$ is the typical value of magnetic field, $\mathrm{Gi}_{(3)}(H)$ is the width of fluctuation region. After Ref. (Koshelev and Varlamov, 2014).

the following form:

$$\mathcal{O}\left(\mathbf{r},\mathbf{r}'\right) = \widetilde{\mathcal{O}}\left(\mathbf{r}-\mathbf{r}'\right)\exp\left(-2ie\int_{\mathbf{r}}^{\mathbf{r}'}\mathbf{A}(\mathbf{s})d\mathbf{s}\right). \quad (106)$$

Then, the operator can be written as

$$\widehat{\mathcal{O}} = \int \widetilde{\mathcal{O}}(\mathbf{r})\exp\left(-i\mathbf{r}\widehat{\pi}\right)d^d\mathbf{r}\,,$$

where $\widehat{\pi} = [\widehat{\mathbf{p}} - 2ie\mathbf{A}(\mathbf{r})]$ is the kinetic momentum, which can be expressed in terms of creation and annihilation operators in Landau representation. One can see that all the operators involved in the above calculations satisfy the Helfand-Werthamer theorem. Namely, the particle-particle bubbles, current vertex, and the four Green function blocks of the AL diagram in coordinate representation can be written as a product of a function of the coordinate difference and the gauge factor. Magnetic field effects can be treated semiclassically, which means that the factor $\widetilde{\mathcal{O}}\left(\mathbf{r}-\mathbf{r}'\right)$ in Eq. (106) can be considered in zero field.

A corresponding approach was realized in Refs. (Galitski and Larkin, 2001a; Kurkijärvi *et al.*, 1972) in the studies of fluctuation diamagnetism and conductivity in clean superconductors.

D. Fluctuation spectroscopy of artificial nanosolids

Nanosolids are artificially designed arrays of nanocrystals composed of tiny crystals ranging in size from 2 to 100 nanometers (they are also called *granular systems*). Due to the electron confinement effect, nanocrystals can be viewed as quantum dots and the behavior of their physical properties lie in between that of molecules and bulk materials. The study of transport properties of granular metals has gained significant attention (Beloborodov *et al.*, 2007; Goldman and Markovič, 1998) since the groundbreaking experiments on the superconductor-insulator transition in granular samples (Haviland *et al.*, 1989). Altering the nanocrystal composition and size allows modifying bulk material properties, in particular enabling the study of the interplay between electron correlations and mesoscopic effects of disorder.

A clear experimental signature of granularity in superconducting system was given in (Lerner *et al.*, 2008). Nanosolids are characterized by the following two one-electron transport mechanisms: the intragrain diffusion (with diffusion coefficient $\mathcal{D}_{\rm g}$) and the intergrain tunneling (with effective diffusion coefficient $\mathcal{D}_{\rm T} = \Gamma a^2$, where Γ is the electron tunneling rate between nano-grains and a is the average grain size). Typically, $\mathcal{D}_{\rm g} \gg D_{\rm T}$ and these two mechanisms result in the appearance of two different Ginzburg-Landau lengths. The first one, $\xi_{\mathrm{GL,g}}(\epsilon) = (\mathcal{D}_g/T_{c0}\epsilon)^{1/2}$, is a result of intragrain pairing, while the second, $\xi_{\mathrm{GL,T}}(\epsilon) = (\mathcal{D}_{\rm T}/T_{c0}\epsilon)^{1/2}$ corresponds to pairing across (intergrain) grains. As as consequence, there are three distinct temperature regimes in the vicinity of the critical temperature. In the first one, far from T_{c0}, where $\epsilon > \mathcal{D}_{\rm g}a^{-2}T_{c0}^{-1} = E_{\rm Th}/T_{c0}$ ($E_{\rm Th}$ is the Thouless energy), the pairing has intergrain nature. In this region the FCPs of each grain are independent and their motion has 3D character, corresponding to a critical exponent of the paraconductivity of $-1/2$. When temperature approaches T_{c0} and $\xi_{\mathrm{GL,g}}(\epsilon)$ becomes larger than the grain size, while $\xi_{\mathrm{GL,T}}(\epsilon)$ remains smaller, the pairing still has the intergrain nature, but the size of FCPs in this temperature range ($\Gamma/T_{c0} \ll \epsilon \ll E_{\rm Th}/T_{c0}$) exceeds the grain diameter. Here, each grain acts as its own zero-

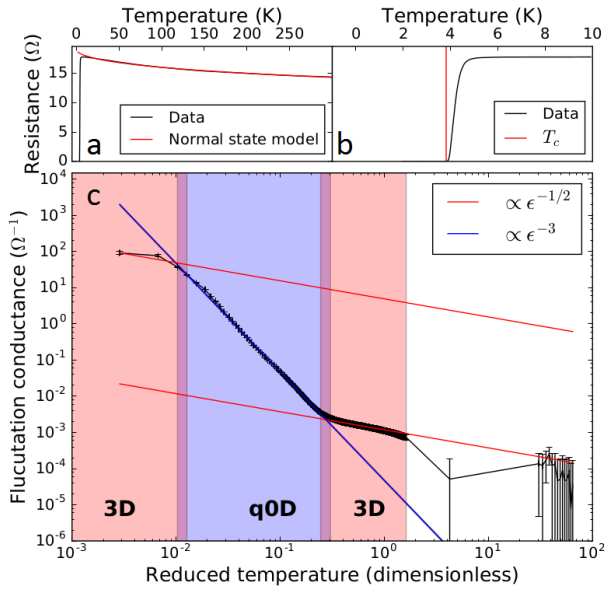

FIG. 44 (Color online) Fluctuation spectroscopy of a 564nm thick BNCD film. (a) A fit to the high temperature region reveals a $T^{0.5}$ dependence, and allows extraction of the value of normal conductance. (b) T_c is defined as the point at which the conductance diverges, depicted as vertical line. (c) Fluctuation conductance as a function of reduced temperature ϵ. *Figure reprinted from Ref. (Klemencic* et al., *2017) (Fig. 3) with permission by authors (2017).*

dimensional (0D) superconductor for which the paraconductivity is expected to be proportional ϵ^{-2}. However, an intergrain FCP transport requires two electrons to hop within one GL lifetime $\tau_{\rm GL} \sim \epsilon^{-1}$ such that the AL contribution in a quasi-0D array of grains should in fact be $\sim \epsilon^{-3}$. Finally, in the immediate vicinity of the critical temperature, $\epsilon \ll \Gamma/T_{c0}$, the coherence length $\xi_{\rm GL,T}(\epsilon)$ exceeds the grain size and the pairing involves electrons of different grains such that the system becomes becomes effectively 3D and the critical exponent of the paraconductivity is $-1/2$, the same as in region $E_{\rm Th}/T_{\rm c0} < \epsilon$. This qualitative picture was supported by the rigorous calculations in Ref. (Lerner *et al.*, 2008). Another type of dimensional double-crossover of fluctuation conductivity as function of temperature was predicted for multilayer superconducting films in Ref. (Varlamov and Yu, 1991).

Very recently the authors of Ref. (Klemencic *et al.*, 2017) presented measurements for the resistance versus temperature in a series of boron-doped nanocrystalline diamond (BNCD) films with different grain sizes, varied by changing the film thickness. Upon extracting the fluctuation conductivity near to the critical temperature, they indeed observed three distinct scaling regions (3D intragrain, quasi-0D, and 3D intergrain, see Fig. 44), confirming the prediction of Ref. (Lerner *et al.*, 2008). The location of the crossovers between these scaling regions allowed them to determine the tunneling energy and the Thouless energy for each film.

The tunneling energy, or Γ, is an energy associated with the transfer of carriers across grain boundaries. Therefore, it does not depend much on the morphology of the grains and is almost invariant between different film. In work (Klemencic *et al.*, 2017), Γ was extracted from the 3D to quasi-0D crossover for all samples and the authors found a value of $\Gamma = 4.2 \pm 2.0 \mu$eV. On the other hand, the Thouless energy should be proportional to the inverse square of the mean grain size with proportionality factor being the intragrain diffusion coefficient. Using this relation they found a value of $\mathcal{D}_{\rm g} = 11.5 \pm 5.7 {\rm cm}^2/{\rm s}$.

Overall, this experimental work is another example of fluctuation spectroscopy, which allows to extract information about the granular structure in nanosolids from the observation of dimensional crossovers in the fluctuation regime. The authors conclude that this is a remarkably simple yet valuable tool for the characterization of microscopic properties of nanocrystalline superconductors.

E. Fluctuation spectroscopy of inhomogeneous films: pseudogap and confinement

In this review, we considered fluctuations as deviations of the superconducting order parameter from its mean field solution and their effect on various transport properties of SCs. I.e., we remained in the framework of the fermionic scenario of superconductivity relating the SC transition temperature to the appearance of a supercurrent as response to an applied vector potential. Or, in other words, one identifies T_{c0} with the temperature at which a stable condensate of Cooper pairs with $\langle \Delta(\mathbf{r}, t) \rangle \neq 0$ appears.

The role of a weak disorder on the properties of SCs in the framework of the BCS theory was elucidated a long time ago in the seminal papers of Anderson (Anderson, 1959), and Abrikosov and Gor'kov (Abrikosov and Gor'kov, 1959a,b). It was demonstrated that in the case of SCs with isotropic spectrum and s-type pairing, which contain a not too high concentration of elastic impurities (the electronic mean free path is supposed to be much larger than the inter-atomic distance), the so-called Anderson theorem is valid. The latter states that in first approximation the presence of impurities does not effect the thermodynamic properties of SCs.

Later, as the focus of attention shifted towards the study of properties of disordered and low-dimensional superconductors, this traditional understanding of the role of impurities become subject of revisions. Remaining in the fermionic paradigm of superconductivity, Finkel'stein demonstrated (Finkel'shtein, 1987) that the delay in screening of the Coulomb interaction in a disordered two-dimensional SC leads to a decrease of the effective electron attraction and, as result, a suppression of Cooper

pair formation when the electronic mean free path becomes of the order of the inter-atomic distance.

Nowadays, the so-called bosonic scenario is discussed in which strong disorder may destroy the phenomenon of superconductivity by means of localization of unbroken Cooper pairs, giving rise to a specific normal pseudogap state. The way in which superconductivity is destroyed in such systems is still debated. A numerical approach to study the properties of uniformly disordered superconductors (Bouadim *et al.*, 2011) suggested that there is a continuous crossover (Trivedi *et al.*, 2012) from the weak disorder limit, where the system has a rather homogeneous fermionic character, to the strong disorder limit, where characteristic inhomogeneities appear in the superconducting order parameter. The latter has an emergent bosonic nature and is characterized by a single-particle gap, which persists on the insulating side of the transition.

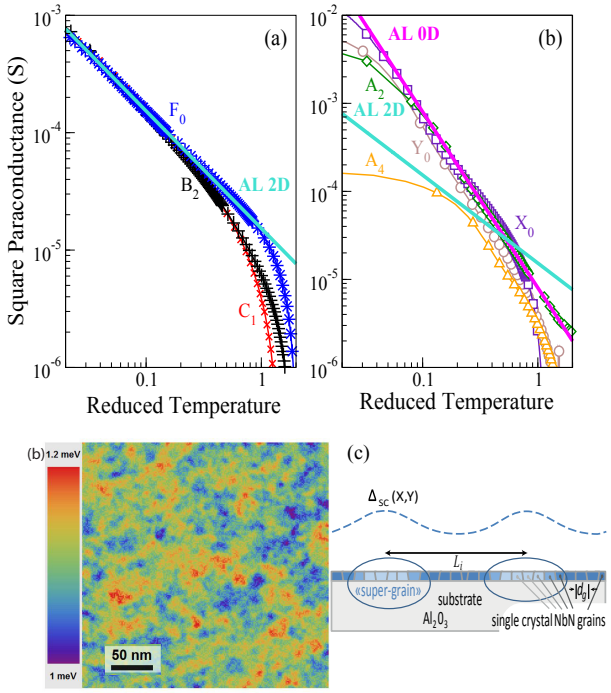

FIG. 45 (a) Extracted square paraconductance for three different, relatively thick samples B_2 ($T_{c0} = 7.1$K, pluses), C_1 ($T_{c0} = 9.4$K, crosses), and F_0 ($T_{c0} = 9.0$K, asterisks) as a function of the reduced temperature $\epsilon = \ln(T/T_{c0})$. The agreement with the Aslamasov-Larkin prediction for a 2D system (cyan solid line) is excellent, without any adjustable parameter. (b) Extracted square paraconductance for the thinner samples Y_0 ($T_{c0} = 4.3$K, open circles), X_0 ($T_{c0} = 3.8$K, open squares), A_2 ($T_{c0} = 4.5$K, open diamonds), and A_4 ($T_{c0} = 2.4$K, open triangles). The pink solid line corresponds to $\sigma = 0.03e^2/(\epsilon^2)$. The expected AL 2D square paraconductance is also shown (thick cyan [light gray] solid line). (c) Map displaying the superconducting gap inhomogeneities at 300mK. Adapted figure from Ref. Carbillet *et al.*, 2016 with permission by authors.

Recent experiments on ultrathin NbN films seem to find indications of an intermediate regime between such fermionic and bosonic scenarios, where Cooper pairs start to localize, while still keeping their character of pairs of Fermions. By combining transport and nanoscale studies of superconducting ultrathin NbN films, it was found in Ref. (Carbillet *et al.*, 2016) that nanoscopic inhomogeneities emerge when the film thickness is reduced. For the thinnest films, scanning tunneling spectroscopy at low temperature unveils inhomogeneities in the superconducting properties, of typical size L_i, that are *not* directly correlated to any structural inhomogeneity and that are found to persist above the critical temperature in the form of a pseudogap [Fig. 45(c)]. Remarkably enough, while the thickest films display a purely two-dimensional behavior of SFs above the critical temperature [Fig. 45(a)], the paraconductivity in the pseudogap regime of the thinnest samples demonstrates SFs of the order parameter which formally corresponds to a zero-dimensional (0D) regime [Fig. 45(b)]. This 0D behavior eventually crosses over to 2D paraconductivity when T_{c0} is approached. Such behavior was ascribed by the authors to an anomalous slowing-down of the diffusion process at long/intermediate wave vectors.

When $\Delta\sigma$ is converted into the measured paraconductance per square by means of the length scale l_{sg}, which represents the size of the 0D *supergrain* (sg) fluctuating domains, one obtains (analogously to subsection X.D)

$$\sigma_{0D}^{(AL)} = \left(\frac{\xi}{l_{sg}}\right)^2 \frac{\pi e^2}{4\hbar\epsilon^2}\,.$$

Deducing $\xi \sim 5.5 \pm 0.5$ nm from the critical field H_{c2}, it is possible to extract the value of l_{sg} from the paraconductivity data. One finds, e.g., $l_{sg} = 28$ nm for samples A_2 ($T_{c0} = 4.5$K) and X_0 ($T_{c0} = 3.8$K), $l_{sg} = 35$ nm for sample Y_0 ($T_{c0} = 4.3$K), and $l_{sg} = 40$nm for sample A_4 ($T_{c0} = 2.4$K). These values of l_{sg} are in quantitative agreement with the typical domain size $L_i/2 \sim 50$nm extracted from STS data at 300mK and at 4.2K for sample X_0 ($T_{c0} = 3.8$K). This means that it is the length $L_i/2 \sim l_{sg}$ instead of the real grain size $d_g \ll l_{sg}$ sets the scale for the 0D fluctuating domains. Such situation remains until the temperature approaches T_{c0} so close that the coherence length $\xi_{GL}(\epsilon)$ becomes larger than L_i and the 2D behavior is recovered.

This scenario leads to a "temporary confinement" of SFs, which allows to explain the paradoxical simultaneous presence of a pseudogap and 0D *amplitude* fluctuations of the order parameter (if the pseudogap indicates simple localization of bosonic pairs, only phase fluctuations would be expected).

XI. NUMERICAL FLUCTUATION SPECTROSCOPY

In order to utilize the complete expressions for fluctuation corrections of conductivity $\sigma_{xx}^{(\mathrm{fl})}(t,h)$ (Eq. (55)), NMR relaxation rate $W^{(\mathrm{fl})}$ (Eq. (103)), Nernst coefficient $\nu^{(\mathrm{fl})}$ (Eq. (80)), or tunneling current I_{qp} (Eq. (91)) to analyze experimental data, an efficient and accurate method to evaluate those expressions numerically is needed. Here we review the numerical methods used for their evaluation with examples – we avoid discussing the actual implementation or technical programming issues, like parallelization (which is straight-forward for the problem discussed here). As supplementary information we provide a C++ implementation for the evaluation of all the fluctuation corrections mentioned above.

A first important ingredient for all expressions is an efficient and accurate algorithm for the evaluation of the real and complex poly-Gamma functions $\psi^{(n)}(z)$. The former is readily available in standard numerical toolkits like GSL (Gough, 2009), but a complex version is a bit more difficult to find and we refer the interested reader to Ref. (Zhang and Jin, 1996). Another complication of most evaluations is that the summation cut-off parameter M_t can reach extremely large values at low temperatures [experimental values $(T_{c0}\tau)_{\mathrm{exp}}^{-1}$ for materials near the superconductor-insulator transition can be on the order 10^6], which slows the numerical procedure down significantly. The latter difficulty can be partially overcome by evaluation of the slowly divergent tails of the m-sums, in e.g. Eq. (55), as integrals. Here, we should also note that for fitting purposes one does not need to choose actual, often extremely small, experimental values $(T_{c0}\tau)_{\mathrm{exp}}$. To save CPU time, one can assume the value $(T_{c0}\tau)_{\mathrm{num}}$ of this parameter to be much larger than $(T_{c0}\tau)_{\mathrm{exp}}$ (but still much less than $T_{c0}\tau_\phi$). After the evaluation of the complete expression, the result can then be shifted by $\ln\ln\frac{(T_{c0}\tau)_{\mathrm{num}}}{(T_{c0}\tau)_{\mathrm{exp}}}$, which approximates the summands not evaluated explicitly Nevertheless, the numerical task remains challenging: e.g., for the surface plot in Fig. 15 we evaluated 10^6 values for $\delta\sigma$ with the modest assumption $(T_{c0}\tau)_{\mathrm{num}} = 0.01$, yet it still took three months of single core CPU time (in 2011) for its calculation.

The (convergent) integral contributions (typically z-integrations) are least difficult to calculate and can be straight-forwardly evaluated using a suitable quadrature scheme. It was found that the Gauss-Legendre 5-point method was efficient and accurate, allowing also the integration of integrable poles or principle values. In practice, due to the presence of the $\sinh^{-2}(\pi z)$ term in the integrand, we can restrict the integration support to $z \in [-5,5]$. Outside this interval the integrand is smaller than the numerical accuracy of double precision floating point numbers. Sums over Landau-levels are calculated up to the cutoff $M_t = (tT_{c0}\tau)^{-1}$ explicitly.

In contrast, summations over k are more involved and only slowly converging (or not converging at all as in the case for the susceptibility $\chi^{(\mathrm{fl})}$ (Eq. (38), where the cutoff for Matsubara frequencies has to be taken into account). For the numerical summation of the k-sum we separate the $k=0$ term and sum from $k=1$ to $k_{\max}$ (with coefficiet 2, due to symmetry) which is determined by the arguments of the $\psi^{(n)}$ functions being equal to $\Omega = 1000$. For $k \geq k_{\max}$ we transform the sum into an integral and use only the asymptotic expressions for the poly-Gamma functions as the difference to the exact expression is again below the floating point accuracy. Then the integration variable is inverted and we have a finite integral for the remaining part of the sum. In the case when the k-sum is not converging, this integral was two non-zero finite limits.

Exemplary, we show the transformation of the k-sum appearing in the NMR contribution, Eq. (103), to a suitable form for numerical evaluation (Glatz *et al.*, 2015):

$$S_m^{(\mathrm{MT})} \equiv \sum_{k=-\infty}^{\infty} \frac{\mathcal{E}_m''(t,h,|k|)}{\mathcal{E}_m(t,h,|k|)}$$

and write

$$\begin{aligned} S_m^{(\mathrm{MT})} &\doteq \left[\sum_{k=0}^{k_{\max}-1}(2-\delta_{0,k}) + 2\int_{k_{\max}}^{\infty} dk\right] \frac{\mathcal{E}_m''(t,h,|k|)}{\mathcal{E}_m(t,h,|k|)} \\ &\equiv S_m^{(\mathrm{MT})(\mathrm{s})} + S_m^{(\mathrm{MT})(\mathrm{i})} \end{aligned}$$

with

$$k_{\max} = \max\left\{2\Omega - \left\lfloor \frac{4h}{\pi^2 t}(2m+1)\right\rfloor, 1\right\}.$$

Here we use $\doteq$ to indicate "equal" in floating point precision.

The sum part $S_m^{(\mathrm{MT})(\mathrm{s})}$ is calculated straightforwardly, which leaves the calculation of the "rest-integral" $S_m^{\mathrm{MT(i)}}$:

$$\begin{aligned} S_m^{(\mathrm{MT})(\mathrm{i})} &= \frac{1}{2}\int_{k_{\max}}^{\infty} dk\, \frac{\psi''\left(\frac{1+k}{2}+x_m\right)}{\ln t - \psi\left(\frac{1}{2}\right) + \psi\left(\frac{1+k}{2}+x_m\right)} \\ &\doteq -\frac{1}{2}\int_{k_{\max}}^{\infty} dk\, \frac{\left(\frac{1+k}{2}+x_m\right)^{-2}}{\ln t - \psi\left(\frac{1}{2}\right) - \ln(2) + \ln(1+k+2x_m)} \end{aligned}$$

where we used the asymptotic behavior of the poly-Gamma functions with $x_m \equiv \frac{2h}{t}\frac{(2m+1)}{\pi^2}$.

A convenient substitution is

$$\begin{aligned} \frac{1}{z} &= \frac{8}{\pi^2} + \frac{(1+k)t}{h\,(m+1/2)} = \frac{8}{\pi^2 x_m}\left[x_m + \frac{1+k}{2}\right], \\ \frac{dz}{z^2} &= -\frac{t}{h\,(m+1/2)}dk = -\frac{4}{\pi^2}\frac{dk}{x_m}, \\ z_{\max} &= \frac{\pi^2}{4}\left(2 + \frac{1+k_{\max}}{x_m}\right)^{-1}. \end{aligned}$$

Therefore,

$$S_m^{(\mathrm{MT})(\mathrm{i})} = \frac{\pi^2}{8}\int_{z_{\max}}^{0} \frac{dz}{z^2 \ln\left(t\pi^2 x_m/4\right) - \psi\left(\frac{1}{2}\right) - \ln(2) - \ln(z)} \frac{x_m\left(\frac{8z}{\pi^2 x_m}\right)^2}{}$$
$$= -\frac{8}{\pi^2 x_m}\int_0^{z_{\max}} dz \frac{1}{A_m - \ln z}$$
$$= -\frac{2t}{h\,(m+1/2)}\int_0^{z_{\max}} dz \frac{1}{A_m - \ln z}$$

with $A_m \equiv \ln\left[h\,(m+1/2)\right] - \psi\left(\frac{1}{2}\right) - \ln(2)$.

This integral is integrable and calculated by the Gauss-Legendre 5-point method (which avoids the singular point at $z = 0$) with only a few support points in the small interval 0 to $z_{\max}$ (125 support points are sufficient to reach floating point precision).

Overall this yields a highly accurate numerical value of the k-sums.

In the quasi-two-dimensional case the additional finite q-integral is calculated by the Gauss-Legendre 5-point method using 25 support points, which is sufficient to obtain high accuracy.

The k-summations for all other fluctuation corrections can be treated in a similar fashion.

ACKNOWLEDGMENTS

We express our deep gratitude to A. Chubukov, Yu. Galperin, M. Grilli, A. Kavokin, A. Koshelev, V. Krasnov, V. Kravtsov, W. Kwok, K. Levin, A. Rigamonti, and M.P. Smylie for reading the manuscript and valuable comments. We want to thank our coauthors T. Baturina, V. Galitsky, M. Serbyn, M. Skvortsov, and V.M. Vinokur for collaboration on several works on fluctuation spectroscopy, which are partially reviewed here. A.V. acknowledges the financial support from the project CoExAn (HORIZON 2020, grant agreement 644076), from Italian MIUR through the PRIN 2015 program (Contract No. 2015C5SEJJ001). This work was supported by the U.S. Department of Energy, Office of Science, Office of Advanced Scientific Computing Research and Materials Sciences and Engineering Division, Scientific Discovery through Advanced Computing (SciDAC) program.

REFERENCES

Abeles, B., R. Cohen, and C. Fuselier (1971), Physica **55**, 275 .

Abrahams, E., R. Prange, and M. Stephen (1971), Physica **55**, 230.

Abrahams, E., M. Redi, and J. W. F. Woo (1970), Phys. Rev. B **1**, 208.

Abrikosov, A., and L. Gor'kov (1959a), Sov. Phys. JETP **8**, 1090, russian original - ZhETF, Vol. 35, No. 6, p. 1558, 1959.

Abrikosov, A., and L. Gor'kov (1959b), Sov. Phys. JETP **9**, 220, russian original - ZhETF, Vol. 36, No. 1, p. 319, 1959.

Abrikosov, A. A. (1988), *Fundamentals of Metal Theory* (Elsevir).

Abrikosov, A. A., L. P. Gor'kov, I. Y. Dzyaloshinskii, and D. Brown (1965), *Quantum field theoretical methods in statistical physics*, Vol. 2 (Pergamon Press Oxford).

Altshuler, B., M. Reizer, and A. Varlamov (1983), Soviet JETP **57**, 1329.

Anderson, P. W. (1959), J. Phys. Chem. Solids **11**, 26.

Angilella, G. G. N., R. Pucci, A. A. Varlamov, and F. Onufrieva (2003), Phys. Rev. B **67**, 134525.

Aronov, A., S. Hikami, and A. Larkin (1995), Physical Review B **51** (6), 3880.

Aronov, A., and A. Rapoport (1992), Modern Physics Letters B **6** (16n17), 1083.

Artemenko, S., I. Gorlova, and Y. Latyshev (1989), Physics Letters A **138** (8), 428.

Aslamasov, L., and A. Larkin (1968), Physics Letters A **26** (6), 238 .

Aslamasov, L., and A. Varlamov (1980), Journal of Low Temperature Physics **38** (1-2), 223.

Aslamazov, L., and A. Larkin (1974), Soviet Phys. JETP **40**, 321.

Bardeen, J., L. N. Cooper, and J. R. Schrieffer (1957a), Phys. Rev. **106**, 162.

Bardeen, J., L. N. Cooper, and J. R. Schrieffer (1957b), Phys. Rev. **108**, 1175.

Baturina, T. I., S. V. Postolova, A. Y. Mironov, A. Glatz, M. R. Baklanov, and V. M. Vinokur (2012), EPL (Europhysics Letters) **97** (1), 17012.

Beasley, M. R., J. E. Mooij, and T. P. Orlando (1979), Phys. Rev. Lett. **42**, 1165.

Behnia, K., and H. Aubin (2016), Reports on Progress in Physics **79** (4), 046502.

Beloborodov, I. S., and K. B. Efetov (1999), Phys. Rev. Lett. **82**, 3332.

Beloborodov, I. S., K. B. Efetov, and A. I. Larkin (2000), Phys. Rev. B **61**, 9145.

Beloborodov, I. S., A. V. Lopatin, V. M. Vinokur, and K. B. Efetov (2007), Rev. Mod. Phys. **79**, 469.

Belogolovskii, M., A. Khachaturov, and O. Chernyak (1986), Sov. Low Temp. Phys. **12** (6), 630.

Bennemann, K.-H., and J. B. Ketterson, Eds. (2008), *The Physics of Superconductors* (Springer Berlin Heidelberg, Berlin, Heidelberg).

Bergmann, G. (1984), Physical Review B **29** (11), 6114.

Bernardi, E., A. Lascialfari, A. Rigamonti, L. Romanò, V. Iannotti, G. Ausanio, and C. Luponio (2006), Phys. Rev. B **74**, 134509.

Blonder, G. E., M. Tinkham, and T. M. Klapwijk (1982), Phys. Rev. B **25**, 4515.

Bouadim, K., Y. L. Loh, M. Randeria, and N. Trivedi (2011), Nature Physics **7**, 884.

Brenig, W., M. Paalanen, A. Hebard, and P. Wölfle (1986), Physical Review B **33** (3), 1691.

Breznay, N. P., and A. Kapitulnik (2013), Phys. Rev. B **88**, 104510.

Breznay, N. P., K. Michaeli, K. S. Tikhonov, A. M. Finkel'stein, M. Tendulkar, and A. Kapitulnik (2012), Phys. Rev. B **86**, 014514.

Brinkmann, D. (1995), Applied Magnetic Resonance **8** (1), 67.

Bruynseraede, Y., M. Gijs, C. Van Haesendonck, and G. Deutscher (1983), Physical review letters **50** (4), 277.

Bulaevskii, L. (1974), Soviet Phys. JETP **39**, 1090.

Capan, C., K. Behnia, J. Hinderer, A. G. M. Jansen, W. Lang, C. Marcenat, C. Marin, and J. Flouquet (2002), Phys. Rev. Lett. **88**, 056601.

Caprara, S., J. Biscaras, N. Bergeal, D. Bucheli, S. Hurand, C. Feuillet-Palma, A. Rastogi, R. C. Budhani, J. Lesueur, and M. Grilli (2013), Phys. Rev. B **88**, 020504.

Caprara, S., M. Grilli, L. Benfatto, and C. Castellani (2011), Physical Review B **84** (1), 014514.

Caprara, S., M. Grilli, B. Leridon, and J. Lesueur (2005), Phys. Rev. B **72**, 104509.

Caprara, S., M. Grilli, B. Leridon, and J. Vanacken (2009), Phys. Rev. B **79**, 024506.

Carbillet, C., S. Caprara, M. Grilli, C. Brun, T. Cren, F. Debontridder, B. Vignolle, W. Tabis, D. Demaille, L. Largeau, K. Ilin, M. Siegel, D. Roditchev, and B. Leridon (2016), Phys. Rev. B **93**, 144509.

Carlson, R. V., and A. M. Goldman (1973), Phys. Rev. Lett. **31**, 880.

Carretta, P., A. Lascialfari, A. Rigamonti, A. Rosso, and A. Varlamov (2000), Phys. Rev. B **61**, 12420.

Carretta, P., D. V. Livanov, A. Rigamonti, and A. A. Varlamov (1996), Phys. Rev. B **54**, R9682.

Mitrović, V. F., H. N. Bachman, W. P. Halperin, M. Eschrig, J. A. Sauls, A. P. Reyes, P. Kuhns, and W. G. Moulton (1999), Phys. Rev. Lett. **82**, 2784.

Mitrović, V. F., H. N. Bachman, W. P. Halperin, A. P. Reyes, P. Kuhns, and W. G. Moulton (2002), Phys. Rev. B **66**, 014511.

Chang, J., N. Doiron-Leyraud, O. Cyr-Choiniere, G. Grissonnanche, F. Laliberte, E. Hassinger, J.-P. Reid, R. Daou, S. Pyon, T. Takayama, H. Takagi, and L. Taillefer (2012), Nature Physics **8** (10), 751.

Chen, Q., J. Stajic, S. Tan, and K. Levin (2005), Physics Reports **412** (1), 1 .

Chubukov, A. (2012), Annu. Rev. Condens. Matter Phys. **3** (1), 57.

Chubukov, A. V., D. Pines, and J. Schmalian (2008), "The physics of superconductors," Chap. A Spin Fluctuation Model for *d*-Wave Superconductivity, in (Bennemann and Ketterson, 2008), pp. 1349–1413.

Cimberle, M. R., C. Ferdeghini, E. Giannini, D. Marré, M. Putti, A. Siri, F. Federici, and A. Varlamov (1997), Phys. Rev. B **55**, R14745.

Cohen, R. W., B. Abeles, and C. R. Fuselier (1969), Phys. Rev. Lett. **23**, 377.

Corti, M., B. J. Suh, F. Tabak, A. Rigamonti, F. Borsa, M. Xu, and B. Dabrowski (1996), Phys. Rev. B **54**, 9469.

Cucolo, A. M., M. Cuoco, and A. A. Varlamov (1999), Phys. Rev. B **59**, R11675.

Di Castro, C., R. Raimondi, C. Castellani, and A. A. Varlamov (1990), Phys. Rev. B **42**, 10211.

Dinter, M. (1977), Journal of Low Temperature Physics **26** (1), 39.

Dorin, V. V., R. A. Klemm, A. A. Varlamov, A. I. Buzdin, and D. V. Livanov (1993), Phys. Rev. B **48**, 12951.

Emery, V. J., and S. A. Kivelson (1995), Nature **374** (6521), 434.

Eschrig, M., D. Rainer, and J. A. Sauls (1999), Phys. Rev. B **59**, 12095.

Fay, D., J. Appel, C. Timm, and A. Zabel (2001), Phys. Rev. B **63**, 064509.

Feigel'man, M. V., L. B. Ioffe, and M. Mézard (2010), Phys. Rev. B **82**, 184534.

Ferrando, V., I. Pallecchi, A. Malagoli, M. Putti, X. Xi, A. Varlamov, A. Koshelev, and C. Ferdeghini (2007), Physica C: Superconductivity and its applications **460**, 608.

Finkelshtein, A. (1983), Sov. Phys. JETP **57** (1), 97, (Zh. Eksp. Teor. Fiz. **84**, 168 (1983).).

Finkel'shtein, A. M. (1987), JETP Letters **45**, 46, russian original - Pis'ma Zh. Eksp. Teor. Fiz., 45, No. 1, 37-40, 1987.

Fiory, A., A. Hebard, and W. Glaberson (1983), Physical Review B **28** (9), 5075.

Forro, L., and A. Hamzić (1989), Solid state communications **71** (12), 1099.

Fukuyama, H., H. Ebisawa, and T. Tsuzuki (1971), Progress of Theoretical Physics **46** (4), 1028.

Galffy, M., and E. Zirngiebl (1988), Solid state communications **68** (10), 929.

Galitski, V. M., and A. I. Larkin (2001a), Phys. Rev. Lett. **87**, 087001.

Galitski, V. M., and A. I. Larkin (2001b), Phys. Rev. B **63**, 174506.

Gantmakher, V. F., S. N. Ermolov, G. E. Tsydynzhapov, A.A.Zhukov, and T.I.Baturina (2003), JETP Letters **77**, 498.

Geballe, T. H., A. Menth, F. J. Di Salvo, and F. R. Gamble (1971), Phys. Rev. Lett. **27**, 314.

Gershenzon, M., V. Gubankov, and Y. E. Zhuravlev (1983), Sov. Phys.-JETP (Engl. Transl.);(United States) **58** (1), (Zh. Eksp. Teor. Fiz. **85**, 287 (1983).).

Geshkenbein, V. B., L. B. Ioffe, and A. I. Larkin (1997), Phys. Rev. B **55**, 3173.

Giaever, I., and K. Megerle (1961), IRE Trans. Electron Devices **ED-9**, 459.

Ginzburg, V. (1960), Soviet Solid State Physics **2**, 61.

Glatz, A., A. Galda, and A. A. Varlamov (2015), Phys. Rev. B **92**, 054513.

Glatz, A., and A. A. Varlamov (2017), in preparation **xx**, xxxxxx.

Glatz, A., A. A. Varlamov, and V. M. Vinokur (2011a), Phys. Rev. B **84**, 104510.

Glatz, A., A. A. Varlamov, and V. M. Vinokur (2011b), EPL (Europhysics Letters) **94** (4), 47005.

Glatz, A., A. A. Varlamov, and V. M. Vinokur (2014), EPL (Europhysics Letters) **107** (4), 47004.

Glover, R. (1967), Physics Letters A **25** (7), 542 .

Goldman, A. M., and N. Markovič (1998), Physics Today **51** (11), 39, http://dx.doi.org/10.1063/1.882069.

Gollub, J. P., M. R. Beasley, R. Callarotti, and M. Tinkham (1973), Phys. Rev. B **7**, 3039.

Gordon, J. M., and A. Goldman (1986), Physical Review B **34** (3), 1500.

Gordon, J. M., C. Lobb, and M. Tinkham (1984), Physical Review B **29** (9), 5232.

Gor'kov, L. (1960), Soviet Physics JETP **37** (10), 998.

Gorny, K., O. M. Vyaselev, J. A. Martindale, V. A. Nandor, C. H. Pennington, P. C. Hammel, W. L. Hults, J. L. Smith, P. L. Kuhns, A. P. Reyes, and W. G. Moulton (1999), Phys. Rev. Lett. **82**, 177.

Gough, B. (2009), *GNU Scientific Library Reference Manual - Third Edition*, 3rd ed. (Network Theory Ltd.).

Graybeal, J. M., J. Luo, and W. R. White (1994), Phys. Rev. B **49**, 12923.

Gusynin, V., V. Loktev, and I. Shovkovyi (1995), Journal of Experimental and Theoretical Physics **80** (6), 1111.

Hagen, S., C. Lobb, R. Greene, M. Forrester, and J. Kang (1990), Physical Review B **41** (16), 11630.

Hagen, S. J., A. W. Smith, M. Rajeswari, J. L. Peng, Z. Y. Li, R. L. Greene, S. N. Mao, X. X. Xi, S. Bhattacharya, Q. Li, and C. J. Lobb (1993), Phys. Rev. B **47**, 1064.

Halperin, B. I., and D. R. Nelson (1978), Phys. Rev. Lett. **41**, 121.

Halperin, B. I., and D. R. Nelson (1979), Journal of Low Temperature Physics **36** (5), 599.

Hartnoll, S. A., P. K. Kovtun, M. Müller, and S. Sachdev (2007), Phys. Rev. B **76**, 144502.

Haviland, D. B., Y. Liu, and A. M. Goldman (1989), Phys. Rev. Lett. **62**, 2180.

Helfand, E., and N. R. Werthamer (1966), Phys. Rev. **147**, 288.

Heym, J. (1992), Journal of Low Temperature Physics **89** (5-6), 869.

Hirschfeld, P. J., M. M. Korshunov, and I. I. Mazin (2011), Reports on Progress in Physics **74** (12), 124508.

Howson, M. A., M. B. Salamon, T. A. Friedmann, J. P. Rice, and D. Ginsberg (1990), Phys. Rev. B **41**, 300.

Inoue, T., S. Miwa, K. Okamoto, and M. Awano (1979), Journal of the Physical Society of Japan **46** (2), 418.

Ioffe, L., and A. Larkin (1981), Soviet Physics-JETP **54** (2), 378, (Zh. Eksp. Teor. Fiz. **81**, 707 (1981).).

Ioffe, L. B., A. I. Larkin, A. A. Varlamov, and L. Yu (1993), Phys. Rev. B **47**, 8936.

Iye, Y., S. Nakamura, and T. Tamegai (1989), Physica C: Superconductivity **159** (5), 616.

Jacobs, T., S. O. Katterwe, and V. M. Krasnov (2016), Phys. Rev. B **94**, 220501.

Jin, K., B. Y. Zhu, B. X. Wu, J. Vanacken, V. V. Moshchalkov, B. Xu, L. X. Cao, X. G. Qiu, and B. R. Zhao (2008), Phys. Rev. B **77**, 172503.

Johnston, D. C. (2010), Advances in Physics **59** (6), 803, http://dx.doi.org/10.1080/00018732.2010.513480.

Kapitulnik, A., A. Palevski, and G. Deutscher (1985), Journal of Physics C: Solid State Physics **18** (6), 1305.

Kartsovnik, M., G. Logvenov, K. Maki, and N. Kushch (1999), Synthetic Metals **103** (1), 1827 , international Conference on Science and Technology of Synthetic Metals.

Kavokin, A. V., and A. A. Varlamov (2015), Phys. Rev. B **92**, 020514.

Kittel, C. (2012), *Introduction to Solid State Physics*, 8th ed. (John Wiley & Sons, Inc., New York).

Klein, T., D. Braithwaite, A. Demuer, W. Knafo, G. Lapertot, C. Marcenat, P. Rodière, I. Sheikin, P. Strobel, A. Sulpice, and P. Toulemonde (2010), Phys. Rev. B **82**, 184506.

Klemencic, G. M., J. M. Fellows, J. M. Werrell, S. Mandal, S. R. Giblin, R. A. Smith, and O. A. Williams (2017), ArXiv e-prints arXiv:1706.05845 [cond-mat.supr-con].

Kokubo, N., J. Aarts, and P. H. Kes (2001), Phys. Rev. B **64**, 014507.

Komendová, L., M. V. Milošević, A. A. Shanenko, and F. M. Peeters (2011), Phys. Rev. B **84**, 064522.

Koshelev, A., and A. Varlamov (2014), Superconductor Science and Technology **27** (12), 124001.

Koshelev, A. E., and A. A. Golubov (2004), Phys. Rev. Lett. **92**, 107008.

Koshelev, A. E., A. A. Varlamov, and V. M. Vinokur (2005), Phys. Rev. B **72**, 064523.

Krasnov, V. M., H. Motzkau, T. Golod, A. Rydh, S. O. Katterwe, and A. B. Kulakov (2011), Phys. Rev. B **84**, 054516.

Kuboki, K., and H. Fukuyama (1989), Journal of the Physical Society of Japan **58** (2), 376.

Kulik, I., O. Entin-Wohlman, and R. Orbach (1981), Journal of Low Temperature Physics **43** (5), 591.

Kurkijärvi, J., V. Ambegaokar, and G. Eilenberger (1972), Phys. Rev. B **5**, 868.

Landau, L. (1930), Zeitschrift für Physik **64** (9-10), 629.

Lang, W., G. Heine, W. Kula, and R. Sobolewski (1995), Phys. Rev. B **51**, 9180.

Larkin, A. (1980), JETP Lett **31**, 219.

Larkin, A., and A. Varlamov (2009), *Theory of Fluctuations in Superconductors*, International Series of Monographs on Physics (OUP Oxford).

Lascialfari, A., and A. Rigamonti (2017), Il Nuovo Saggiatore **33**, 5.

Lascialfari, A., A. Rigamonti, and I. Zucca (2005), Phys. Rev. B **71**, 214510.

Lawrence, W. E., and S. Doniach (1971),.

Leridon, B., J. Vanacken, T. Wambecq, and V. V. Moshchalkov (2007), Phys. Rev. B **76**, 012503.

Lerner, I. V., A. A. Varlamov, and V. M. Vinokur (2008), Phys. Rev. Lett. **100**, 117003.

Levanyuk, A. (1959), Sov. Phys. JETP **9**, 571.

Levchenko, A., M. R. Norman, and A. A. Varlamov (2011), Phys. Rev. B **83**, 020506.

Li, P., and R. L. Greene (2007), Phys. Rev. B **76**, 174512.

Liu, W., T. W. Clinton, A. W. Smith, and C. J. Lobb (1997), Phys. Rev. B **55**, 11802.

Livanov, D. V., G. Savona, and A. A. Varlamov (2000), Phys. Rev. B **62**, 8675.

Lowe, A. J., S. Regan, and M. A. Howson (1993), Phys. Rev. B **47**, 15321.

Mahan, G. D. (2013), *Many-particle physics* (Springer Science & Business Media).

Maki, K. (1968), Progress of Theoretical Physics **39** (4), 897.

Maki, K. (1973), Phys. Rev. Lett. **30**, 648.

Maki, K., and H. Takayama (1971), Journal of Low Temperature Physics **5** (3), 313.

Maniv, T., and S. Alexander (1977), Journal of Physics C: Solid State Physics **10** (13), 2419.

Matsuda, A., S. Sugita, and T. Watanabe (1999), Phys. Rev. B **60**, 1377.

Michaeli, K., and A. M. Finkel'stein (2009a), EPL (Europhysics Letters) **86** (2), 27007.

Michaeli, K., and A. M. Finkel'stein (2009b), Phys. Rev. B **80**, 214516.

Michaeli, K., K. S. Tikhonov, and A. M. Finkel'stein (2012), Phys. Rev. B **86**, 014515.

Micklitz, T., and M. R. Norman (2009), Phys. Rev. B **80**, 220513.

Mineev, V. P., and M. Sigrist (2001), Phys. Rev. B **63**, 172504.

Morris, R. C., and R. V. Coleman (1973), Phys. Rev. B **7**, 991.

Mosconi, P., A. Rigamonti, and A. Varlamov (2000), Applied Magnetic Resonance **19** (3-4), 345.

Moskalenko, V. (1959), in *Fiz. Met. Metalloved. 4 503* (Citeseer).

Nagaoka, T., Y. Matsuda, H. Obara, A. Sawa, T. Terashima, I. Chong, M. Takano, and M. Suzuki (1998), Phys. Rev.

Lett. **80**, 3594.
Nelson, D. R., and B. I. Halperin (1979), Phys. Rev. B **19**, 2457.
Nelson, D. R., and J. M. Kosterlitz (1977), Phys. Rev. Lett. **39**, 1201.
Obraztsov, Y. N. (1964), Soviet Physics-Solid State **6** (2), 331.
Paalanen, M. A., A. F. Hebard, and R. R. Ruel (1992), Phys. Rev. Lett. **69**, 1604.
Paglione, J., and R. L. Greene (2010), Nature physics **6** (9), 645.
Palestini, F., A. Perali, P. Pieri, and G. C. Strinati (2012), Phys. Rev. B **85**, 024517.
Park, M., M. S. Isaacson, and J. M. Parpia (1995), Phys. Rev. Lett. **75**, 3740.
Patton, B. R., V. Ambegaoker, and J. W. Wilkins (1969), Solid State Communications **7** (18), 1287 .
Perali, A., C. Castellani, C. Di Castro, M. Grilli, E. Piegari, and A. A. Varlamov (2000), Phys. Rev. B **62**, R9295.
Perali, A., P. Pieri, G. C. Strinati, and C. Castellani (2002), Phys. Rev. B **66**, 024510.
Podolsky, D., S. Raghu, and A. Vishwanath (2007), Phys. Rev. Lett. **99**, 117004.
Pourret, A., H. Aubin, J. Lesueur, C. Marrache-Kikuchi, L. Berge, L. Dumoulin, and K. Behnia (2006a), Nature Physics **2** (10), 683.
Pourret, A., H. Aubin, J. Lesueur, C. A. Marrache-Kikuchi, L. Bergé, L. Dumoulin, and K. Behnia (2007), Phys. Rev. B **76**, 214504.
Pourret, A., K. Behnia, D. Kikuchi, Y. Aoki, H. Sugawara, and H. Sato (2006b), Phys. Rev. Lett. **96**, 176402.
Prando, G., P. Carretta, A. Lascialfari, A. Rigamonti, S. Sanna, L. Romanò, A. Palenzona, M. Putti, and M. Tropeano (2011), Advances in Science and Technology **75**, 141.
Prange, R. E. (1970), Phys. Rev. B **1**, 2349.
Pratt, F., J. Caulfield, L. Cowey, J. Singleton, M. Doporto, W. Hayes, J. Perenboom, M. Kurmoo, and P. Day (1993), Synthetic Metals **56** (1), 2289 , proceedings of the International Conference on Science and Technology of Synthetic Metals (ICSM'92).
Raffy, H., R. Laibowitz, P. Chaudhari, and S. Maekawa (1983), Physical Review B **28** (11), 6607.
Raghu, S., D. Podolsky, A. Vishwanath, and D. A. Huse (2008), Phys. Rev. B **78**, 184520.
Randeria, M., and A. A. Varlamov (1994), Phys. Rev. B **50**, 10401.
Ranninger, J., J. M. Robin, and M. Eschrig (1995), Phys. Rev. Lett. **74**, 4027.
Reggiani, L., R. Vaglio, and A. A. Varlamov (1991), Phys. Rev. B **44**, 9541.
Reizer, M. Y. (1993), Phys. Rev. B **48**, 13703.
Reizer, M. Y., and A. V. Sergeev (1994), Phys. Rev. B **50**, 9344.
Renner, C., B. Revaz, J.-Y. Genoud, K. Kadowaki, and O. Fischer (1998), Phys. Rev. Lett. **80**, 149.
Ri, H.-C., R. Gross, F. Gollnik, A. Beck, R. P. Huebener, P. Wagner, and H. Adrian (1994), Phys. Rev. B **50**, 3312.
Richardson, W. (1997), Physics Letters A **235** (2), 186.
Rigamonti, A., F. Borsa, and P. Carretta (1998), Reports on Progress in Physics **61** (10), 1367.
Sacépé, B., C. Chapelier, T. I. Baturina, V. M. Vinokur, M. R. Baklanov, and M. Sanquer (2008), Phys. Rev. Lett. **101**, 157006.
Sacépé, B., C. Chapelier, T. I. Baturina, V. M. Vinokur, M. R. Baklanov, and M. Sanquer (2010), Nature Communications **1**, 140.
Sacepe, B., T. Dubouchet, C. Chapelier, M. Sanquer, M. Ovadia, D. Shahar, M. Feigel'man, and L. Ioffe (2011), Nat Phys **7** (3), 239.
Samoilov, A. V. (1994), Phys. Rev. B **49**, 1246.
Santhanam, P., and D. Prober (1984), Physical Review B **29** (6), 3733.
Lopes dos Santos, J. M. B., and E. Abrahams (1985), Phys. Rev. B **31**, 172.
Scalapino, D. J. (1970), Phys. Rev. Lett. **24**, 1052.
Scalapino, D. J. (2012), Rev. Mod. Phys. **84**, 1383.
Scherpelz, P., D. Wulin, K. Levin, and A. K. Rajagopal (2013), Phys. Rev. A **87**, 063602.
Schmid, A. (1969), Phys. Rev. **180**, 527.
Schmidt, H. (1968), Zeitschrift für Physik **216** (4), 336.
Schmidt, V. V. (1966), Pis'ma v ZhETF **3**, 141.
Serafin, A., A. I. Coldea, A. Y. Ganin, M. J. Rosseinsky, K. Prassides, D. Vignolles, and A. Carrington (2010), Phys. Rev. B **82**, 104514.
Serbyn, M. N., M. A. Skvortsov, A. A. Varlamov, and V. Galitski (2009), Phys. Rev. Lett. **102**, 067001.
Skocpol, W., and M. Tinkham (1975), Reports on Progress in Physics **38** (9), 1049.
Slichter, C. P. (1990), *Principles of magnetic resonance*, Vol. 1 (Springer Verlag, Berlin).
Smith, A. W., T. W. Clinton, C. C. Tsuei, and C. J. Lobb (1994), Phys. Rev. B **49**, 12927.
Sondheimer, E. (1948), *Proceedings of the Royal Society of London A: Mathematical, Physical and Engineering Sciences*, **193** (1035), 484.
Steiner, M., and A. Kapitulnik (2005), Physica C: Superconductivity **422** (1), 16.
Stewart, G. R. (2011), Rev. Mod. Phys. **83**, 1589.
Suhl, H., B. T. Matthias, and L. R. Walker (1959), Phys. Rev. Lett. **3**, 552.
Suzuki, M., S.-i. Karimoto, and K. Namekawa (1998), Journal of the Physical Society of Japan **67** (3), 732.
Suzuki, T., and T. Tsuboi (1977), Journal of the Physical Society of Japan **43** (2), 444.
Tafti, F. F., F. Laliberté, M. Dion, J. Gaudet, P. Fournier, and L. Taillefer (2014), Phys. Rev. B **90**, 024519.
Tan, S., and K. Levin (2004), Phys. Rev. B **69**, 064510.
Tao, H., F. Lu, and E. Wolf (1997), Physica C: Superconductivity **282**, 1507 , proceedings of the International Conference on Materials and Mechanisms of Superconductivity High Temperature Superconductors V.
Teller, E. (1931), Zeitschrift für Physik **67** (5-6), 311.
Thompson, R. S. (1970), Phys. Rev. B **1**, 327.
Tikhonov, K. S., G. Schwiete, and A. M. Finkel'stein (2012), Physical Review B **85** (17), 174527.
Trivedi, N., Y. L. Loh, K. Bouadim, and M. Randeria (2012), Journal of Physics: Conference Series **376** (1), 012001.
Tsuboi, T., and T. Suzuki (1977), Journal of the Physical Society of Japan **42** (2), 437.
Tsuei, C. C., and J. R. Kirtley (2000), Rev. Mod. Phys. **72**, 969.
Ullah, S., and A. T. Dorsey (1990), Phys. Rev. Lett. **65**, 2066.
Ullah, S., and A. T. Dorsey (1991), Phys. Rev. B **44**, 262.
Ussishkin, I. (2003), Phys. Rev. B **68**, 024517.
Ussishkin, I., and S. L. Sondhi (2004), International Journal of Modern Physics B **18** (25), 3315.
Ussishkin, I., S. L. Sondhi, and D. A. Huse (2002), Phys. Rev. Lett. **89**, 287001.

Varlamov, A., and V. Dorin (1983), Soviet Phys. JETP **57**, 1089.
Varlamov, A., and D. Livanov (1990), Sov. Phys. JETP **71**, 325.
Varlamov, A. A., and V. V. Dorin (1986), Sov. Phys. JETP **64**, 1159.
Varlamov, A. A., and A. V. Kavokin (2009), EPL (Europhysics Letters) **86** (4), 47007.
Varlamov, A. A., and L. Yu (1991), Phys. Rev. B **44**, 7078.
V.M. Loktev, Y. P. (2015), *Dopants and Impurities in High-Tc superconductors* (Academperiodica, Kiev).
Wang, Y., L. Li, and N. P. Ong (2006), Phys. Rev. B **73**, 024510.
Wang, Y., N. P. Ong, Z. A. Xu, T. Kakeshita, S. Uchida, D. A. Bonn, R. Liang, and W. N. Hardy (2002), Phys. Rev. Lett. **88**, 257003.
Wang, Y., Z. Xu, T. Kakeshita, S. Uchida, S. Ono, Y. Ando, and N. Ong (2001), Physical Review B **64** (22), 224519.
Watanabe, T., T. Fujii, and A. Matsuda (1997), Phys. Rev. Lett. **79**, 2113.
Watanabe, T., T. Fujii, and A. Matsuda (2000), Phys. Rev. Lett. **84**, 5848.
Wen, H. H., Z. Y. Liu, Z. A. Xu, Z. Y. Weng, F. Zhou, and Z. X. Zhao (2003), EPL (Europhysics Letters) **63** (4), 583.
Wu, C., and J. Lin (1994), Physical Review B **50** (1), 385.
Xi, X. X. (2008), Reports on Progress in Physics **71** (11), 116501.
Xu, Z. A., N. P. Ong, Y. Wang, T. Kakeshita, and S. Uchida (2000), Nature **406** (6795), 486.
Xu, Z. A., J. Q. Shen, S. R. Zhao, Y. J. Zhang, and C. K. Ong (2005), Phys. Rev. B **72**, 144527.
Yamashita, T., Y. Shimoyama, Y. Haga, T. Matsuda, E. Yamamoto, Y. Onuki, H. Sumiyoshi, S. Fujimoto, A. Levchenko, T. Shibauchi, *et al.* (2015), Nature Physics **11** (1), 17.
Zhang, S., and J.-M. Jin (1996), *Computation of Special Functions*, 1st ed. (Wiley-Interscience).
Zheng, G.-q., W. G. Clark, Y. Kitaoka, K. Asayama, Y. Kodama, P. Kuhns, and W. G. Moulton (1999), Phys. Rev. B **60**, R9947.
Zheng, G.-q., H. Ozaki, W. G. Clark, Y. Kitaoka, P. Kuhns, A. P. Reyes, W. G. Moulton, T. Kondo, Y. Shimakawa, and Y. Kubo (2000), Phys. Rev. Lett. **85**, 405.
Zimmermann, H., M. Mali, M. Bankay, and D. Brinkmann (1991), Physica C: Superconductivity **185**, 1145.
Zuo, F., J. A. Schlueter, and J. M. Williams (1999), Phys. Rev. B **60**, 574.